CO_2 Foam Monitoring using Pressure and Resistivity Measurements

A Scientific Approach to Validating CO_2 Foam Pilots

Metin Karakas

Thesis for the degree of Philosophiae Doctor (PhD)
University of Bergen, Norway
2023

UNIVERSITY OF BERGEN

CO_2 Foam Monitoring using Pressure and Resistivity Measurements

A Scientific Approach to Validating CO_2 Foam Pilots

Metin Karakas

Thesis for the degree of Philosophiae Doctor (PhD)
at the University of Bergen

Date of defense: 15.11.2023

Year: 2023

Title: CO_2 Foam Monitoring using Pressure and Resistivity Measurements

Name: Metin Karakas

Print: Skipnes Kommunikasjon / University of Bergen

Contents

SUMMARY 6

ACKNOWLEDGEMENTS 11

LIST OF PAPERS 12

1. INTRODUCTION AND THEORY 13

1.1 FOAM IN POROUS MEDIA 13

1.2 FOAM CONSIDERATIONS 14

1.3 FOAM TYPES 15

1.4 FOAM FOR MOBILITY CONTROL 18

1.5 CO_2 FOAM AS MOBILITY CONTROL METHOD 19

1.6 RESERVOIR WORKFLOW 21

1.7 RESERVOIR MONITORING 22

1.7.1 Pressure Monitoring *22*

1.7.2 Resistivity Monitoring *23*

1.7.3 Resistivity Monitoring Using Reservoir Cores *26*

1.8 MAIN MOTIVATIONS AND RESULTS 27

2. FOAM MODELING 30

2.1 TRANSPORT MODELING 32

2.2 TRANSPORT MODELS 33

2.2.1 Analytical Model *33*

2.2.2 Explicit Population-Based Foam Model *37*

2.2.3 Transient Foam Equations *38*

2.2.4 Steady State Condition – PBE *39*

3. PRESSURE RESPONSE DURING CO_2-FOAM DISPLACEMENTS 40

3.1 CROSSWELL PRESSURE TESTING 42

3.2 FORWARD PRESSURE MODELLING 47

4. CO_2 FOAM RESISTIVITY CHARACTERISTICS AND MODELING 49

4.1 CO_2 FOAM RESISTIVITY CHARACTERISTICS 49

4.2 CO_2 FOAM RESISTIVITY MODELLING - PBE SOLUTION 52

4.3 CO_2 FOAM DISPLACEMENT WITH OIL PRESENT 53

5. FIELD PILOT 56

5.1 FOAM FORMULATION 58

5.2 FOAM PARAMETERS 59

5.3 INJECTION STRATEGY 59

5.4 SURFACTANT DELIVERY 60

5.5 RESERVOIR MONITORING 61

5.6 ANALYSIS OF PRESSURE DATA 62

5.7 FOAM MODEL 63

5.8 SIMULATION MODEL 64

5.9 HISTORY MATCHING 65

5.10 COMPARISON OF FINAL SAG AND WAG CYCLES 69

5.11 DERIVATIVE ANALYSIS 70

5.12 PRODUCTION ANALYSIS 71

5.13 INJECTION PROFILING 73

6. CONCLUSIONS AND FUTURE PERSPECTIVES 74

6.1 FUTURE PERSPECTIVES 76

7. CONCLUDING REMARKS/LESSONS LEARNED 78

7.1 LABORATORY LESSONS LEARNED 78

7.2 FIELD LESSONS LEARNED 78

ABBREVIATIONS **80**

NOMENCLATURE **81**

BIBLIOGRAPHY **85**

SCIENTIFIC PAPERS **94**

Summary

In this PhD study, we focus on the use of pressure and resistivity measurements to monitor the effectiveness of foam as a CO_2 mobility control agent in oil-producing reservoirs. When it is applied optimally, foam has excellent potential to improve reservoir sweep efficiency, as well as CO_2 utilization and storage, during CO_2 Enhanced Oil Recovery (EOR) processes. In this study, we present an integrated and novel workflow involving laboratory measurements, reservoir modeling and reservoir monitoring. Using the recorded bottom-hole pressure data from a CO_2 foam pilot study, we demonstrate how transient pressures could be used to monitor CO_2 foam development inside the reservoir. Results from a CO_2 foam pilot trial in a heterogeneous carbonate field in Permian Basin, USA are presented. We demonstrate how the injection pressure could be used to evaluate the development of foam during various foam injection cycles. For this purpose, we utilized a high-resolution radial simulator to study the effect of foam on well injectivity, as well as on CO_2 mobility in the reservoir during this surfactant-alternating gas (SAG) process.

Our analysis of the injection data indicates constant temperature behavior during all SAG cycles. On the other hand, differential pressures consistently increased during the surfactant injection and decreased during the subsequent CO_2 injection periods. Pressure buildup during the periods of surfactant injection indicated the development of a reduced mobility zone in the reservoir. The radial model proved to be useful to assess the reservoir foam strength during this pilot study. Transient analysis revealed that the differential pressures during the SAG cycles were higher than the pressures observed during the water-alternating gas (WAG) cycle which, in turn, showed foam generation and reduced CO_2 mobility in the reservoir. Our results show that in this pilot, the reservoir foam strength was most likely weaker than that expected in the laboratory.

In this PhD study, we also examine the inter-dependency between various foam parameters. To study this uniqueness problem, we utilize published experimental data from a nano-particle foam study. We show that the pressure measurements during

steady-state foam flow will give rise to an ill-posed parameter estimation problem, and, for most reservoir applications, pressure measurements alone will not adequately describe the transient foam effects.

In this work, we propose the use of combined resistivity and pressure measurements for foam monitoring. We present a theoretical framework to describe the expected resistivity changes during CO_2-foam displacements. With this objective, we first provide equations to estimate the resistivity for CO_2-foam systems and then utilize two distinct foam models to quantify these effects. Using analytical solutions based on the fractional flow theory, we present resistivity and mobility distributions for ideal and non-ideal reservoir displacement scenarios.

Our results show that transient pressure measurement could be used to gauge the overall foam strength in reservoir applications . However, additional measurements may be needed to describe the complex physics of in situ foam generation. Therefore, we propose the use of combined pressure and resistivity measurements in time-lapse mode in field applications of the (CO_2) foam processes. The proposed methods are novel as they could be employed to predict under-performing CO_2-foam floods and improve oil recovery and CO_2 storage.

In summary, this work shows that pressure data are a strong indicator of CO_2 foam development and, through combined pressure and resistivity measurements; it is possible to gather critical reservoir information to assess the effectiveness of the CO_2 foam displacements. These findings have been also corroborated through laboratory studies. Our work also shows that, through relatively simple foam transport models (either population based or implicit or local equilibrium approaches) it will be possible to quantify these resistivity changes.

This thesis is based upon eight scientific papers presenting various components for the CO_2 foam monitoring. These involves theoretical investigations using mathematical models, experimental studies in core samples as well as a field research project demonstrating the utility of various monitoring techniques during the CO_2 foam mobility applications in heterogeneous systems,

Papers 1 and 7 present the analysis of transient pressure measurements from the CO_2 foam pilot in Texas, USA. Bottom Hole Pressure (BHP) and temperature data from the downhole pressure gauge (DHPG) was used to evaluate the pilot response during surfactant and CO_2 injection. The analysis was conducted by examining the differential pressure (dP) and differential temperature (dT) through time for the Surfactant-Alternating-Gas (SAG) and Water-Alternating-Gas (WAG) injection cycles. A high-resolution, two-dimensional radial numerical model was used to history match the measured transient pressure data. The simulation model included the porosity and permeability distribution from a validated sector-scale model of the pilot pattern and surrounding producers. The radial flow model was used to examine the impact of foam on injectivity and mobility reduction when switching between surfactant solution and CO_2 injection processes.

Transient analysis showed that the temperature responses were quite similar during most SAG cycles. On the other hand, differential pressures consistently increased during periods of surfactant injection and decreased during the subsequent CO_2 injection periods. The pressure increase (buildup) during surfactant injection was due to a decrease in mobility, showing development of a mobility bank in the reservoir. The analysis was also extended to the Pressure Fall-Off tests when the injection well was shut-in for extended periods. These analyses strongly suggest a foam development in the reservoir conditions. However, the foam strength (or stability) was less than expected from lab works.

Papers 2 and 5 present a combined pressure and resistivity monitoring method during reservoir flooding using CO_2 foam. In this paper, a theoretical framework is described to estimate the expected resistivity changes during CO_2-Foam displacements. With this objective, a procedure is provided to estimate the resistivity for CO_2-Foam systems and then these effects are quantified using both Population Based (PBE) and Local Equilibrium foam models. In this paper, we present, by using analytical solutions based on the fractional flow theory, the corresponding resistivity and mobility distributions for both ideal and non-ideal reservoir displacement scenarios. Additionally, we present the inter-dependency between various foam parameters if only pressure measurements

are utilized. In this paper, we also propose combination of Pressure and Resistivity measurements in time-lapse mode as a rigorous monitoring method for monitoring the (CO_2) Foam processes. The proposed method is novel as it could be employed to predict under-performing CO_2-Foam floods as well as improve oil recovery and CO_2 storage.

Paper 3 presents an experimental investigation of CO_2 foam development during alternating injection of surfactant solution and CO_2 at reservoir conditions. The experimental work captured unsteady-state CO_2 foam generation during SAG injection and shed light onto field-scale CO_2 foam flow processes. Using foam models, apparent viscosity was calculated for each surfactant-alternating-gas (SAG) injection cycle. All experimentally derived foam models indicated reduced CO_2 mobility and the foam propagation into the core based upon the increasing pressure build-up for each SAG cycle |Furthermore, these results showed increased flow resistance compared to an identical water-alternating-gas (WAG) injection process, without surfactant. This experimental work confirmed our findings from the CO_2 foam pilot in Texas that foam generation is a transient process and that foam propagates into the reservoir during each SAG injection cycle.

Paper 4 presents a monitoring technique to track quality of the foam while core-flooding. This monitoring is used to capture the onset of foam formation, development, and foam breakthrough across the length of core-plugs. This method complements the conventional method of measuring pressure response across the core and allows tracking of the foam generation and propagation. During this study, various brine formulations were alternatively injected with the non-ionic surfactant, co-injected with gas, to generate foam in-situ in carbonate reservoir samples. In addition, a new idea involving resistivity and pressure measurements for the optimization of CO_2 foam injection process is discussed.

Paper 6 describes the design and monitoring program from a CO_2 foam pilot in East Seminole Field, Permian Basin, USA. In this field a tertiary miscible CO_2 injection has been implemented and the results indicated poor areal sweep efficiency due to reservoir

heterogeneity and an unfavorable mobility ratio between CO_2 and reservoir fluids. With this objective, a surfactant-stabilized foam was selected for mobility control. The foam system was designed using reservoir cores form this field. This was done to ensure the success of foam generation and strength during this field experiment. A field injection unit was constructed to meet the requirements of surfactant delivery, mixing, and storing. The injected fluids were routinely analyzed to validate the foam formulation consistency during this field experiment. The reservoir monitoring program included downhole pressure and temperature measurements, injection profiles and tracer tests. Produced fluids were also collected and analyzed to determine surfactant breakthrough in producing wells in the area.

Paper 8 presents the complete field results and analysis from the implementation of CO_2 foam mobility control in a CO_2 foam pilot that was conducted in a heterogeneous carbonate reservoir in East Seminole Field, Permian Basin USA. The effectiveness of foam in improving overall recovery was determined by comparing the production response before and after surfactant injection. The production analysis shows the effectiveness of foam in improving the overall oil recovery in this pilot.

Acknowledgements

I would like to extend many thanks to my supervisor Professors Arne Graue and Professor Geir Ersland for an opportunity to work on an exciting project and for thoughtful guidance and discussions. My special thanks go to Prof. George Hirasaki at Rice University for sharing his deep knowledge, experience, and the lab facilities at Rice University with us during the Pilot project.

Special thanks to Research Scientist Zachary Paul Alcorn at the University of Bergen for sharing the reservoir model used in history matching. I also want to acknowledge my research colleagues Tore Føyen and Leilei Zhang with whom I spent considerable time at the field site during the pilot. Thanks to the field operator Tabula Rasa Energy, for data sharing and access to the East Seminole Field, Permian Basin, USA.

I also wish to acknowledge the Norwegian Research Council CLIMIT program for their financial support under grant number 249742 (CO_2 Storage from Lab to On-Shore Field Pilots Using CO_2-Foam for Mobility Control in CCUS) and Gassnova project number 618069 as well as our industry partners; Shell Global Solutions, TOTAL E&P USA, Equinor ASA, and Occidental Petroleum.

Finally, I extend my deepest gratitude to my beloved wife Feza Karakas for her endless support during this process.

List of Papers

1. **Karakas, M.**, Alcorn, Z. P., Aminzadeh, F., & Graue, A., (2022) Pressure Measurements for Monitoring CO_2 Foam Pilots. Published in Energies, 15(9), 3035.
2. **Karakas, M.**, Aminzadeh, F., & Graue, A. (2022), CO_2-Foam Monitoring using Resistivity and Pressure Measurements. Published in Global Journal of Research In Engineering.
3. Alcorn, Z. P., Sæle, A., **Karakas, M.**, & Graue, A. (2022). Unsteady-state CO_2 Foam Generation and Propagation: Laboratory and Field Insights. Published in Energies, 15(18), 6551.
4. Haroun, M., Mohammed, A. M., Somra, B., Punjabi, S., Temitope, A., Yim, Y., Anastasiou, S., Baker, J. A., Haoge, L., Kobaisi, M. A., **Karakas, M**., Aminzadeh, F. and Francisco C., Real-time resistivity monitoring tool for in-situ foam front tracking. Paper presented at the Abu Dhabi International Petroleum Exhibition & Conference. November 2017.
5. **Karakas, M**. and Aminzadeh, F., 2018. Optimization of CO_2-Foam Injection through Resistivity and Pressure Measurements. Paper presented at the SPE Western Regional Meeting, April 2018.
6. Alcorn, Z. P., Føyen, T., Zhang, L., **Karakas, M**., Biswal, S. L., Hirasaki, G., and Arne G., CO_2 Foam Field Pilot Design and Initial Results. Paper presented at the SPE Improved Oil Recovery Conference, Virtual, August 2020.
7. **Karakas, M**., Alcorn, Z. P., & Graue, A. CO_2 Foam Field Pilot Monitoring Using Transient Pressure Measurements. Paper presented at the SPE Annual Technical Conference and Exhibition. October 2020.
8. Alcorn, Z. P., Graue, A., & **Karakas, M**., CO_2 Foam Pilot in a Heterogeneous Carbonate Reservoir: Analysis and Results. Paper presented at the SPE Improved Oil Recovery Conference. April 2022.

1. Introduction and Theory

In this chapter a theoretical background on CO_2 foam injection as well as the motivations for this work are presented. Later in the thesis, we present the field pilot research program with a discussion on laboratory and reservoir measurements.

1.1 Foam in Porous Media

Foam in porous media refers to the phenomenon where a stable foam, consisting of gas bubbles dispersed in a liquid, flows through a porous media such as sandstone and carbonate rocks (Rossen and Gauglitz 2000). In Enhanced Oil Recovery (EOR) operations, foam can be used to improve the sweep efficiency of injected fluids, diverting them from high-permeability zones to low-permeability ones. This diversion helps to increase oil recovery and minimize channeling effects (Kuuskraa et al. 2006 and Enick et al. 2012). Foam is also employed in soil and groundwater remediation processes to control the migration of contaminants. By reducing the mobility of contaminated fluids, foam helps to enhance the retention and immobilization of pollutants, facilitating their removal. Recently, foam has been proposed for subsurface storage of carbon dioxide (CO_2) in carbon capture and storage (CCS) applications.

Foam can act as a trapping mechanism, immobilizing the injected gas and reducing the risk of leakage. Overall, foam in porous media offers a range of benefits in terms of stability, flow resistance, and mobility control. Its unique characteristics make it a valuable tool in various industries where precise control of fluid flow through porous media is essential. The behavior of foam in porous media is influenced by factors such as the liquid-to-gas ratio, bubble size distribution, liquid properties, porous medium characteristics, and flow conditions (Kim et al., 2005). Understanding the dynamics of foam flow in porous media is essential for optimizing these processes and improving our knowledge.

Foam can alter the flow characteristics in porous media by reducing the effective permeability (or mobility) of the porous media, affecting fluid flow and transport processes. Foam also increases the viscosity of the liquid phase, which further

influences flow behavior. Foam can also exhibit non-Newtonian behavior, which means that its viscosity could change with the applied shear rate, leading to non-linear flow patterns.

The stability of foam in porous media is essential for successful industrial applications (Valincius et al. 2007). In this context, foam stability refers to the ability of the foam to maintain its structure and functionality over extended period. Foam stability depends on the properties of the liquid and gas phases, gas phase, and the porous medium itself. Foam is generally stabilized by adding surfactants, which reduce the surface tension between the gas and liquid phases, preventing bubble coalescence and collapse. The presence of surfactants could also alter the wetting properties of the porous medium and could affect the foam flow.

The study of foam in porous media involves a combination of experimental techniques (Lai and Radke 1991), theoretical models (Gauglitz and Radke 1990, Kam et al. 2004), and numerical simulations (Rossen and Gauglitz 2000). Mathematical models and numerical simulations have been developed to predict and understand foam flow dynamics and to optimize foam-based processes (Ma et al. 2015).

Overall, the study of foam in porous media is a multidisciplinary effort and combines various disciplines such as physics, fluid mechanics and reservoir engineering. Understanding the behavior of foam in porous media is crucial for optimizing oil recovery and CO_2 storage, developing efficient oil recovery techniques, and addressing environmental challenges.

1.2 Foam Considerations

Foam flow in porous media can exhibit different flow regimes depending on foam quality (gas fraction in the foam), pressure gradient, and the characteristics of the porous medium such as permeability and wettability. Capillary forces could also play a significant role in foam flow in porous media. The presence of small capillary channels in the porous medium can lead to preferential trapping and immobilization of gas bubbles, affecting the foam flow patterns and the overall transport of fluids through the porous medium. Foam flow in porous media may exhibit hysteresis, which means

that its flow characteristics could depend on the previous history of the foam flow. This hysteresis effect is attributed to the trapping and mobilization of gas bubbles within the pore spaces, leading to variations in the foam behavior during flow reversal or changes in flow conditions.

Foam in porous media utilizes different displacement mechanisms to mobilize and displace fluids. These mechanisms include snap-off, where gas bubbles break off from the main foam body and enter new flow paths, and film flow, where thin liquid films bridge adjacent gas bubbles and aid in fluid transport.

Understanding foam flow at the pore-scale level is crucial for predicting and optimizing foam behavior in porous media. Pore-scale models simulate the interactions between individual gas bubbles, liquid films, and the solid surfaces of the porous medium, providing insights into foam dynamics and the underlying physics. Pressure drop across the porous medium during foam flow is commonly measured to assess the resistance to flow. Researchers analyze foam behavior and determine key parameters such as apparent viscosity and gas mobility by monitoring the pressure drop as a function of gas and liquid flow rates.

Various visualization methods, including X-ray computed tomography (CT) and optical microscopy, are employed to observe the foam structure, and understand the foam propagation dynamics in porous media. These techniques provide insights into foam distribution, bubble size distribution, and foam stability. Capillary pressure curves are used to analyze the foam displacement behavior in porous media. By measuring the pressure drop across the porous medium at different liquid saturations, researchers can determine the capillary pressure relationship and understand the foam imbibition and drainage processes.

1.3 Foam Types

Foam in porous media is typically generated by injecting a gas and surfactant solution into the porous medium. The gas bubbles become trapped in the pore spaces, forming a foam structure. The stability of foam in porous media is influenced by factors such

as surfactant concentration, brine salinity, temperature, and the rock characteristics (Rossen and Gauglitz, 2000).

There are basically three types of foam in porous media (Kam et al. 2004):

a. Strong Foam

b. Coarse of Weak Foam

c. Intermediate Foam

Strong foam in porous media exhibits sustained stability and enhanced flow resistance when flowing through a porous medium. Strong foam maintains its structure and stability even under high pressure gradients or shear forces. It resists coarsening and drainage, which are typical challenges for industrial foam applications. The formation of strong foam in porous media involves the injection of a gas phase (CO_2, air, or nitrogen) mixed with a surfactant solution into the porous medium. The surfactant reduces the interfacial tension between gas and liquid phases, allowing the formation of stable foam lamellae. The surfactant solution is typically injected into the porous medium first, followed by the gas phase. The gas flows through the surfactant solution, generating bubbles and creating a foam structure. As the foam propagates through the porous medium, it undergoes complex interactions with the pore surfaces and the resident fluids.

Coarse or weak foam in porous media refers to a type of foam structure that exhibits larger bubble size and lower stability compared to strong foam. The foam bubbles in coarse foam are larger in size compared to strong foam. This is often attributed to the limited availability of surfactant molecules or the presence of high capillary pressures within the porous medium, which hinder the formation of smaller bubbles. Coarse foam has lower stability and is more prone to coalescence and bubble rearrangement compared to strong foam. The larger bubbles have a higher tendency to merge, leading to a decrease in the overall foam stability. This can result in faster drainage and destabilization of the foam structure. Weak foam exhibits higher mobility compared to

strong foam. The larger bubble size and reduced foam stability allow for easier flow through the porous medium, resulting in lower flow resistance.

Insufficient surfactant concentration in the foam formulation can lead to the formation of coarse foam. The limited availability of surfactant molecules results in weaker interfacial forces, larger bubble size, and reduced foam stability. The size and distribution of pore spaces in the porous medium can also affect foam formation. If the pore throats are relatively large, the bubbles formed may be inherently larger, leading to the development of coarse foam. Finally, high capillary pressures within the porous medium could also promote the coalescence of foam bubbles and result in the formation of weak foam. The larger bubble size and less than desired mobility of weak foam can result in reduced sweep efficiency during enhanced oil recovery operations. The foam may bypass significant portions of the reservoir, leading to decreased oil recovery. Therefore, weak foam may have limited effectiveness as a mobility control agent in certain applications.

It is important to consider the specific characteristics and implications of weak foam in porous media when designing and implementing foam-based processes or technologies. The understanding of foam behavior can help optimize foam formulations and operating conditions to achieve the desired outcome in reservoir applications.

Intermediate foam in porous media refers to a foam structures that exhibits flow characteristics between strong foam and weak foam. The bubble size in intermediate foam falls between that of fine, strong foam and coarse, weak foam. These bubbles are larger than those in strong foam but smaller than those in weak foam. The moderate bubble size contributes to a balance between foam stability and mobility. Intermediate foam in general exhibits a moderate level of stability compared to strong and weak foam. It resists coarsening and drainage to a certain extent but is more susceptible to bubble rearrangement and coalescence compared to strong foam.

1.4 Foam for Mobility Control

As part of Carbon Capture, Utilization, and Storage (CCUS) processes, CO_2 together with mobility control foam could be injected into existing oil reservoirs to improve sweep efficiency (oil recovery) and CO_2 storage. When compared to conventional CO_2 injection processes, these benefits could provide the necessary financial means for the industry while working towards achieving global CO_2 storage targets to mitigate the climate change.

Due to its ability to enhance hydrocarbon recovery beyond levels possible with primary and secondary recovery methods, Carbon Dioxide (CO_2) injection has been identified as one of the most promising Enhanced Oil Recovery (EOR) methods worldwide. While high oil recoveries are theoretically and scientifically possible, the actual performance of CO_2-EOR in real reservoir applications has been considerably less than that predicted in laboratory conditions.

One of the main reasons for less-than-optimum performance is due to limited contact of the injected CO_2 with the remaining or residual oil in the reservoir. The poor sweep efficiency is typically caused by the gravity override, viscous fingering and channeling of the less dense and higher mobility CO_2 phase in heterogeneous reservoirs with contrasting permeabilities.

The main CO_2-EOR Challenges can be summarized as follows (Kuuskraa et al. 2006):

- Low sweep efficiency under conditions of high (unfavorable) mobility ratios
- Gravity override by the less dense CO_2 phase
- Viscous fingering of the CO_2 through the reservoir's oil
- Channeling of the CO_2 in highly heterogeneous reservoirs

It is expected that some of these undesirable effects could be offset, in additional to traditional mechanical means, by injection of CO_2 Foam (Talebian et al. 2014). Therefore, reservoir conformance is one of the main considerations for any successful CO_2-EOR implementation.

CO_2 foams have emerged as one of the most promising, cost-effective techniques to achieve increased oil recovery through improving the CO_2 mobility ratio and sweep efficiency (Bernard et al. 1980; Ferno et al. 2016). The use of foam for mobility control was first proposed by Bond and Holbrook in 1958. CO_2 foams are typically generated in-situ through the simultaneous injection of a water-soluble surfactant and CO_2 (co-injection) or alternating injection of surfactant solution and CO_2 (SAG).

1.5 CO_2 Foam as Mobility Control Method

CO_2 Foam is a fluid, where CO_2 phase is dispersed within a liquid phase as bubbles which are separated by thin films called lamellae. Foams are thermodynamically unstable and require a minimum pressure gradient to form. They also collapse with time and lamellae plays an important role for stability. Therefore, in wide range of applications surfactants are used to prevent coalescence of bubbles. The foam texture and its properties are determined by the density of the lamellae. Normally, the CO_2 mobility is larger than that of the foam and this can cause less-than-optimal displacement in porous media. As shown in Fig. 1, in an ideal (or optimal) displacement, both foam and the miscible CO_2 fronts should travel at the same speed.

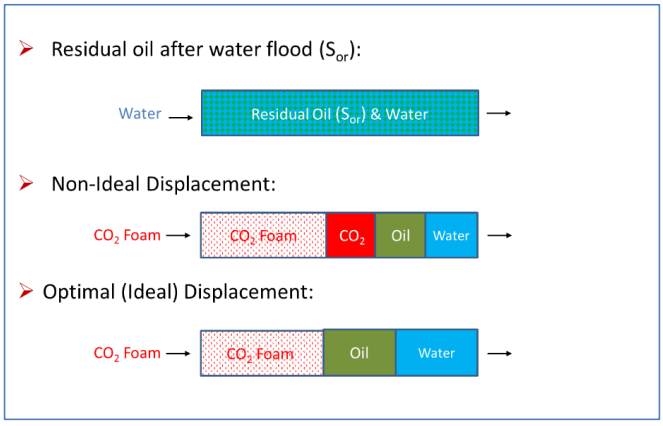

Figure 1. Optimal CO_2-Foam Injection. In a non-ideal displacement, the CO_2 front moves a head of the Foam front. In an ideal displacement, both CO_2 and Foam phases travel at the same speed.

The mobility of foam depends on its texture: the finer the foam's texture, the lower the CO_2 mobility. Laboratory studies clearly show that foam strength is very important in achieving the desired reservoir displacement efficiency. Additionally, solubility of surfactant in CO_2 and Water phases as well as the adsorption of CO_2 on the rock, play a crucial role in an optimal CO_2-Foam displacement. At a given reservoir temperature, the partitioning of the CO_2 soluble surfactants is dependent on pressure. This is strongly influenced by the attractiveness (CO_2-philicity) of the selected surfactant for foam application. Research indicates that various (cationic, nonionic and zwitterionic) surfactants are the main candidates for CO_2 foams in EOR.

Several studies have been conducted to examine the texture and stability of CO_2 foams as a function of the surfactant structure and formulation. These variables include the water/CO_2 ratio, surfactant concentration, water salinity, etc. Research shows that surfactant characteristics, along with foam strength, can be adjusted to ensure optimum foam displacement during CO_2 EOR processes. However, surfactant-based foams break down in the formation due to the presence of oil and the adsorption of the surfactant to rock, and at high temperatures and salinities. Therefore, it is also important to maintain foam strength (or stability) during the entire injection period in field applications. Recent work suggests that the addition of silica nanoparticles to surfactant-stabilized CO_2 foams may increase the strength and stability of foam systems (Rognmo et al. 2018).

There are also several strategies to generate foam in porous media. These include the co-injection of gas (CO_2)/surfactant or surfactant-alternating gas (CO_2) injection (the SAG method). In the co-injection process, the gas (CO_2) and the surfactant solution are simultaneously injected, and foam is formed in situ. In the SAG method, the surfactant and CO_2 are injected in alternating slugs. In low-permeability reservoirs, SAG injection may be preferred due to increased gas injectivity. Additionally, with the use of the SAG method, the contact between CO_2 and water is minimized, which may reduce corrosion in surface facilities and piping (Haroun et al. 2017). Laboratory studies using reservoir

cores are used to define the optimum recipe at a given reservoir pressure, temperature, and water salinity.

1.6 Reservoir Workflow

A key component of successful reservoir application of foam is the implementation of a well-defined reservoir workflow. In general terms, reservoir workflow in petroleum industry refers to the systematic and organized set of activities and processes undertaken to characterize, develop, produce, and monitor a hydrocarbon reservoir. In the case of mobility control applications of foam, the reservoir workflow involves laboratory studies, reservoir modelling, pilot design, field implementation, ad finally, reservoir monitoring to verify the foam design and injection strategy. This process encompasses multiple disciplines such as fluid engineering, petrophysics, geology and reservoir engineering. The workflow provides a framework for integrating data, models, and expert knowledge to make informed decisions about each stage of the overall process. By integrating diverse data sources and disciplines, reservoir engineers can make informed choices about foam design, reservoir implementation strategies, production optimization, and reservoir surveillance. This helps identify and mitigate risks associated with reservoir implementation. By integrating data from different disciplines and incorporating uncertainty analysis, the workflow could improve the understanding of subsurface uncertainties and their impact on recovery forecasts, reducing the likelihood of costly surprises. By systematically capturing and analysing data, monitoring reservoir performance, and comparing it with predictions, valuable insights could be gained for future reservoir management projects, leading to iterative improvement. The figure below illustrates a sample of this optimization process.

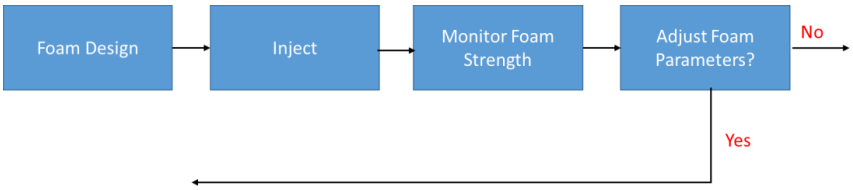

Figure 2. Foam (and CO_2-Foam) Optimization Process. Laboratory studies using reservoir cores are used to define the optimum recipe at a given the reservoir pressure, temperature, and water salinity. Based on reservoir monitoring results, the foam design and/or injection strategy could be adjusted (Yes Option). If the results are satisfactory, the selected foam design and injection strategy is used for the full field (No Option).

1.7 Reservoir Monitoring

For field applications of foam, reservoir monitoring is essential to assess the foam development under reservoir conditions. While seismic, resistivity, electromagnetic and pressure measurements have been suggested in the oil industry, foam monitoring is typically carried out through bottom hole pressure measurements, injection logging and the use of fluid tracers. These measurements are, in turn, used to assess the effectiveness of foam as a mobility control method and, hence, provide a way in which to remedy any underperforming CO_2 floods.

1.7.1 Pressure Monitoring

In the petroleum industry, transient pressure testing is typically used to investigate reservoir characteristics such as permeability, reservoir boundaries, etc., as well as the well performance such as productivity or injectivity, skin effects, etc. Fall-off testing is an effective method for monitoring water or foam injection. Typically, fall-off tests are conducted by ceasing the injection and analyzing the transient pressure to assess any mobility changes near the injector (Gargar et al. 2015). In such tests, bottom-hole pressures are recorded at the injection well, and the data are used to examine the reservoir mobility changes caused by the injection. Foam injection affects the mobility distribution in the reservoir; therefore, the location of the foam front can be monitored, in principle, by fall-off tests. These tests rely on single-point pressure measurements

and may lack the resolution required in layered formations. Based on previous comparable studies with CO_2 injections, it has been suggested that crosswell pressure testing, in addition to seismic and electromagnetic data, could be deployed for CO_2 foam monitoring (Karakas and Aminzadeh 2018). In crosswell pressure testing, a series of pressure pulses is induced by shutting down the injector, and the pressure measurements are taken at the observation well. These measurements could be used to examine the inter-well reservoir connectivity. The main advantage of these tests is the larger investigation volume away from the injector. This test procedure is shown in the figure below:

Figure 3. Crosswell Testing. For this testing method, an observer well between the injector and producer well is required to conduct a cross-well measurements.

The cross-well testing procedure is as follows:

- Pulses are generated by step changes in the injection rate (shutting the injector)
- Pressure is monitored at the observer.
- Travel time and amplitude of the pressure response recorded.

1.7.2 Resistivity Monitoring

Recently several reservoir technologies have been introduced for reservoir mapping and front tracking between wells. Time-Lapse Seismic and Electromagnetic (EM) measurements has been suggested and used to track the position of Water and CO_2 fronts in the reservoir between wells and the in some cases map the fluid saturation.

It should be noted that, while seismic provide a detailed information about reservoir heterogeneities (structures), the fluid identification with time-lapse seismic is challenging in certain conditions such as supercritical CO_2 injection in primary oil

applications (Altundas 2015, Nakamura 2015). The fluid identification is enhanced using Electromagnetic (EM) and Resistivity (ERT) methods which provide stronger fluid signature (or distinguishability) when CO_2 is injected into formations with saline water (Zhou et al. 2000). The resistivity is a very sensitive parameter to formation fluids and, when used in time-lapse mode, can be used to track saturation changes.

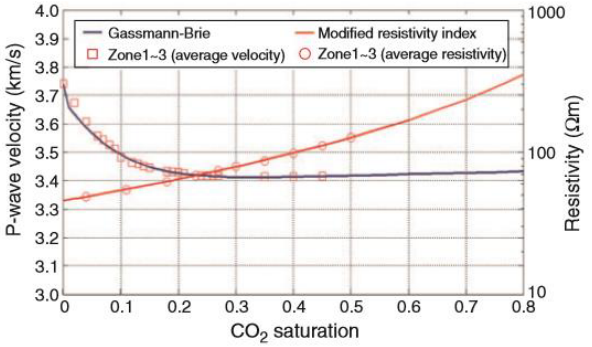

Figure 4. P-Wave and Resistivity Change vs CO_2 Saturation (from Kim et al. 2010). These results show a flattening sensitivity of the compressional velocity (Vp) to the CO_2 saturation. On the other hand, Resistivity increases monotonically with CO_2 saturation.

Kim et al. (2010) conducted several CO_2 injection experiments using water saturated cores. They monitored both seismic velocity and electrical resistivity during these experiments. In this work, simultaneous measurements of Compressional Velocity (Vp) and Resistivity (Rt) were made during CO_2 drainage or imbibition processes. The result showed a decrease in Vp and increase in Rt with increasing CO_2 Saturations. However, the main effect on Vp comes during the first 20% increase in CO_2 saturation, as shown in the above plot. On the other hand, the resistivity effect is significantly more dominant and continuous with increasing CO_2 Saturations.

Kim et al. (2010) also showed that CO_2 saturations can be estimated from measured resistivity data using a modified version of Archie's Equation as shown in the graph below.

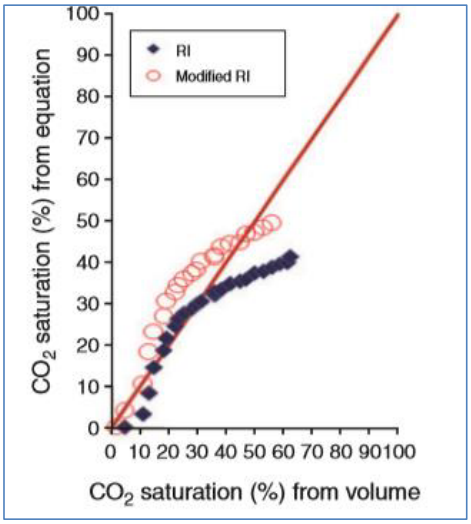

Figure 5. CO_2 Saturations from Modified Archie Eqn. (from Kim et al. 2010).

Archie's equation has been also reservoir history matching utilized to convert the time-lapse EM resistivity data to saturation (Biterge et al. 2014):

$$S_w = \sqrt[n]{\frac{a}{\phi^m}\frac{R_w}{R_{DL}}} \tag{1}$$

Where: S_w is apparent water saturation, ϕ is porosity, R_w is formation water resistivity, RDL is inverted formation resistivity from EM, n is saturation exponent, a is a constant, m is the cementation factor.

These laboratory observations suggest that, in formations undergoing tertiary CO_2 floods where the injected water has high salinity, resistivity could be used to estimate CO_2 saturation. The expected changes associated with miscible CO_2 injection typically involve displacement of the original in-situ reservoir fluids, by the miscible CO_2 phase. Under these conditions, it is possible to determine which reservoir layers are carrying the miscible CO_2 phase and how it is changing the saline water saturation. Repeat resistivity measurements could be used to track the CO_2 front before it arrives at the producers and this information could be used to estimate its velocity.

Wu et al. (2012) ran foam experiments on unsaturated soil samples to investigate the possibility of using electrical measurements for foam monitoring. Wo et al. reported large changes in electrical properties with foam formation. Karakas and Aminzadeh (2017) proposed time-lapse measurements with an array of permanently deployed sensors to detect and estimate the change in the Foam-CO_2-Oil interface in the reservoir due to CO_2-Foam injection and as a function of time. With the proposed method, resistivity and pressure measurements are acquired simultaneously during the CO_2-Foam Injection into reservoir as shown in the figure below:

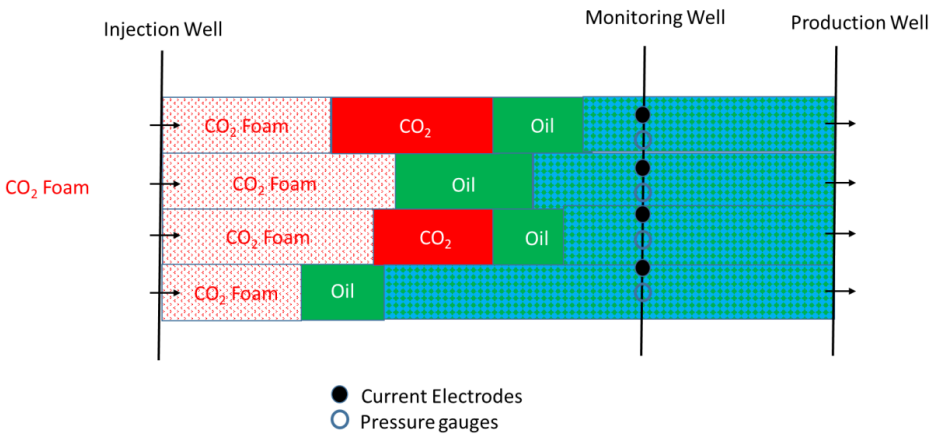

Figure 6. Example of Pressure and Resistivity Monitoring during a CO_2 Foam Flood. Pressure gauges and the current electrodes are deployed at the observation to track fluid saturations.

1.7.3 Resistivity Monitoring Using Reservoir Cores

Typically, foam development is confirmed by taking the pressure measurements along core samples. These measurements are used to infer the mobility reduction factor (MRF) during gas/surfactant (foam) injection.

Since electric measurements are sensitive to salt concentration, porosity, rock mineralogy and fluid saturation, they have been employed as a fluid tracking tool in the petroleum industry. In terms of laboratory studies, Adebayo et al. (2017) monitored resistivity across core samples during different stages of core displacement processes.

Their results showed the potency of resistivity as a tracking tool at core scale. An increase in resistivity at oil flooding and a corresponding decrease during imbibition (with sea water) were observed. The effect of wettability changes was notable as a further increase in resistivity after aging was detected. Injection of CO_2 into the sample provided the most significant increase highlighting the highly resistive nature of gas.

Since foam drainage is one of the factors responsible for the destabilization of foam, resistivity measurements have been also utilized to characterize this process in lab conditions. In these experiments, liquid content and the foam height is monitored using electrical resistance as a function of time.

Berge, C. (2017) conducted resistivity measurements while injecting CO_2 and surfactant solution into saturated cores and Haroun et al. (2017) monitored resistivity and pressure changes during foam generation in formation-brine saturated carbonate core plug samples.

Haroun, M. et al. (2017) observed large increase in resistivity and pressure with foam development. In this study, resistivity measurements were made to determine whether foam was generated in-situ during core flood experiments. A high-pressure high temperature dual core flooding cell was used for foam injection. The core holder was equipped with high resolution multi-range differential pressure sensors and the pressure drop was tracked across the core sample. During these experiments, a resistivity meter was used to monitor the resistance across the core sample.

1.8 Main Motivations and Results

The following summarizes main motivations for this work:

- To provide a theoretical framework to describe the expected resistivity changes during CO_2-foam displacements.
- To generate resistivity and mobility distributions for ideal and non-ideal reservoir displacement scenarios.
- To examine the inter-dependency between various foam parameters.
- To show resistivity and pressure monitoring possibilities during CO_2 foam injection displacements.

- To assess the effectiveness of CO_2 foam in a pilot study using pressure measurements.
- To demonstrate the pressure monitoring part of the integrated workflow.
- To gather knowledge for future CO_2 EOR field applications.

In this study, we present a novel technique to study the development of foam in reservoir conditions. The reservoir workflow was used to assess the effectiveness of CO_2 foam in a pilot study conducted in the East Seminole Field, Permian Basin, West Texas. It involved, reservoir characterization, laboratory measurements, reservoir modelling and monitoring. Specific objectives for the pilot application were as follows:

- To evaluate whether foam has been generated in the reservoir.
- Tune the foam model if foam has formed.
- To determine the foam propagation distance/rate in the reservoir.

The laboratory program was aimed at determining the optimal foam formulation for the field test. The laboratory studies were conducted on reservoir core samples to determine the optimal foam formulation. This included surfactant-screening studies, evaluations of the optimal foam quality (gas fraction) and surfactant concentration and quantification of CO_2 EOR and CO_2 storage potential.

The laboratory studies were conducted on reservoir core samples to determine the optimal foam formulation. Reservoir modeling was carried out to decide on optimum injection strategy, and extensive reservoir monitoring was conducted to assess the effectiveness of the designed foam under reservoir conditions. The results of this integrated research work provide important knowledge for future CO_2 EOR field applications.

Reservoir modelling was carried out to decide on optimum injection strategy. A surfactant-alternating gas (SAG) injection strategy was adapted, with 10 days of surfactant solution injection followed by 20 days of CO2 injection. Reservoir monitoring was conducted to assess the effectiveness of the designed foam and injection strategy under reservoir conditions.

Surfactant screening studies identified the non-ionic water-soluble Huntsman L24-22, a linear ethoxylated alcohol (C12-14 EO22), for the field pilot study based upon minimal loss to the formation due to adsorption, adequate foam strength, and chemical stability (Jian et al. 2019). Once the reservoir-specific surfactant was selected, the foam formulation was evaluated by determining the impact of surfactant concentration, gas fraction (foam quality) and flow velocity on foam strength at reservoir conditions (Alcorn et al, 2020). The foam strength was quantitatively evaluated by the apparent foam viscosity, which was calculated from the steady-state pressure gradient at each gas fraction during foam quality scans and at each injection rate during foam rate scans (Rognmo et al. 2018). Foam model parameters for numeral modelling were derived from the foam quality and foam rate scans by curve-fitting regression (Sharma et al. 2017).

Transient pressure analyses were conducted for all injection cycles. A high- resolution two-dimensional radial flow model was used to history-match the measured differential pressures. The proposed method of transient analysis has been found to be quite useful in assessing the development and progression of foam in the reservoir. The radial model proved to be useful for assessing the reservoir foam strength during this pilot study. This study showed that the pressure data alone may not be sufficient to describe the complex physics of in situ foam generation. In the pilot application, analysis of measurements suggests that the reservoir foam strength was weaker than expected based on laboratory measurements.

The results from this research work provide important knowledge for future CO_2 EOR field applications.

2. Foam Modeling

The foam exhibits complex flow behavior due to the interactions between gas bubbles, liquid films, and the rock matrix in the porous medium. Understanding and modeling these interactions are crucial for accurately predicting foam behavior in porous media.

Foam flow in porous media is governed by several mechanisms, including bubble generation, coalescence, drainage, and trapping. Bubble generation refers to the formation of gas bubbles within the liquid phase due to the injection of surfactant solution. Coalescence occurs when bubbles collide and merge, leading to the formation of larger bubbles. Drainage is the process by which liquid films thin and rupture, causing the release of gas and liquid from the foam structure. Trapping refers to the entrapment of gas bubbles within the porous matrix, impeding their flow.

To model foam flow in porous media, a set of governing equations is used. These equations include the conservation of mass for both the liquid and gas phases, as well as the conservation of momentum for each phase. Additionally, constitutive relationships are employed to describe the interactions between phases, such as the pressure drop across liquid films and the relative permeability of the foam.

Foam flow in porous media can be modeled using various approaches, ranging from simplistic empirical models to more complex mechanistic models. Empirical models are based on experimental data and correlations, providing simple relationships to estimate foam properties and behavior. Mechanistic models aim to capture the underlying physical processes using mathematical equations, accounting for bubble size distribution, film thickness, and capillary forces. Numerical techniques such as finite difference, finite element, or finite volume methods are commonly employed to solve the governing equations and simulate foam flow in porous media.

Validating foam models requires experimental data obtained through laboratory-scale studies or field trials. Researchers conduct experiments to measure foam properties, including foam texture, stability, and mobility reduction. These data are then compared with model predictions to assess the accuracy and reliability of the foam models.

Additionally, advanced imaging techniques, such as X-ray computed tomography (CT) or magnetic resonance imaging (MRI), are employed to visualize and quantify the foam structure within porous media.

While foam models can be effective in certain situations, it's important to be aware of their constraints and potential drawbacks. Foam models typically provide a simplified representation of complex systems or phenomena. They rely on assumptions and approximations to capture the essential characteristics of the system, which may result in oversimplification and loss of critical details. This can limit their accuracy in capturing the intricacies of the real-world system.

Foam models are typically built at a smaller physical scale compared to the actual system being studied. This reduction in scale can affect the accuracy of the model, especially when phenomena such as fluid dynamics or structural behavior are involved. Scaling laws and adjustments need to be considered to ensure accurate representation, but even then, there may be limitations in capturing the full-scale behavior. Foam models often use samples with properties that may differ from those of the actual reservoir. These material differences can impact the behavior of the model and lead to discrepancies between the model's predictions and real-world observations. Ensuring accurate representation of material properties is crucial for reliable results.

It is important to acknowledge these limitations when working with foam models. Their usefulness lies in their ability to provide insights and approximate behavior, but they should be used alongside other modeling techniques and supported by empirical data whenever possible to ensure more robust and reliable results.

Understanding and accounting for these limitations can help researchers make informed decisions when utilizing foam models. It is essential to recognize that foam models are tools for approximation and insight, and their limitations should be considered alongside other approaches, empirical data, and expert judgment.

2.1 Transport Modeling

The transport of foam can be described by several methods (Ma, K. et al. 2015). These include mechanistic methods such as the population balance approach as well as the semi-empirical methods based on fractional flow theory. The semi-empirical model is widely used in the oil industry for various foam injection scenarios. Abbasszadeh et al. (2014) presented a validation of the empirical foam simulation method. In this work, Abbaszadeh et al. (2014) matched the experimental foam data on sand-packs using a commercial simulator and concluded that the empirical foam modelling approach could also be applied to large-scale reservoir simulations. For more physically accurate representation of phase behavior of the CO_2-Oil system, a compositional model may also be required. Grid resolution is also important for accurate calculation of the CO_2 front. For some reservoir applications high resolution simulation models may be unfeasible. Under certain conditions upscaling may be required to simulate these miscible injection processes.

The scaling problem during chemical flooding has been studied by Moreno et al. (2011). These researchers have investigated the fluid displacement behavior in different reservoir architectures and the scaling effects to capture the underlying physics of the displacement. Also, Masoudi et al. (2015) presents a study in which they used a core-scale compositional model using Gas-Mobility Reduction Factors. They ran simulations to examine the sensitivity to key parameters on foam behavior. The gridding and the foam simulations are shown in the figure below.

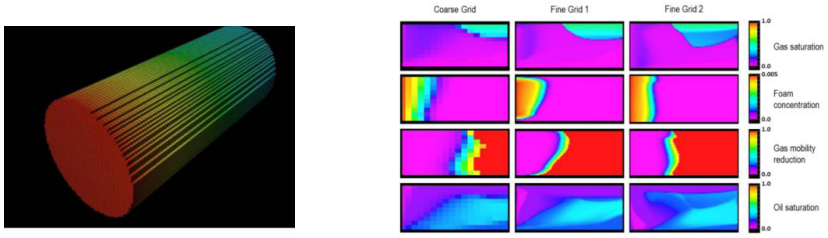

Figure 7. Simulation Gridding and Foam Simulations (From Masoudi et al. 2015)

2.2 Transport Models

The transport of CO_2-foam can be described in several methods. Pore-Network models provide a good insight into the foam transport and, due to large number of unknows, is not practical for reservoir scale applications. The analytical solution for the oil case was described by Ashoori et al. 2010. Population balance models (Falls et al. 1988, Rossen et al. 1999) explicitly represent the dynamics of lamella creation and destruction along with the effect of the resulting foam on gas mobility. Gas mobility is reduced according to bubble size (determined by rates of creation and destruction of lamellae). Implicit or local equilibrium models (Cheng et al. 2000; Farajzadeh et al. 2012) represent the effect of bubble size implicitly by introducing factors for reducing gas mobility by foam as a function of water saturation, oil saturation, surfactant concentration, and shear thinning due to flow rate. Local-equilibrium models assume foam is present anywhere gas and water are present along with an adequate surfactant concentration.

In this study, several of these methods were utilized. The population balance method was used for examining the interaction between various foam model parameters. The analytical approach was utilized for construction of resistivity profiles and a foam numerical simulator for history matching of the pressure data during pilot implementation. These methods are described in subsequent sections.

2.2.1 Analytical Model

In our work, an analytical solution approach (Ashoori et al. 2010) is utilized for resistivity calculations in the presence of oil phase. In this section, we describe the main assumptions and the solutions for ideal and non-ideal displacements for this approach.

Main assumptions include 1D displacement of oil by the injected CO_2 with dissolved surfactant; CO_2 is incompressible; surfactant is dissolved in the CO_2 phase only; reservoir is initially at residual-oil saturation after a waterflood; surfactant is soluble in both water and CO_2 phases and first-contact miscibility. Additionally, some residual oil is allowed behind the CO_2 bank.

For the rest of this section, we will use the following definitions:

C_{sg} is the mass concentration of surfactant in the CO_2 phase.

C_{sw} and C_{so} are the mass concentration of surfactant in the water phase and CO_2 Residual oil, respectfully.

C_{sa} is the mass of surfactant adsorbed on the rock.

S_{oM} is the residual oil saturation behind the CO_2 phase.

f_w and $S_w{}^u$ are the fractional water cut and water saturation behind the foam front, respectfully. Utilizing the fractional flow theory, the velocity of the surfactant front can be expressed as follows (Ashoori et al. 2010):

$$v_s = \frac{f_w^u + \frac{C_{sg}}{C_{sw}-C_{sg}}}{S_w^u + \frac{(1-S_{OM})\,C_{sg} + S_{OM}C_{SO} + S_{OM}C_{Sa}}{C_{sw}-C_{sg}}} \tag{2}$$

On the other hand, the velocity of the miscible (CO_2) front can be expressed as follows:

$$v_w = \frac{f_w^u - f_w^d}{S_w^u - S_w^d} \tag{3}$$

Assuming $C_{sg} > C_{sw}$ and $S_{oM} = 0$, the speed of the foam front could be obtained by connecting point D onto the foam fractional curve as shown in the figure below:

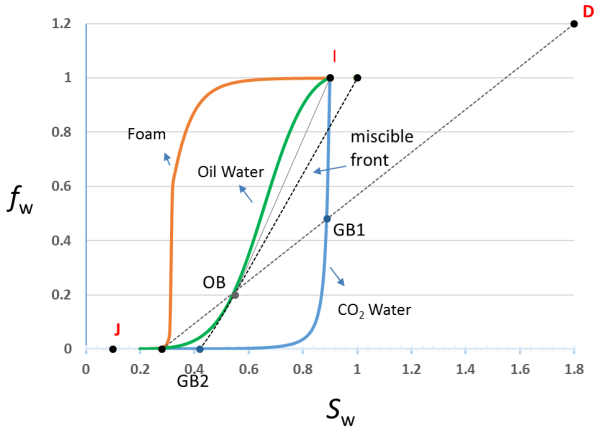

Figure 8. Analytical approach for foam transport model (Non-Ideal Displacement), Ashoori et al. 2010.

Where the point D is defined as follows:

$$D\ (S_w, f_w\ ) = (\ -\ \frac{C_{sg} - C_{sg}}{C_{sw} - C_{sg}}\ ,\ -\ \frac{C_{sg}}{C_{sw} - C_{sg}}\ ) \tag{4}$$

Similarly, the velocity of the miscible CO_2 front could be obtained from a tangent from the (1,1) point onto the oil-water fractional curve. Figure below shows the expected saturation profile for a non-optimal foam flood:

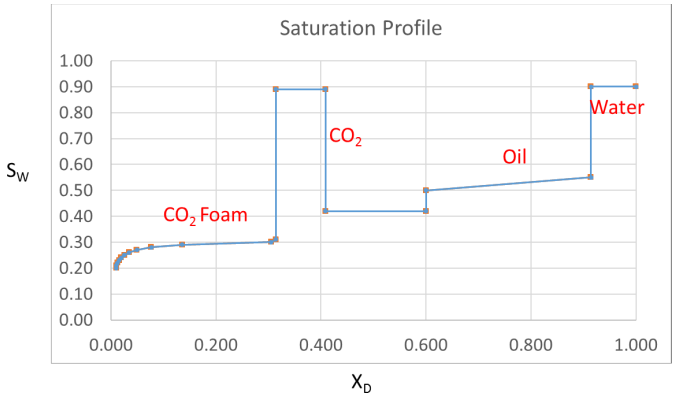

Figure 9. Saturation Profile from Analytical Approach (Non-Ideal Displacement), Ashoori et al. 2010

Then for an optimal displacement, the surfactant (foam) and the CO_2 fronts would have an equal velocity provided that

$C_{sg}/C_{sw} \rightarrow \infty$ and $C_{sa} \rightarrow 0$

In this case, D approaches to (1,1):

$D\ (S_w, f_w) \rightarrow (1, 1)$

The foam front in this case is obtained by connecting point D to the foam fractional curve as follows:

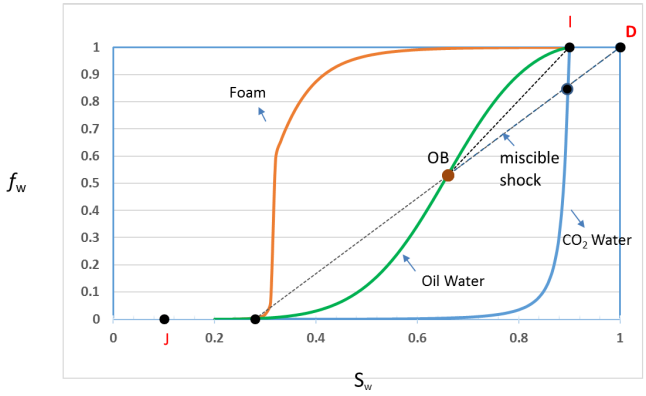

Figure 10. Analytical Approach for foam transport model (Ideal Displacement), Ashoori et al. 2010

Figure below shows the expected saturation profile for an optimal (ideal) CO_2 Foam Flood:

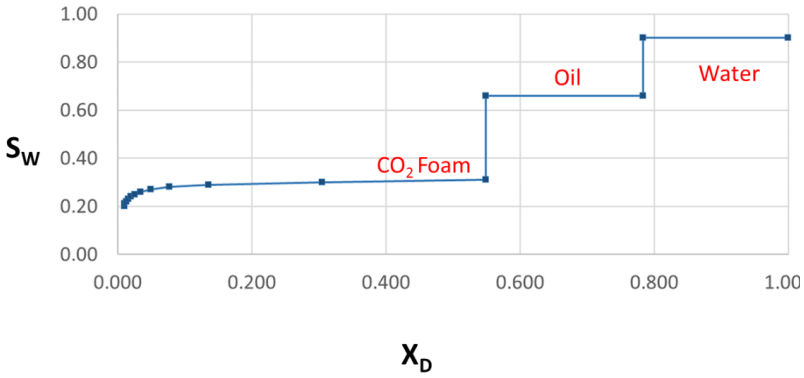

Figure 11. Saturation Profile (Ideal Displacement), Ashoori et al. 2010.

Figure below shows the comparison of total mobility distribution between optimal and non-optimal CO_2 -Foam displacements:

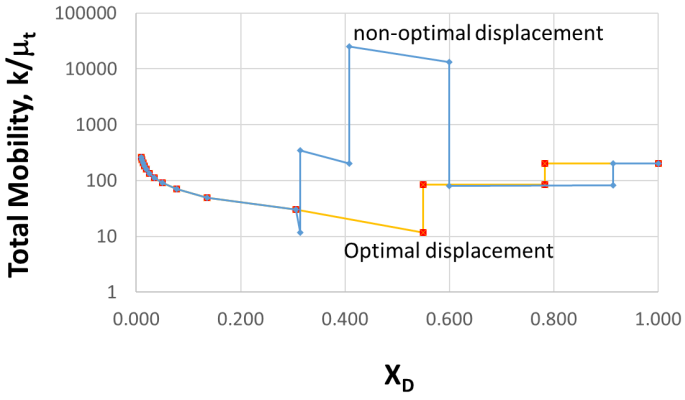

Figure 12. Comparison of Total Mobility Distribution (Ideal vs non-ideal Displacement), Ashoori et al. 2010

Therefore, these three parameters, namely, solubility of surfactant in CO_2 and Water phases as well as the adsorption of CO_2 on the rock, play a crucial role in an optimal CO_2-Foam displacement.

2.2.2 Explicit Population-Based Foam Model

As stated earlier, in our work foam resistivity is linked to foam population density. For this reason, explicit models ideally suit for this purpose. The formulation assumes water and CO_2 phases and does not include the oil phase which is a reasonable assumption as most experimental foam works are done with the main dominant water phase.

In this method main assumptions include incompressible and isothermal two-phase flow (CO_2 & Water); 1-D displacement only (CO_2 foam injection) and the negligible adsorption of the surfactant.

Below, we review the formulation of the PBE approach which is used for our resistivity modeling work.

2.2.3 Transient Foam Equations

Assuming one-dimensional isothermal two-phase flow of CO_2 and water, the material balance equation for Water phase can be written as:

$$\phi \frac{\partial S_w}{\partial t} + u_t \frac{\partial f_w}{\partial x} = 0 \tag{5}$$

In this model, we assume 0 < x < L and for t >0. L is the length of the flood domain. ϕ is the porosity and the u_t is total flux which is assumed to be constant in these displacements. As usual, S_w and f_w denotes the water saturation and the fractional flow of water.

The fractional flow of water can be expressed as follows:

$$f_w = \frac{\frac{k_{rw}}{\mu_w}}{\frac{k_{rw}}{\mu_w} + \frac{k_{rco2}}{\mu^f_{co2}}} \tag{6}$$

Where μ^f_{co2} is the effective viscosity of the CO_2 phase (with foam) and is given by (Hirasaki et al. 1985).

$$\mu^f_{co2} = \mu^0_{co2} + C_f \frac{n_f}{(\frac{u_{co2}}{\phi S_{co2}})^{1/3}} \tag{7}$$

Where μ^0_{co2} is the viscosity of the foam without foam present and C_f is a model parameter.

Foam Population Balance for the density of the lamellae (n_f) can be written as follows (Kovscek et al. 1995, Chen et al. 2010):

$$\phi \frac{\partial (S_{co2}\, n_f)}{\partial t} + u_t \frac{\partial (f_{co2} n_f)}{\partial x} = \phi\, S_{co2}\, (r_g - r_c) \tag{8}$$

The rate of foam generation is given by

$$r_g = C_g \nabla p^m \tag{9}$$

and the rate of foam coalescence is given by

$$r_c = C_c\, n_f\, \left(\frac{S_w}{S_w - S_w^*}\right)^n \tag{10}$$

Where C_g, C_c, m and n are model parameters. S_w^* is the minimum water saturation corresponding to critical capillary pressure for a foam – water flow systems. In high permeability systems, the minimum water saturation is quite low and the foam behavior around this value could be quite abrupt, meaning foam or no-foam development.

The water flux is given by

$$\boldsymbol{u}_w = - \frac{k\, k_{rw}}{\mu_w}\, \nabla p_w \tag{11}$$

And the foam flux is given by:

$$u_{co2} = - \frac{k\, k_{rco2}}{\mu_{co2}^o}\ \ \nabla p_w \tag{12}$$

2.2.4 Steady State Condition – PBE

At local steady state conditions, rate of foam generation is equal to rate of foam coalescence:

$$r_g = r_c \tag{13}$$

when this relationship is inserted into the foam-viscosity equation:

$$\mu_{co2}^{f} = \mu_{co2}^{0} + C_f \frac{n_f}{\left(\frac{u_{co2}}{\phi S_{co2}}\right)^{1/3}} \tag{14}$$

we obtain the following relationship for the effective CO_2 - foam viscosity:

$$\mu_{co2}^{f} = \mu_{co2}^{0} + \frac{C_g\, C_f}{C_c} \frac{\nabla p^m}{\left(\frac{S_w}{S_w - S_w^*}\right)^n \left(\frac{u_{co2}}{\phi S_{co2}}\right)^{1/3}} \tag{15}$$

3. Pressure Response during CO_2-Foam Injection

In this section, we focus on the use of pressure to characterize mobility effects and examine the transient pressure responses during injection and cross well tests with CO_2 foam injection.

The expected pressure response during CO_2-Foam injection will be function of the displacement type. For an ideal displacement case (immediate and uniform foam development), the pressure response at the injector well mainly depends on the mobility of the selected foam system.

As mentioned earlier there are three possible steady foam states at a fixed injection rate:

1. Coarse foam: in this state bubbles are large, foam texture (density) is small, and the gas mobility (velocity) is high. Therefore, pressure gradient is not enough to mobilize existing lamellae. This state is relatively stable to small changes.

2.Strong foam: in this state bubbles are small foam texture or density is large and the gas mobility (velocity) is low.

3.Intermediate foam: between coarse and strong foam, there is an intermediate state which is relatively unstable. In this state, both higher and lower gas velocities can be expected.

For these displacements, the total mobility within the foam bank will be a function of the foam quality. Kam et al. (2004) fit a population-balance model to experimental data for these three foam states. The experimental data were gathered by co-injecting gas and surfactant solution into a vertically mounted bead pack (Gauglitz et al. 2002). Pressure drop was monitored using pressure taps stationed along the bead packs. The figure below shows the model fit to the data.

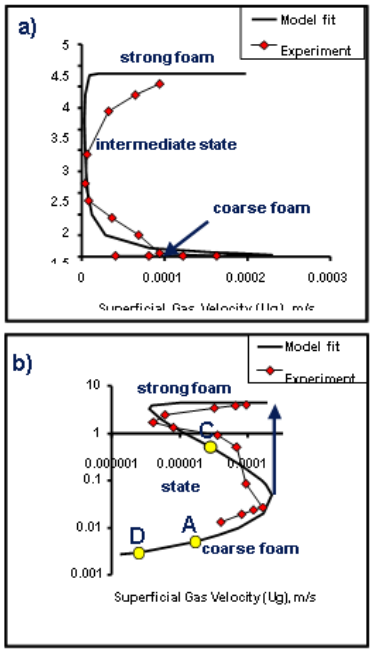

Figure 13. Model fit to experimental data (dark diamonds) for various foam states (Kam et al. 2004).

Table below gives the model parameters obtained by fitting the population-balance model to experimental data (Kam et al. 2004).

Table 1. Population-balance model parameters were obtained by fitting the model to experimental data (Kam et al, 2004).

Foam parameters		Other parameters	
C_g/ C_c	15,488.894	S_w*	0.0585
m	2.4	k (m^2)	$30.4x10^{-12}$
n	0.28	φ	0.31
C_f	$1.007x10^{-16}$	μ_w (Pa s)	0.001
		μ_g^o (Pa s)	0.00002
		S_{wc}	0.04
		S_{gr}	0.0

Where S_w^* is the water saturation at limiting capillary pressure. μ_g^o is the gas viscosity without foam.

To illustrate the expected mobilities for different foam types (strong–intermediate-weak foam systems), we utilized these model parameters in the table below.

Table 2. Estimated Total Mobility for different foam types.

	Strong Foam	**Intermediate Foam**	**Weak Foam**
Water Saturation	0.10	0.10	0.63
CO_2 Saturation	0.90	0.90	0.38
Water Viscosity (Pa.s)	1.0E-03	1.0E-03	1.0E-03
Foam Density ($1/m^3$)	8.0E+13	3.2E+12	7.0E+08
CO_2 Foam Viscosity (Pa.s)	4.6E-01	1.0E-02	2.3E-05
Relative Permeability to Water	0.003	0.003	0.299
Relative Permeability to CO_2	0.863	0.872	0.117
Foam Mobility (1/Pa.s)	5.3	86.9	5432.6
Mobility Ratio (Foam/Water)	0.005	0.087	5.433

As indicated in the above table, the foam mobility is expected to be significantly less than that of water for most strong or intermediate foam systems. Therefore, one can expect to see development of a reduced mobility bank around the injector with continuous foam injection.

3.1 Crosswell Pressure Testing

In petroleum industry, the crosswell tests or interference tests are commonly deployed by shutting the producers or injection wells and observing the pressure response at a selected observation well. During crosswell tests without any fluid injection, the transient pressure at the observation well is largely used to quantify the inter-well transmissibility. In these cases, the pressure change (or amplitude) at the observation

is a function of the inter-well transmissibility. Also, due to distance from the source well, the maximum pressure change is observed with a delay (time-lag) from the time the source well is shut-in. The figure below shows a typical pressure response during a standard crosswell test without any injection.

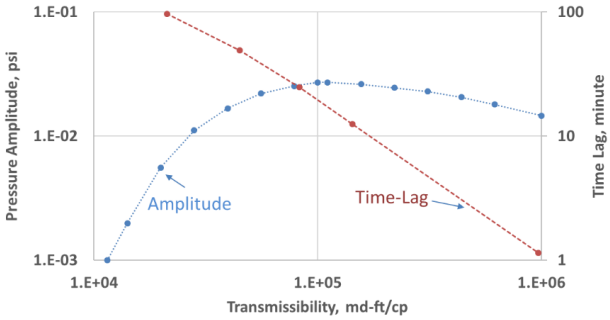

Figure 14. Pressure Amplitude and time lag for a single mobility crosswell test

As seen from this figure, the pressure magnitude at the observation well initially increases with increasing transmissibility due to faster propagation of the pressure pulse in the reservoir and later, levels down due to smaller pressure pulse created at the source for a fixed rate change. The time-lag, on the other hand is inversely related to the transmissibility for a fixed storage (porosity-compressibility) system in the reservoir and decreases with increasing inter-well transmissivity.

1.1 Pressure Response during Miscible CO_2 Displacement

During CO_2 injection, there are two important changes that effect the pressure response at the observation well: mobility increases significantly within the CO_2 bank (mobility ratio of around 20) and storativity increase due to large compressibility of the CO_2 phase (compressibility ratio around 9).

These mobility and compressibility effects are shown in the figures below for a miscible CO_2 injection into reservoir:

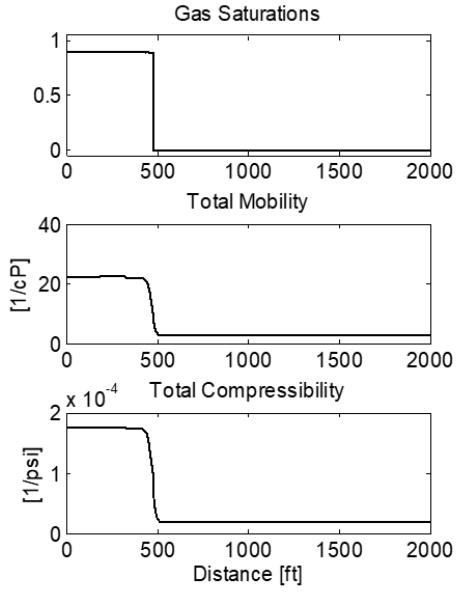

Figure 15. Mobility and Compressibility profiles during CO_2 Injection (Karakas and Morten, 2010).

The above calculated gas saturations are idealized as it ignores gravity override, viscous fingering and channeling through high-permeability zones. However, these results are useful as they provide an upper limit of the expected pressure response with CO_2 injection.

Based on the fixed rate change, the pressure response at the observation well is calculated at different times of CO_2 injection. These results are shown in the figure below:

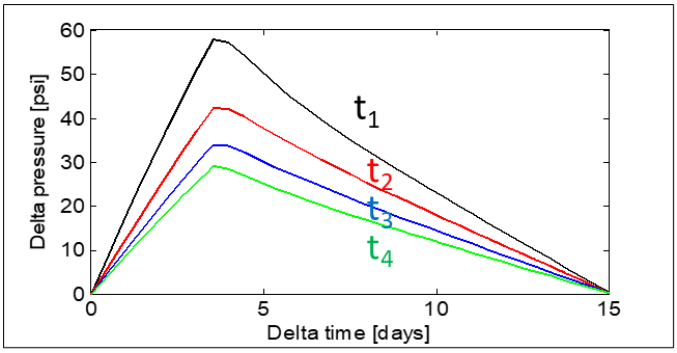

Figure 16. Pressure Response at the Observation Well during CO_2 Injection (Karakas and Morten, 2011). Different colors show the evolution of the pressure response at different shut-in times ($t_4>t_3>t_2>t_1$) during CO_2 injection.

In the figure above, delta pressure is the calculated pressure drop from the last established pressure before the well is shut in. Similarly, delta time is the time difference from the time well is shut in. As seen from this figure, the pressure amplitude decreases with growing mobility CO_2 bank. This is expected since the pressure pulse at the source is smaller for a fixed rate. It is also interesting to note that observed time-lag is almost constant due to increased compressibility of the system which counteracts the effect of increased inter-well transmissibility on the time-lag.

1.2 Pressure Response during CO_2-Foam Displacements

The expected pressure response during CO_2-Foam injection will be function of the displacement type. For an ideal foam displacement situation, the system is like that observed with CO_2 displacement case since there is a single mobility bank. However, the pressure changes will be significantly higher compared to CO_2 injection case due to decreased mobility. Hence, the pressure response depends on the mobility and the compressibility of the selected foam system.

Based on parameters listed in Table 2, it is expected that the pressure amplitude response of a weak foam system will be similar to that of CO_2 injection. On the other hand, the relative mobility for a strong foam system is significantly lower and hence, will be the pressure amplitude. In the case of a strong foam system, the mobility reduction is very severe and the magnitude of the pressure pulse at the observation well will be very large. These results suggest that it might be possible to distinguish various foam types based on observed pressure response. Obviously, a base CO_2 injection scenario (no foam case) would be very useful.

As mentioned before, the time-lag is function of the system storativity which depends on the compressibility of the system. To examine this effect, we estimated the total system compressibility assuming the following parameters:

Table 3. Rock and Fluid Properties for compressibility calculations.

Pressure (MPa)	27.6
Temperature (deg C)	126.7
Rock Compressibility (1/Pa)	5.80E-10
Water Compressibility (1/Pa)	4.4E-10
Oil Compressibility (1/Pa)	1.5E-09
CO_2 Compressibility (1/Pa)	3.3E-08
Foam Compressibility (1/Pa)	2.7E-08

For foam compressibility, we scaled down the CO_2 compressibility by a factor of 0.8 which is an assumption and should be validated. Based on these numbers, we total compressibility for various systems is calculated as follows:

Table 4. Total compressibility for different foam systems.

	Strong Foam	**Intermediate Foam**	**Weak Foam**
Water Saturation	0.10	0.10	0.63
CO_2 Saturation	0.90	0.90	0.38
Total Compressibility (1/Pa)	2.46E-08	2.48E-08	1.09E-08
Compressibility Ratio (Foam/Oil)	12	12	5
Compressibility Ratio (Foam/Water)	24	24	11

As expected, the compressibility for the foam bank is significantly higher than that of the displaced fluids (water/oil). Hence, time-lag response would be similar to that observed during pure CO_2 injections.

3.2 Forward Pressure Modelling

In this section, we examine the fluid compressibility effects. As usual, the pressure equations are obtained from the general mass balance and phase equilibrium. These nonlinear equations are typically solved numerically for phase pressures and saturations. However, the problem can be simplified further by assuming a slight compressibility for the supercritical CO_2 phase. In this case, the fluid density changes with pressure as follows:

$$\rho = \rho_0 \, e^{c\,(P-P0)} \tag{22}$$

The slightly compressible assumption for CO_2 phase should be considered as a rough approximation since it assumes a first-contact miscibility with reservoir pressures above the supercritical pressure (1070 psi at 88 deg F). The following table shows a comparison of CO_2 density obtained using the slightly compressible approximation and compares them with the actual density values (at 260 deg F).

Table 5. CO_2 Density Modeling above the Critical Pressure

P (psi)	ρ_{co2} (lb/ft3)	ρ_{co2} predicted	% Error
3000	24.97		
3500	29.22	28.0	4%
4000	32.71	31.4	4%
4500	35.74	35.3	1%

In this table, the CO_2 densities were calculated using CO_2 compressibility (c) of 2.30E-04 psi^{-1}.

With the slightly compressible assumption and ignoring capillarity and gravity, the pressure equation can be written as follows:

$$\phi\, c_t \frac{\partial P}{\partial t} - \nabla K\, \lambda_t\, \nabla P = q \qquad (23)$$

where:

c_t is the total compressibility.

λ_t is the total mobility.

K is the permeability.

Φ is the porosity.

q is the source term representing production and injection.

Please note that, in the equation above, total compressibility (c_t) and the total mobility (λ_t) are both functions of space and time.

4. CO_2 Foam Resistivity Characteristics and Modeling

In this section, a method is presented to relate foam resistivity data to foam density as well as validation of this through laboratory measurements. We will also calculate expected resistivity profiles for various foam scenarios, including CO_2 foam injection with oil present. These results show that resistivity response will be quite similar to those obtained using the foam in absence of oil simulations and will provide a distinct jump at the foam front. On the other hand, the same is not true for non-ideal displacements. In this case, the resistivity profile extends into the miscible CO_2 bank. Hence, by itself, Resistivity measurements may not be enough to distinguish these multiple fluid banks. However, for these non-ideal displacement cases, as shown, the mobility contrast is very large and, as discussed in the next chapter, complimentary crosswell pressure measurements could provide key reservoir data for quantification of these largely contrasting mobility banks.

4.1 CO_2 Foam Resistivity Characteristics

Typically, nonionic surfactants are dissolved in CO_2 phase and the foam generation occurs in situ when injected CO_2 plus surfactant meets the formation brine. CO_2 is highly resistive whereas the thin water film could be conductive (depending on the salinity of the in-situ reservoir fluid). During foam injection, these films enhance the electrical conductivity. With growing bubble size, these conduits become less effective and overall, the resistivity of the foam system increases.

In the following section, we define the foam conductivity with foam population or texture. For this purpose, we will utilize the following definitions:

K_b is the bulk foam conductivity

X_f represents the foam population density or (foam texture)

D is the volumetric liquid fraction or = $(1-X_f)$

$c1$ is a constant

S_{co2}^{f} is CO_2 saturation with foam

σ_s is conductivity of the thin film around bubbles

Assuming uniform hexagonal prism shape foams, the foam conductivity σ_f can be obtained using the following relationship proposed by Lemlich, R. (1985):

$$Kb = \frac{D}{3} \tag{24}$$

The same relationship can also be utilized for CO_2 foam displacements as follows:

$$Kb = \frac{conductivity\ of\ dispersion}{conductivity\ of\ continous\ phase} = \frac{\sigma_f}{\sigma_s} \tag{25}$$

Using these relationships, we obtain:

$$\sigma_f = \frac{1}{3}\sigma_s\ (1 - X_f) \tag{26}$$

or another expression would be:

$$\sigma_f = c1 * \sigma_s * (1\text{-}S_{co2}^{f}) \tag{27}$$

Assuming, σ_s = 1.0 S/m and X_f= 0.90 (foam quality), we obtain the following values for foam conductivity:

σ_f = 0.033 S/m (foam conductivity) or R_f = 30 ohm.m (foam resistivity)

These results suggest that foam conductivity will be order of (1 to 2) higher compared to that of CO_2 phase only. We also propose to scale the foam conductivity with foam density as follows:

$$\sigma_f = c1\ \ \sigma_s\ (1\text{-}S_{co2}^{f})\ (\frac{n_f}{n_{fmax}}) \tag{28}$$

where: n_{fmax} is the maximum population density.

For the computation of total system (rock and fluid) conductivity, the mixing (or the Archie's) law is used. For a CO_2-Water system, lab results show that the Archie's equation will provide a reasonable approximation (Bergmann, Peter, et al. 2013).

Assuming a CO_2 Foam - Water system and utilizing the mixing law, the total system conductivity can be calculated as follows:

$$\sigma = \phi^2 [S_{co2}^f \sigma_f^{1/2} + S_w \sigma_w^{1/2}] \quad (29)$$

Recently, resistivity and pressure measurements were made at high temperature and pressure using carbonate cores (Haroun, M. et al. 2017). During these experiments, sharp increases in both resistivity and pressure were observed with the formation of CO_2-Foam. These experimental results are in line with the theoretical results provided in here.

It should be noted that Archie's Law is a fundamental relationship used to describe the electrical conductivity (or resistivity) of porous media, particularly in the field of petrophysics. It is widely used in the petroleum industry for reservoir characterization, saturation estimation, and fluid typing and therefore, we will review some of its limitations here.

Archie's Law is based on several simplifying assumptions that may not hold true in all situations. It assumes that the porous medium is homogenous, isotropic, and electrically conductive. Archie's Law does not also account for situations where multiple immiscible fluids are present, such as oil, gas, and water. Archie's Law is most accurate for rocks with moderate to high porosity. Finally, Archie's Law assumes that the electrical resistivity is primarily controlled by fluid conductivity which may not be true for some cases. These effects need to be considered and corrected for accurate interpretations. Therefore, it is important to use Archie's (or Mixing) Law with caution and together with other petrophysical data and measurements to account for these limitations.

4.2 CO_2 Foam Resistivity Modelling - PBE Solution

Using the simulated Saturations as well as the foam densities, we calculated the estimated resistivity (along with relative mobility) distributions. For these calculations, we used the following bulk conductivity values for different phases:

Table 6. Bulk Conductivity for Resistivity Simulations

σ_w	5.00	S/m
σ_{CO2}	0.001	S/m
σ_f	0.100	S/m
σ_{oil}	0.001	S/m

The figure below shows the resistivity profile from one dimensional CO_2 Foam flood assuming a moderately conductive water scenario. The resistivity profile has been calculated using the simulated foam population from the foam simulator as well as the CO_2 Foam Resistivity Model. The foam simulator has a high-resolution grid with more than 100 subdivisions.

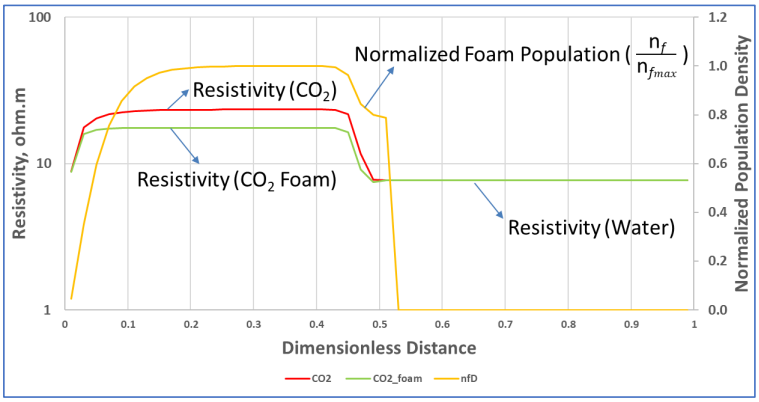

Figure 17. Calculated Resistivity Profile during CO_2-Foam Injection (PBE Solution)

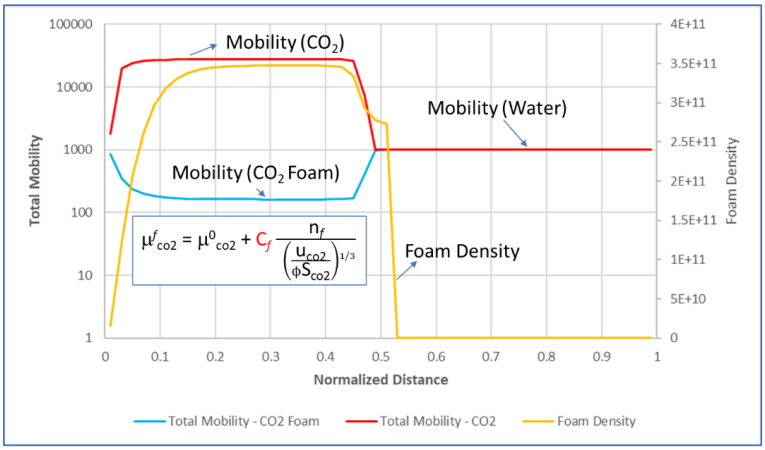

Figure 18. Combined Resistivity and Mobility Profile during CO_2-Foam Injection (PBE Solution)

4.3 CO_2 Foam Displacement with Oil Present

The resistivity calculations were also made for CO_2-Foam displacement with Oil. For this case, the solution was obtained using the analytical solution approach provided by Ashoori et al. (2010). In this solution, the mobility effects were calculated using the steady-state parameters provided in Appendix B. The resistivity calculations were done assuming similar bulk conductivities as given in Table 6. The figures below show the calculated resistivity profiles for both ideal as well as non-ideal foam displacements:

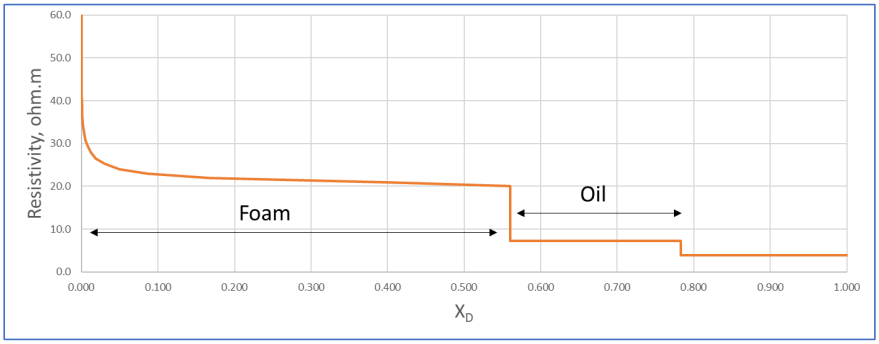

Figure 19. Resistivity profile during Ideal CO_2-Foam Displacement

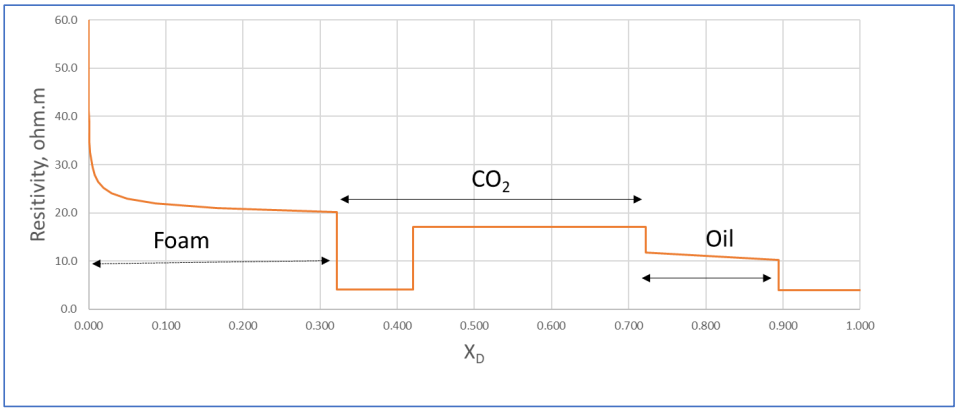

Figure 20. Resistivity profile during non-ideal CO_2-Foam Displacement

The figures below show the mobility distribution along with the resistivity profiles.

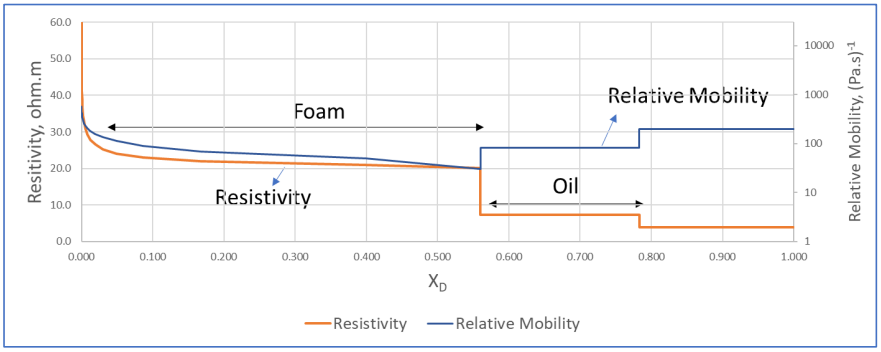

Figure 21. Combined Resistivity and Mobility Profile during CO_2-Foam Injection (Analytical Solution – Ideal Displacement)

As seen from these figures, resistivity profile during ideal displacement is similar to that of PBE simulations shown earlier. In both cases, a distinctive resistivity response at the foam front is observed. On the other hand, the same is not true for the non-ideal displacement. In this case, the resistivity profile, as shown in Figures below, is a staircase and extends into the Miscible CO_2 bank.

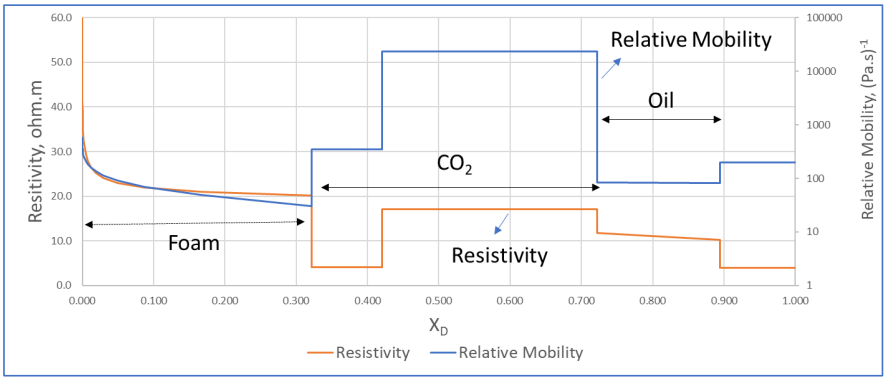

Figure 22. Combined Resistivity and Mobility Profile during CO_2-Foam Injection (Analytical Solution – Non-Ideal Displacement)

5. Field Pilot

In this section, we present results from a recent CO_2 foam pilot study in a heterogeneous carbonate field in Permian Basin, USA. The pilot was part of an integrated and novel workflow involving laboratory measurements, reservoir modelling and monitoring. Using the recorded bottom-hole pressure data from this CO_2 foam pilot, we demonstrate how transient pressures could be used to monitor CO_2 foam development inside the reservoir. The injection pressure was used to evaluate the development of foam during various foam injection cycles. A high-resolution radial simulator was utilized to study the effect of foam on well injectivity, as well as on CO_2 mobility in the reservoir during the surfactant-alternating gas (SAG) process.

The objectives of this study were as follows:

Evaluate whether foam has been generated based upon comparisons with measured BHP and injection rates; tune foam model to observed pressures during pilot if foam has formed; and determine the foam propagation distance/rate if foam has formed.

The CO_2 foam field pilot is in East Seminole Field in the Permian Basin of west Texas. The field produces from a heterogeneous cyclical carbonate in the San Andres formation. In this field, the oil recovery using CO_2 injection has been poor due to reservoir heterogeneity and the unfavourable mobility ratio between the injected CO_2 and in-situ reservoir fluids.

An inverted 40 acre 5-spot was selected to pilot to test the designed foam strategy at reservoir conditions. The pilot included a central injection well, and four surrounding producers. The main features of this pilot pattern were as follows: short well distances, rapid CO_2 breakthrough, and high CO_2-oil-ratios (or GOR) at the producing wells. The figure below shows the pilot pattern:

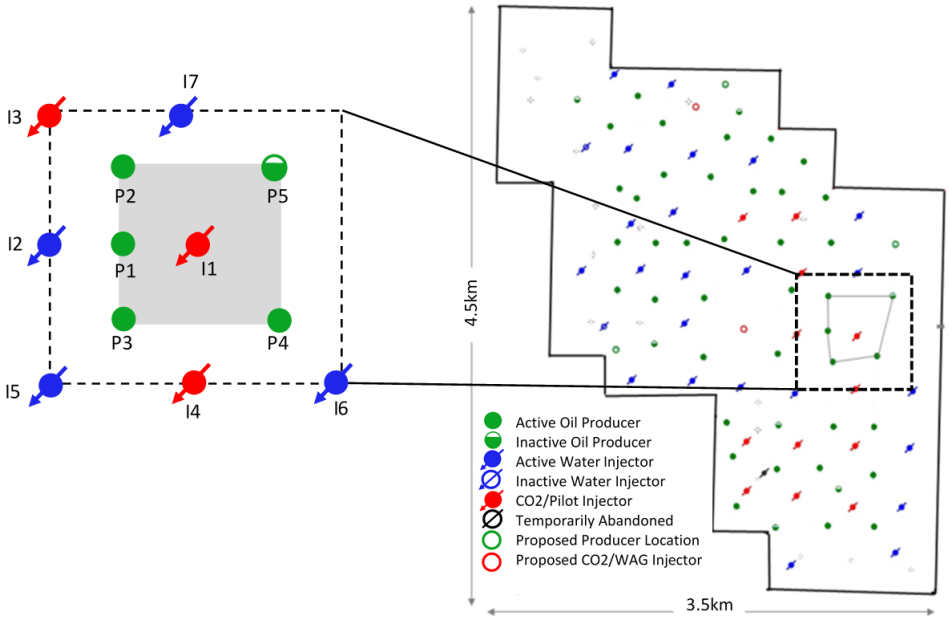

Figure 23. Pilot pattern (shaded area) and surrounding wells in East Seminole Field. The pilot injection well was I1 and the monitored producers were P1 through P4.

Two production wells, P1 and P4, were the focus of the baseline data collection and pilot monitoring because they experienced the most rapid CO_2 breakthrough time from tertiary CO_2 injection. The reservoir interval has an average permeability of 13 mD, pay thickness of 110 ft, and consists of six flow zones separated by impermeable flow barriers. Composite logs from the pilot injection well indicated a 10 ft thick high permeability streak of 200 mD. Historical injection profiles showed that this zone has been taking most of the injected CO_2. Therefore, this high permeability zone was targeted since foam can form in high permeability streaks and diverting flow to unswept regions of the reservoir with lower permeabilities. The reservoir and fluid properties are shown in the table below:

Table 7. Reservoir and fluid properties of the San Andres unit in East Seminole Field.

Reservoir Characteristic	**Value**
Depth	5200 ft
Permeability	1 to 300 md (average: 13 md)
Porosity	3 to 28% (average: 12%)
Pay Thickness	110 ft
Reservoir pressure (initial)	2500 psig
Reservoir pressure (current)	3400 psig
Fracture pressure	3900 psig
Reservoir Temperature	104ºF
Oil gravity	31 ºAPI
Formation brine salinity	70,000 ppm

5.1 Foam Formulation

A laboratory program was conducted to determine the optimal foam formulation before the field test. This included surfactant-screening studies, evaluation of the optimal foam quality (gas fraction), and quantification of CO_2 EOR and CO_2 storage potential of the optimized foam formulation at the core-scale. The laboratory program included surfactant-screening studies (Jian et al. 2016) as well as simulation studies (Alcorn et al. 2019).

A nonionic water-soluble surfactant was selected for the pilot test based on low adsorption characteristics. The effect of high temperatures was evaluated for the selected nonionic surfactant is known to degrade at high temperatures under aerobic conditions. An oxygen scavenger was used to prevent surfactant degradation at elevated temperatures. A scale inhibitor compatible with the selected surfactant was used. A stable foam was generated when the oxygen scavenger and scale inhibitor was used in reservoir brine with surfactant.

5.2 Foam Parameters

Two water components were used to model foam behaviour: one for surfactant solution and one for only water. The base-case foam parameters were derived from laboratory foam quality and rate scans and fit to the empirical local-equilibrium foam model by curve fitting regression (Rognmo et al. 2019; Sharma et al. 2017). Figure below shows the foam quality and rate scan used to derive the model parameters.

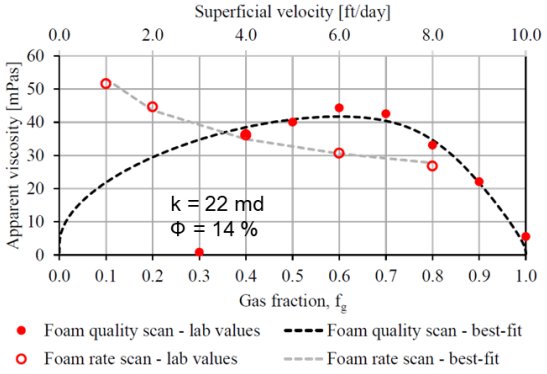

Figure 24. Laboratory foam characteristics (from Rognmo et al. 2019). It shows apparent viscosity variations as a function of gas fraction as well as velocity. The model fits to the laboratory measurements which are shown as symbols in this graph.

5.3 Injection Strategy

There are several strategies to generate foam in porous media. These include co-injection of gas (CO_2)/surfactant or surfactant alternating gas (CO_2) injection (the SAG

method). In co-injection process, the gas (CO_2) and the surfactant solution are simultaneously injected, and foam is formed in-situ. In the SAG method, surfactant and CO_2 are injected in alternating slugs. In low permeability reservoirs, SAG injection may be preferred due to increased gas injectivity. Additionally, with the use of SAG method, the contact between CO_2 and water is minimized which may reduce corrosion in surface facilities and piping (Haroun et al. 2017).

In the Seminole CO_2 foam pilot, a rapid surfactant-alternating-gas (SAG) injection strategy with 10 days of surfactant solution followed by 20 days of CO_2 Injection was used to generate foam in-situ for in-depth mobility control. This injection strategy and the controlling parameters (durations) were designed to minimize any injectivity restrictions and maximize the chance of success.

Before the pilot, the reservoir pressure was higher than the initial pressure by around 900 psi (close to 3400 psi) due to the injection of produced water. Due to foam development injection bottom hole pressure (BHP) can suddenly increase and exceed the formation fracture pressure (around 3900 psi). Therefore, the injection strategy was designed to mitigate injectivity losses and the risk of fracturing the formation. For this reason, the injection rates (during the SAG cycles) were reduced by half (from historical injection rates) to minimize the risk of fracturing. In addition, the injection strategy targeted a 70% foam quality, as suggested by the laboratory studies.

5.4 Surfactant Delivery

A field injection unit was designed to meet the requirements for surfactant delivery, mixing, and storing. To ensure the success of the pilot test, it was important to keep the injected foam formulation consistent at each cycle. A methodology was established to effectively validate foam formulation consistency in the field.

A refractometer was used to measure surfactant concentration in the holding tank and in the final dilution line. A correlation was established to convert the refractive index (RI) reading to surfactant concentration in weight percent (wt%). Surfactant solutions with known concentrations were first measured and used to calibrate the readings.

Surfactant samples were collected for measurement several days prior to injection and every day during the 10-day surfactant slugs. The method proved to be effective in measuring and validating the foam formulation in the field.

5.5 Reservoir Monitoring

The injection bottom hole pressures (BHP) and temperatures were monitored by mounting a downhole pressure gauge (DHPG) in the pilot injection well. The gauge was installed two weeks before the start of the pilot and pulled every other month during the pilot to download the pressure and temperature data. The monitoring program also included repeat injection profiles, tracer tests and three-phase production rates. Produced fluids were also collected once a week for chemical analysis to determine surfactant breakthrough time.

Figure below shows injection rates of CO_2 (red curve), surfactant solution (green curve), water (blue curve) and the measured BHP (black curve) at the injector well for all SAG and WAG cycles implemented during this pilot.

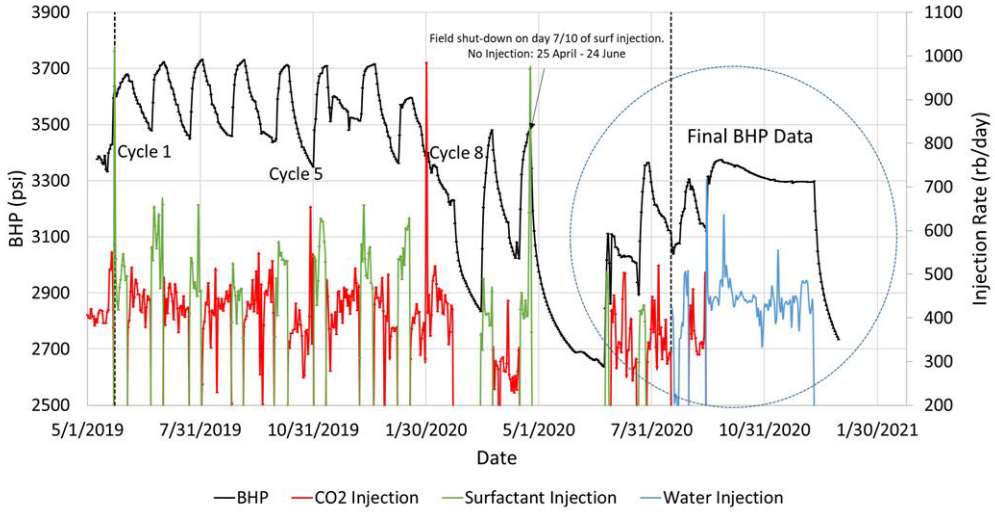

Figure 25. Plot showing the Injection History along with Measured Bottom Hole Pressures during SAG and WAG Cycles.

Injection rates during the pilot were 520 rb/day and 470 rb/day for surfactant solution and CO_2, respectively. The volumetric ratio of injected CO_2 relative to the total volume of CO_2 and surfactant injected was used to evaluate injected foam quality per cycle. The aim was to inject foam at 70% quality (0.70 gas fraction) per cycle as determined in the laboratory studies. The foam qualities ranged from 61% to 71%, which was within the designed target.

At the end of SAG Cycles, a WAG Injection was carried out for comparison purposes. The 'Final' Period is shown in the figure below:

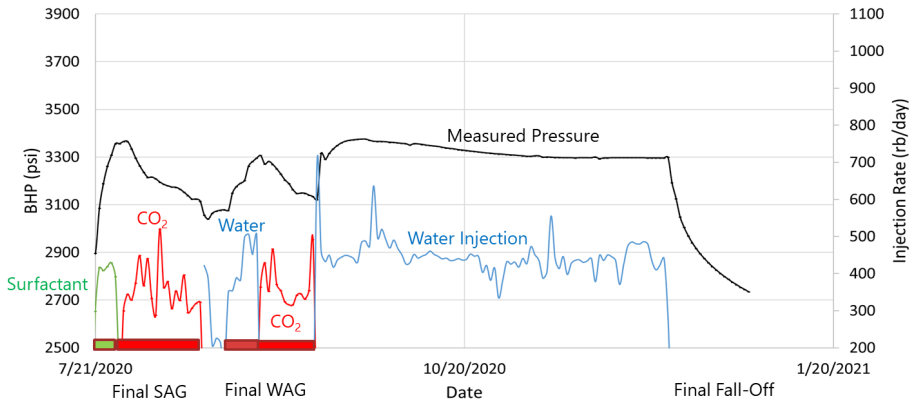

Figure 26. Plot showing the Injection History along with Measured Bottom Hole Pressures during the Final SAG/WAG and Fall-Off Periods.

5.6 Analysis of Pressure Data

The analysis of pressure measurements was carried out using the changes (instead of the absolute pressures) for each SAG cycle. Differential pressures (dP) and temperatures (dT) were calculated by subtracting the absolute values from the last stabilized pressure and temperature reading before each injection cycle, a technique widely used in transient pressure analysis. Similarly, delta t (dt) refers to differential time from the start of a particular injection cycle. Figure below shows the dP (and dT) through time for the first five SAG cycles and the final SAG cycle.

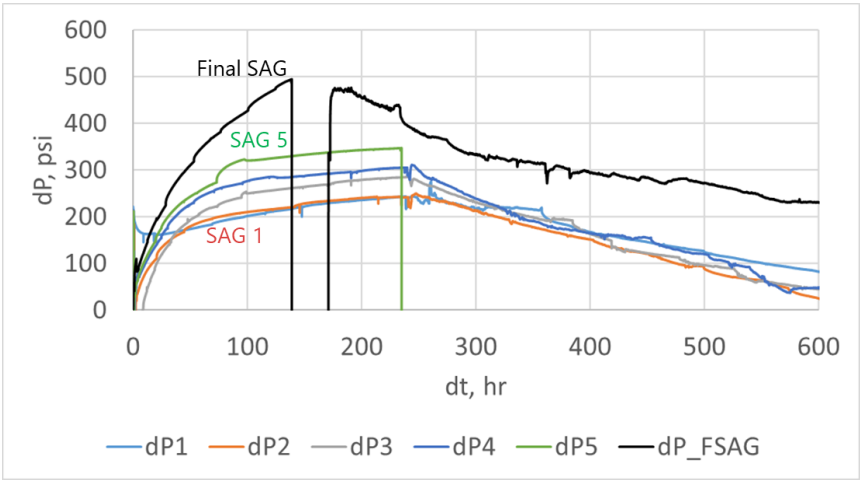

Figure 27. Transient Pressure for the first five SAG cycles and the final SAG cycle. dP1 corresponds to slug 1, dP2 to slug 2, and so on.

Differential pressures (*dP*) increased for each surfactant cycle until the last SAG cycle, which suggests, as expected, a (reduced) mobility bank developing further into the reservoir.

5.7 Foam Model

In this section, the effect of foam was modelled using the local equilibrium approach which implicitly represent the effect of bubble size by introducing factors for reducing gas mobility by foam as a function of water saturation, oil saturation, surfactant concentration, and shear thinning due to the flow rate. It should be noted that local equilibrium models assume that foam is present anywhere gas and present, along with an adequate surfactant concentration.

The decrease in gas mobility during foam floods is accounted for in local equilibrium models by scaling the gas relative permeability for no-foam floods (k_{rg}^{nf}) by a mobility reduction factor (FM), whereas the water relative permeabilities remain unchanged.

$$k_{rg}^{f} = k_{rg}^{nf} \times FM \tag{16}$$

The effect of water saturation, shear rate, surfactant concentration and oil saturation (Farajzadeh et al. 2012) on mobility reduction factor was studied, given by the expression:

$$FM = \frac{1}{1 + fmmmob \times F_{water} \times F_{shear} \times F_{oil} \times F_{surf}} \quad (17)$$

$fmmmob$ refers to the maximum gas mobility reduction that can be achieved. F_{water}, F_{shear}, F_{oil} and F_{surf} capture the water saturation, shear rate, oil saturation and surfactant concentration dependence, all lying in the range of 0 to 1 (Equation 3 through 6). The capillary number N_{ca} represents the relative effect of viscous and capillary forces.

$$F_{water} = 0.5 + \frac{arctan[epdry(S_w - fmdry)]}{\pi} \quad (18)$$

$$F_{shear} = \begin{cases} \left(\frac{fmcap}{N_{ca}}\right)^{epcap} & if\ N_{ca} > fmcap \\ 1 & otherwise \end{cases} \quad (19)$$

$$F_{surf} = \left(\frac{Surfactant\ concentration}{fmsurf}\right)^{epsurf} \quad (20)$$

$$F_{oil} = \left(\frac{fmoil - So}{fmoil}\right)^{epoil} \quad (21)$$

Two water components were used to model foam behavior: one for surfactant solution and one for only water.

5.8 Simulation Model

A radial simulation model was used in this study. A workflow was developed to history-match the cumulative oil production and water-cut in the sector model. A high-resolution two-dimensional radial flow model (r-z) was used to simulate the high injection rates around the wellbore and to capture the main (vertical) heterogeneity in this reservoir. The model was based upon a validated sector-level model of the pilot

pattern and surrounding producers. The base sector model was calibrated to 40 years of waterflood and over 4 years of CO_2 injection data, before the pilot study. The simulation model included the porosity and permeability distribution from a validated sector-scale model of the pilot pattern and surrounding producers. The radial flow model was used to examine the impact of foam and/or relative permeability on injectivity and mobility reduction when switching between surfactant solution and CO_2 in a SAG process.

The model included one injector (I1) to simulate all the SAG cycles as well the final WAG cycle and the two shut-in periods. The grid contained 28 layers, which were refined from the base sector model. Radial grid extended to 700 ft from the injector and the grid sizes increased logarithmically from the injector. Layers and perforations were from the history-matched (HM) sector model (Sharma, M. 2017). The model includes historical water and CO_2 injection before pilot.

5.9 History Matching

The radial simulation model was initially run using the base-case foam parameters. Table below shows these parameters:

Table 8. Base Case Foam Parameters

Foam Parameter	**Value**
fmmob	192
fmdry	0.40
epdry	84
fmcap	9.0e-07
epcap	0.59

Where:

- FMMOB: The reference mobility reduction factor.
- FMDRY: The limiting water saturation below which the foam is no longer effective.
- EPDRY: A weighting factor which controls the sharpness in the change of mobility.
- FOAMSO: The maximum oil saturation above which foam is no longer effective.
-

Due to uncertainty in foam model parameters derived from laboratory data, sensitivity runs were set-up to first test key foam model parameters. Table below shows the parameter ranges for the sensitivity study.

Table 9. Foam Parameters for Sensitivity Simulations.

Simulation Run	**FMMOB**	**FMDRY**	**EPDRY**	**FOAMFSO**
Base Case	192	0.4	84	0.28
S1	19.2			
S2	1.9			
S3		0.45		
S4		0.35		
S5			42	
S6			168	
S7				0.18
S8				0.38

Transient data was used to compare the model pressure response with the measured ones during all Surfactant and CO_2 injection periods. This comparison for the final for the final SAG cycle is shown in the figure below.

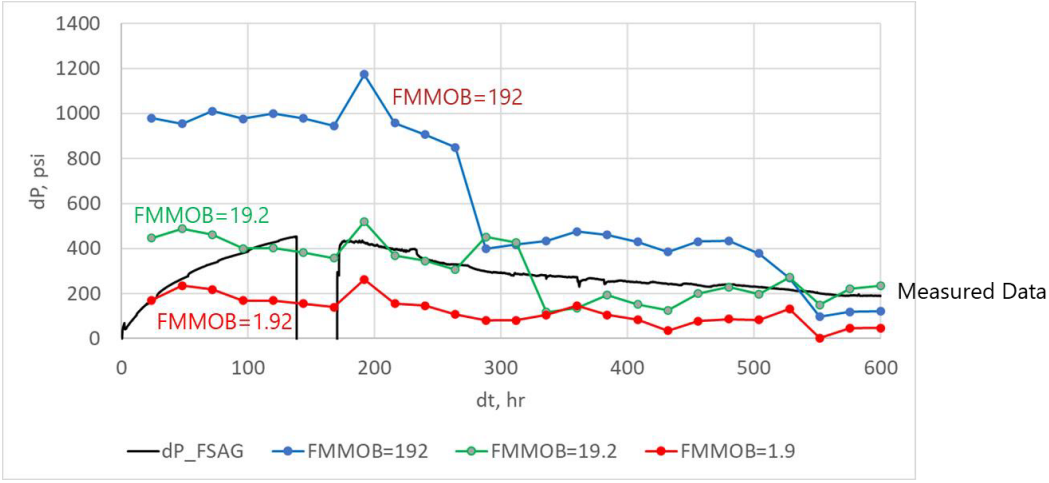

Figure 28. Simulated transient pressures CO_2 Injection during final SAG Cycle with different foam strength parameters.

Similar comparisons were made for the final WAG cycle which followed the final SAG Cycle. Figure below shows the simulated results versus the measured response during the final WAG period. As seen from this match, the simulated case with a lower FMMOB value (red curve) followed the measured response more closely than the cases with higher mobility reduction (green and blue curves).

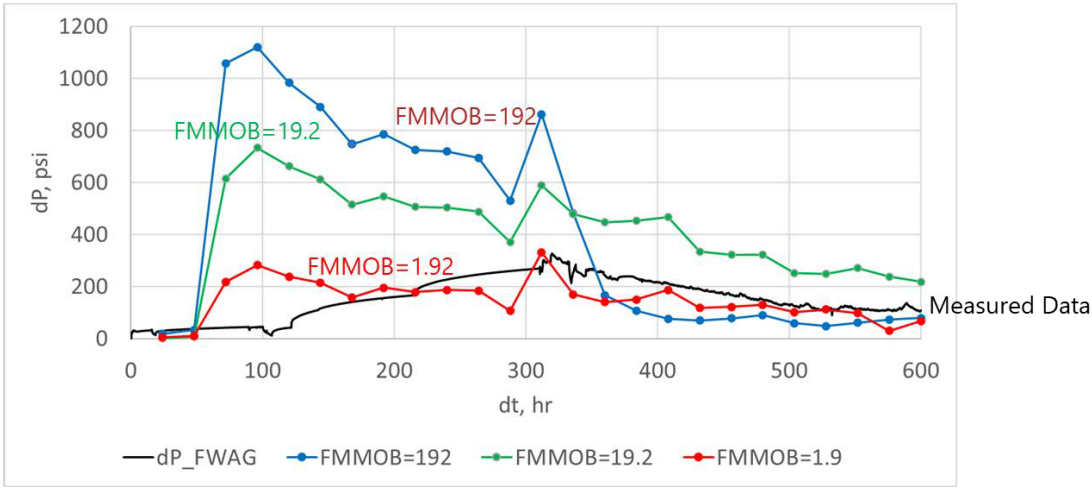

Figure 29. Simulated transient pressures during the Final WAG cycle with different foam strength parameters.

The analysis of the two shut-in (Fall-Off) periods were made separately. Figure below shows the comparison between the intermediate (after the 8th SAG Cycle) Fall Off period and the final Fall Off period. This comparison shows an anomalous pressure increase during the final Fall-Off period.

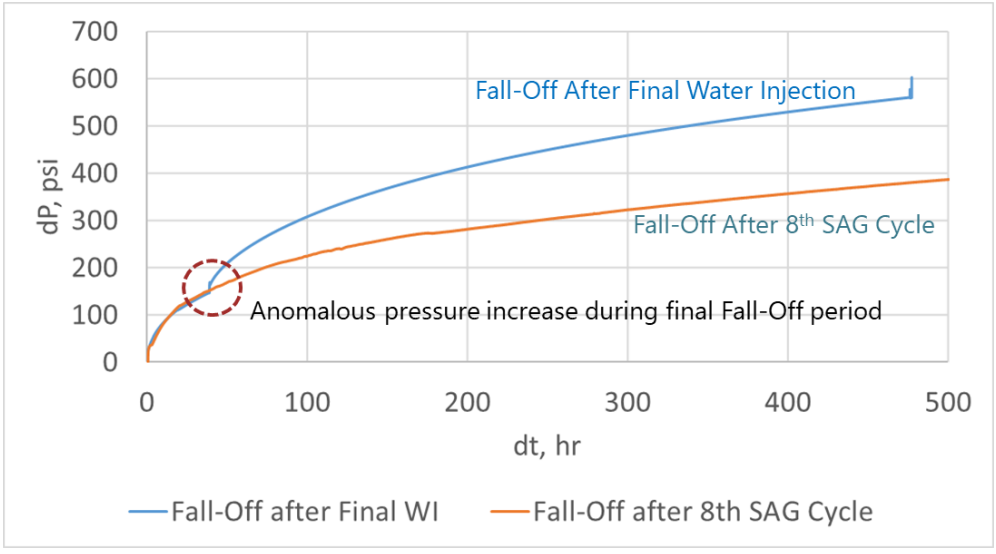

Figure 30. Comparison of the transient pressure response between the Intermediate and Final Fall-Off periods.

A comparison of the Final Fall-Off period was also made, and the figure below shows these results.

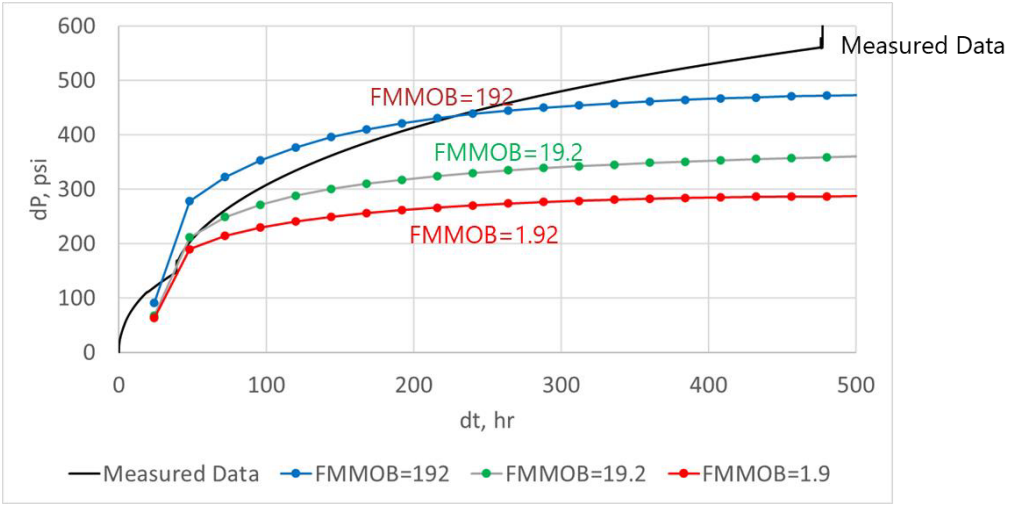

Figure 31. Simulated transient pressures during the Final Fall-Off period with different foam strength parameters.

5.10 Comparison of Final SAG and WAG Cycles

The figure below shows a comparison of delta pressures (dP) during the final SAG and WAG cycles. As can be seen, delta pressures during the Final SAG period are higher than the pressures observed during the final WAG (post pilot test) which indicates lower mobility during the SAG Cycles (and hence foam formation).

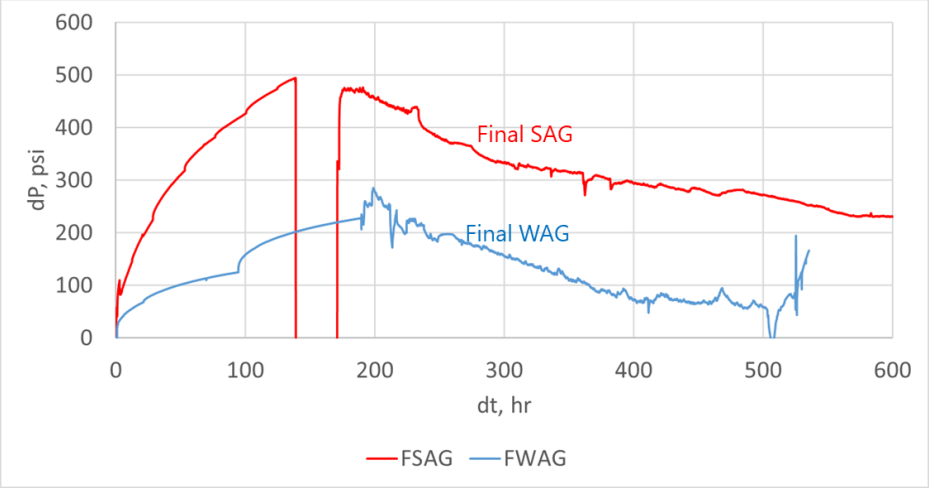

Figure 32. Comparison of the transient pressure response between the Final SAG and WAG Cycles.

5.11 Derivative Analysis

Pressure derivative is commonly used in Petroleum Engineering to identify reservoir flow regimes (such as radial, or linear flow). Diagnostic lines are matched to various regions on log-log pressure and derivative plots, and the corresponding well and reservoir parameters are calculated based on the assumed flow regime (Bourdet et al. 1989).

The pressure derivative is defined as follows:

$$\text{Pressure Derivative} = \Delta t \, \frac{\partial \Delta P}{\partial \Delta t} \tag{30}$$

For pilot test, the pressure derivative analysis is conducted for the fall-off period since this is only period where the rate is kept constant. The figure below shows a log-log plot of delta pressures (dP) and pressure derivative during the final fall-off period. Please note that no smoothing was performed on this derivative plot and the pressure derivative is relatively noisy due to (low) resolution of the downhole pressure gauge.

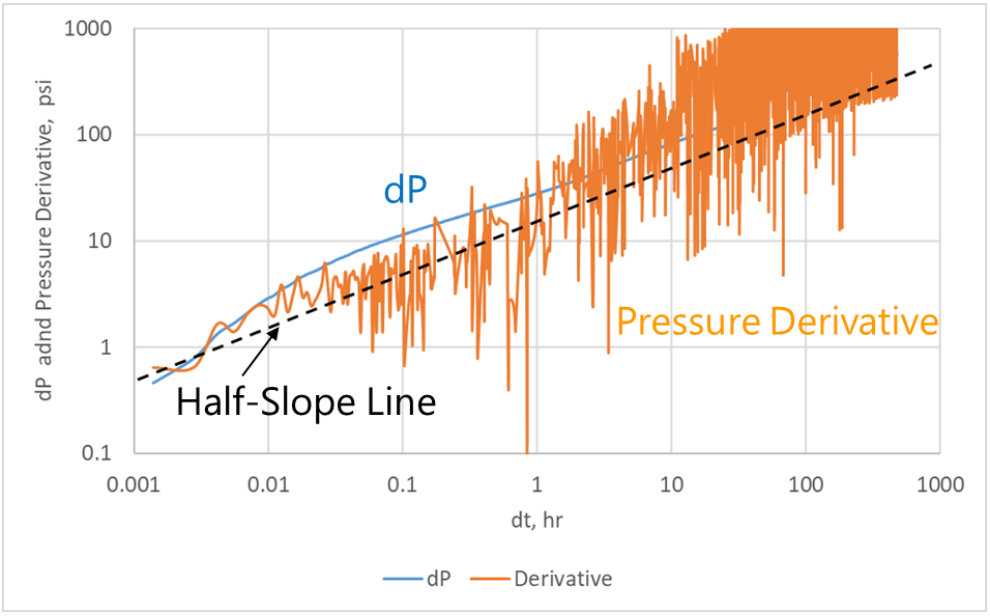

Figure 33. Pressure Derivative Plot for the final Fall-Off Period.

İn the above figure, we also plotted the diagnostic half slope (1/2) line to compare with the actual derivative data. Linear flow is recognized as a positive half (1/2) slope in the pressure derivative on the log-log diagnostic plot. Its presence enables determination of the fracture half-length or the channel or reservoir width if reservoir permeability can be determined independently. In this case, the pressure derivative analysis suggests a half-slope trend on the log-log pressure and derivative plot which suggests linear flow in the reservoir.

5.12 Production Analysis

The effectiveness of foam in improving overall recovery can also be determined by comparing the production response before and after surfactant injection. To do this, a reliable baseline production was first established. This period covered approximately 1.5 years prior to the start of the pilot (from January 2018 to May 2019) where there was consistent data and minimal operational disruptions in the pattern. Trend curves were fitted and extended for all four pilot pattern production wells over time to provide a projection of the baseline performance had there been no foam implemented in the

pattern (Figure below, black dashed line). The observed oil production data from all four producers in the pattern was then used to get the cumulative response realized due to foam implementation in the pilot pattern. Figure below shows cumulative oil recovered as a function of pore volume injected for the pilot pattern.

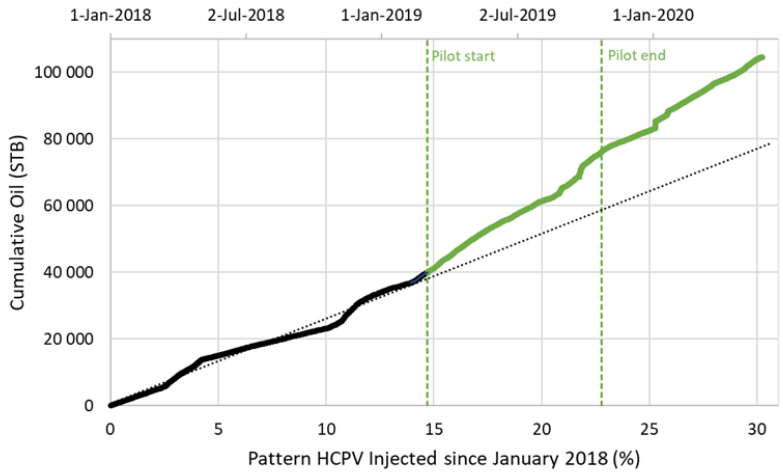

Figure 34. Cumulative oil production from the pilot production wells (P-1, P-2, P-3, and P-4) as a function of hydrocarbon pore volume (HCPV) injected for the baseline period (black curve) and the during the pilot (green curve). The black dashed line shows the projected cumulative oil recovery from the baseline period with no foam injection.

This analysis shows a positive slope change in the cumulative oil recovery shortly after starting foam injection (green curve). A conservative estimate puts the cumulative incremental oil to more than 20,000 STB. This increase in production (compared to the baseline period) could also be related to well operations conducted during the pilot. Nonetheless, the implementation of the foam pilot increased oil recovery despite less pore volumes injected.

5.13 Injection Profiling

Foam was expected to block the high permeability steak, which carried majority of the injected fluids (water and CO_2) historically in this reservoir. Injection logging was deployed as part of the pilot monitoring program to determine any changes in injected intervals after foam generation. A slug of radioactive tracer was added to the injection fluid and several gamma ray logs were recorded at certain time intervals as part of injection logging. Figure below shows the results from these CO_2 and water injection logs from the baseline period, during the 7th SAG cycle and during the last SAG cycle.

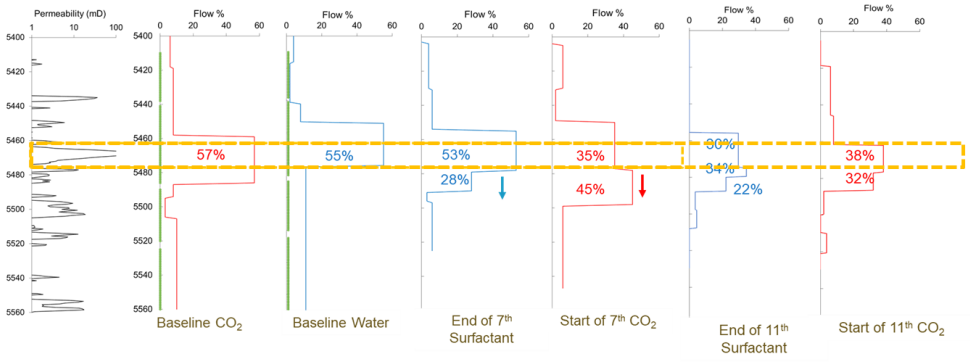

Figure 35. Injection profile logs for the pilot foam injector from before the pilot (baseline CO_2 and water) and for the 7th and 11th cycles of the pilot. Dashed box delineates a high permeability streak shown on the composite log at left.

The analysis of these profiles suggests potential blockage of the high permeability streak during foam generation and increased injection into adjacent reservoir intervals. This could be due to foam formation in the high permeability streak and diversion of the injected CO_2 to other reservoir intervals.

6. Conclusions and Future Perspectives

In this thesis we present resistivity and pressure monitoring possibilities during CO_2 foam injection displacements. Both theoretical foundation and practical applications are discussed. The main conclusions from this thesis are presented here followed by a discussion of continuing work and future perspectives.

Compared to conventional CO_2 injection, CO_2 foam can increase both oil recovery as well as the volume of CO_2 stored during carbon capture, utilization and storage (CCUS) processes. This has been demonstrated in field (and lab) conditions. Foam injection reduces CO_2 mobility which improves the CO_2 sweep efficiency. Reservoir monitoring is crucial for the application of foam (and CO_2 foam) in oil reservoirs where heterogeneity is involved. Our results suggest that combination of Pressure and Resistivity measurements in time-lapse mode could be deployed as an effective monitoring tool in field applications of the (CO_2) foam processes. The proposed method is novel as it could be employed to predict under-performing CO_2-foam floods as well as improve oil recovery and CO_2 storage.

We also utilized some of these methods during this field pilot research project on CO_2 foam monitoring. This CO_2 foam pilot was conducted in East Seminole Field, Permian Basin, west Texas where CO_2 foam was implemented to reduce CO_2 mobility to improve sweep efficiency, oil recovery, and CO_2 storage potential. A surfactant-alternating-gas (SAG) injection strategy was implemented, with 10 days of surfactant solution followed by 20 days of CO_2. The monitoring program included single, fall-off tests to measure injection pressure, and injection profiles to determine zones of injection. Injection BHP and temperature data was used to evaluate the pilot response during surfactant and CO_2 injection. The analysis was conducted by examining the differential pressure (dP) and differential temperature (dT) through time for all the SAG and WAG cycles. A high-resolution two-dimensional radial flow model was developed to history match the measured transient pressure data. This analysis has provided significant insight into injectivity reduction during SAG injection.

Key findings from this work are:

- Resistivity has been proven as a supplementary monitoring tool for foam experiments. The current study concentrated on proving that resistivity can be employed at laboratory scale as an effective technique to identify foam behavior in core flooding.
- Pressure measurements during steady-state foam flow give rise to an ill-posed estimation problem and that grouping of foam parameters is necessary. For most reservoir applications, pressure measurements alone will not adequately describe the transient foam effects.
- Based on our theoretical results we expect the foam conductivity to be order of (1 to 2) higher than that of CO_2 phase and significantly less than that of saline reservoir water.
- Assuming a reasonable conductive water in the reservoir, resistivity profiles during ideal CO_2 foam displacements should exhibit a distinctive character at the foam front.
- During non-ideal CO_2 foam displacements, resistivity measurements by itself may not be enough to differentiate foam and miscible CO_2 banks. However, for these non-ideal cases, the mobility contrast is very large and crosswell pressure measurements would be ideal to detect and quantify these largely contrasting mobility banks.
- Analysis of downhole pressure and temperature data showed that the temperature responses were quite similar during most SAG cycles. On the other hand, differential pressures consistently increased during periods of surfactant injection and decreased during the subsequent CO_2 injection periods. The pressure increase (buildup) during surfactant injection was due to a decrease in mobility, showing development of a mobility bank in the reservoir. Additionally, the comparison of pressure data between WAG and SAG cycles show that the delta pressure is higher with SAG injection which suggest reduced mobility due to foam development.
- Based on the detailed comparisons and the transient analysis of measured bottomhole pressure data, it could be concluded that foam was generated downhole. However, history matched foam model parameters are significantly

different from the expected values based on laboratory studies. Sensitivity studies show that the foam mobility reduction factor (FMMOB) is the most dominant parameter. Foam development in the field trial was weaker than expected.

- Production analysis during the reservoir experiment (pilot) indicated that the oil production in the pilot area increased by 30% during the pilot implementation. Injection profiles show that the injected fluids (CO_2, Surfactant and Water) were diverted from a high-permeability zone into adjacent unswept reservoir intervals. These results suggest improved sweep efficiency with foam development.
- The radial model proved to be useful to assess the reservoir foam strength during the CO_2 Foam pilot. While the pressure data alone may not be enough to describe the complex physics of in-situ foam generation, it is a powerful indicator of foam strength. In this pilot application case, it appears that the reservoir foam strength was weaker than that expected in the laboratory.
- Finally, field results suggest that the reservoir sweep efficiency and oil recovery could be improved by CO_2 foam injection. This is mainly due to CO_2 mobility reduction. Additionally, simulation results show that the volume of CO_2 stored will be increased by CO_2 foam utilization. Therefore, CO_2 foam injection can reduce the operational costs, improve CO_2 storage and result in more oil recovery. These effects can translate into additional benefits for industry operators who participate in combined CO_2 storage and CO_2 EOR in CCUS.

6.1 Future Perspectives

Monitoring the effectiveness of the foam during an CO_2-EOR field application is detrimental in high-salinity, high-pressure and high-temperature reservoirs with heterogeneity involved. This work demonstrated the use of conventional pressure measurements for characterizing foam strength. In addition, we recommend the deployment of distributed pressure sensors for time-lapse crosswell pressure measurements as well as resistivity surveys for saturation (CO_2, Foam and Water) monitoring. The use of nanoparticles for foam stability is an active area of research and

its effectiveness under real reservoir conditions should be investigated in well-designed field pilots.

7. Concluding Remarks/Lessons Learned

Describing and understanding pore, core, and field scale CO_2 foam data is essential for more accurate predictions of CO_2 foam behavior across length and time scales and advance the technology of CO_2 foam in heterogeneous reservoirs. In this research, we utilized CO_2-Foam experiments on cores and field pressure measurements to characterize the CO_2-Foam advancement during a field application. The following summarizes the lessons learned during these works.

7.1 Laboratory Lessons Learned

Further studies are needed to identify better ways to correlate quality of foam with resistivity measurements. These studies should be carried out for both water and oil cases.

7.2 Field Lessons Learned

Based on the history-matched model results, it could be said that foam has advanced in high permeability layers during the CO_2 pilot. However, considering the non-unique nature of estimating the foam parameters, the effect of other foam processes (foam propagation and its effectiveness) should be addressed directly by direct saturation measurements such as resistivity monitoring.

The pilot had elevated reservoir pressures due to the (over) injection of produced water in an offset pattern. The Minimum-Miscibility-Pressure (MMP) was far below these pressures. This excess pressure field trials should be avoided, if possible since it limits higher injection rates.

We had good evidence that proved the foam development in the pilot application (such as SAG vs WAG comparisons, increase in oil production). This pilot had a modest monitoring program, and the pilot design and operation should be taken to a higher level in future applications.

It is likely that more of the surfactant adsorbed to the rock surface in the field trial compared to the laboratory studies due to the presence of more minerals (clays) in the field compared to laboratory adsorption measurements on pure calcite and dolomite. In future pilots, the use of nanoparticles should be considered.

Abbreviations

CCUS	Carbon capture, utilization, and storage
EOR	Enhanced Oil Recovery
SAG	Surfactant Alternating Gas
WAG	Water Alternating Gas
MPZ	Main Producing Zone
ROZ	Residual Oil Zone
BT	Breakthrough
CT	Computed Tomography
TVD	Total Vertical Depth
Wt %	Weight Percent
SCAL	Special Core Analysis
RCA	Routine Core Analysis
PVT	Pressure Volume Temperature
MMP	Minimum Miscibility Pressure
GOR	Gas-Oil Ratio
MRF	Mobility Reduction Factor
PV	Pore Volume
PET	Positron Emission Tomography
MRI	Magnetic Resonance Imaging
OOIP	Original Oil in Place

Nomenclature

$a1$	a constant
C_c	a model parameter
C_c	a model parameter to represent foam coalescence.
C_f	a model parameter to represent effective foam viscosity.
C_g	a model parameter to represent foam generation.
C_{sa}	Mass of Surfactant adsorbed on the rock
C_{sg}	Mass Concentration of Surfactant in CO_2
C_{so}	Mass Concentration of Surfactant in CO_2 Residual Oil
C_{sw}	Mass Concentration of Surfactant in Water
$c1$	a constant in the proposed foam conductivity model
cP	Centipoise
C_{surf}	Surfactant concentration
C_{surf}	Surfactant concentration
D	Volumetric liquid fraction in the foam
d	Value of determinant to capture the conditioning of the parameter estimation problem
epcap	Foam model parameter in Fshear
epdry	Steady-state foam parameter to capture the slope near critical water saturation
epsurf	Foam model parameter in Fsurf
F_n	Objective function used to history match foam parameters.
f_{co2}	CO_2 phase fractional flow
f_g	Gas fraction or foam quality
FM	Mobility reduction factor (foam model)
fmcap	Foam model parameter in Fshear
fmdry	Factor in steady-state foam model to represent the critical water saturation
fmmob	Foam model, maximum gas mobility reduction factor
fmsurf	Foam model parameter in F_{surf}

F_{shear}	Shear rate effect on foam (foam model)
f_w	Water phase fractional flow
Fw	Factor to capture the effect of water saturation on foam mobility reduction
F_{water}	Water saturation effect on foam (foam model)
K_b	bulk foam conductivity (or σ_f)
k	Permeability
k^f_{rg}	Gas relative permeability with foam
k^{nf}_{rg}	Gas relative permeability with no foam
k_{rCO2}	Relative permeability to CO_2 phase
k_{rg},wi	Endpoint relative permeability of gas
$krgnf$	Gas relative permeability with no foam
k_{ro}	Relative permeability to oil phase
k_{rw}	Water phase relative permeability
k_{rw},gi	Endpoint relative permeability of water
m	a model parameter for transient foam generation
M	Measurement Matrix
mD	Millidarcy
MPa	Megapascal
$MRF_{CO2Foam}$	Mobility Reduction Factor by CO_2 foam
$Mscf$	Thousand standard cubic feet
$Mscf/day$	Thousand standard cubic feet per day
n	a model parameter for transient foam coalescence
n_f	Foam texture or density
n_{fmax}	Maximum foam density
$Psig$	Pound per square inch, gauge
R_{CO2}	Resistivity of the CO_2 phase
R_f	Resistivity of the foam
R_{film}	Resistivity of the film
R_w	Resistivity of water phase
r_c	Foam (lamella) destruction rate

r_g	Foam (lamella) generation rate
$r1$	a constant
rb/day	Reservoir barrels per day
$R_{f,CO2\ foam}$	Incremental oil recovery by CO_2 foam
$R_{f,tot}$	Total oil recovery
$R_{f,WF}$	Incremental oil recovery by waterflood
S	Sensitivity Matrix
S^*_w	Water saturation at the limiting capillary pressure, fraction
S_{co2}	CO_2 Saturation
S_g	Gas saturation
S_o	Oil saturation
S_{0M}	Residual saturation behind the CO_2 front,
S_{or}	Residual oil saturation
S_{orm}	Residual oil saturation to miscible flood
S_{orw}	Residual oil saturation to waterflood
S_w	Water saturation
S_{wi}	Irreducible water saturation
t	Time
u_{co2}	CO_2 volumetric flux or superficial velocity
u_{co2}	CO_2 volumetric flux or superficial velocity
u_t	Total velocity
u_t	Total volumetric flux or superficial velocity
u_w	Water volumetric flux or superficial velocity
vf	volumetric fraction of rock and fluids, fraction
v_s	Velocity of the foam front
v_w	Velocity of the miscible (CO_2) front
X	Vector defining the foam parameters.
X_D	Dimensionless distance
X_f	Foam Quality, fraction
∇p	Pressure gradient
∇p_w	Pressure gradient for the water phase

$\mu_{app,CO2}$	Apparent viscosity of CO_2
$\mu_{app,CO2foam}$	Apparent viscosity of CO_2 foam
${}^{0}API$	American Petroleum Institute gravity
$\mu_{co2}{}^{0}$	CO_2 viscosity in absence of foam
$\mu_{co2}{}^{f}$	Effective CO_2 viscosity in presence of foam
ϕ	Porosity
σ_{co2}	CO_2 conductivity (without foam)
$\sigma_{co2}{}^{f}$	CO_2 conductivity (with foam), S/m
σ_{f}	Foam conductivity
σ_{film}	Conductivity of the film
σ_{w}	Conductivity of the water phase

Bibliography

Abbaszadeh, M., Nia Korrani, A. K., Lopez-Salinas, J. L., Rodriguez-de La Garza, F., Villavicencio Pino, A., & Hirasaki, G. 2014. Experimentally-based empirical foam modeling. In SPE improved oil recovery symposium. OnePetro.

Abbaszadeh, M., Varavei, A., Garza, F. R., Pino, A. E., Salinas, J. L., Puerto, M. C., ... & Miller, C. A. 2018. Methodology for the Development of Laboratory–Based Comprehensive Foam Model for Use in the Reservoir Simulation of Enhanced Oil Recovery. SPE Reservoir Evaluation & Engineering, 21(02), 344-363.

Adebayo, A.R., et al., 2017. Measurements of electrical resistivity, NMR pore size and distribution, and x-ray CT-scan for performance evaluation of CO2 injection in carbonate rocks: A pilot study. International Journal of Greenhouse Gas Control.

Adkins, S.S., Chen, X., Chan, I., Torino, E., Nquyen, Q., Sanders, A. 2010. Morphology and Stability of CO2-in-Water Foams with Nonionic Hydrocarbon Surfactants. Langmuir, 26, no. 8, 5335-5348.

Agnihotri, A.K. and Lemlich, R., 1981. Electrical conductivity and the distribution of liquid in polyhedral foam. Journal of Colloid and Interface Science, 84(1), pp.42-46.

Alcorn, Z. P., Fredriksen, S. B., Sharma, M., Rognmo, A. U., Føyen, T. L., Fernø, M. A., & Graue, A. 2018. An Integrated CO2 Foam EOR Pilot Program with Combined CCUS in an Onshore Texas Heterogeneous Carbonate Field. Society of Petroleum Engineers. doi:10.2118/190204-MS

Alcorn, Z.P., Føyen T. Zhang L., Karakas, M., Biswal, S. L., Hirasaki, G., and Graue, A. 2019. CO2 Foam Field Pilot Design and Initial Results. SPE-200450-MS., SPE Improved Oil Recovery Conference 2020.

Alcorn, Z.P., Sharma, M., Fredriksen, S. B., Fernø, M.A., and Graue, A. 2019. An Integrated CO2 Foam EOR Pilot Program with Combined CCUS in an Onshore Texas Heterogeneous Carbonate Field. SPE Reservoir Evaluation and Engineering 22 (04): 1449-1466. https://doi.org/10.2118/190204-PA.

Alcorn, Z.P.; Føyen, T.; Zhang, L.; Karakas, M.; Biswal, S.L.; Hirasaki, G.; Graue, A. CO2 Foam Field Pilot Design and Initial Results; 2020. SPE-200450-MS. In Proceedings of the SPE Improved Oil Recovery Conference 2020, Virtual.

Altundas, Y. Bilgin, et al. 2015. Feasibility of crosswell seismic monitoring in CO2-EOR using an integrated compositional workflow. SEG Technical Program Expanded Abstracts 2015. Society of Exploration Geophysicists, 2015. 5472-5476.

Ashoori, E., van der Heijden, T., & Rossen, W., 2010. Fractional-Flow Theory of Foam Displacements With Oil. Society of Petroleum Engineers. doi:10.2118/121579-PA

Berge, C., 2017. An Experimental Study of Foam Flow in Water Saturated Porous Media, MS thesis, University of Bergen, Bergen, Norway.

Bergmann, P., et al., 2012. Surface-downhole electrical resistivity tomography applied to monitoring of CO2 storage at Ketzin, Germany. Geophysics, 2012. 77(6): p. B253-B267.

Bergmann, P., Ivandic, M., Norden, B., Rücker, C., Kiessling, D., Lüth, S., Schmidt-Hattenberger, C. and Juhlin, C., 2013. Combination of seismic reflection and

constrained resistivity inversion with an application to 4D imaging of the CO2 storage site, Ketzin, Germany. Geophysics, 79(2), pp.B37-B50.

Bernard, G. G., Holm, L. W., & Harvey, C. P. 1980. Use of surfactant to reduce CO2 mobility in oil displacement. Society of Petroleum Engineers Journal, 20(04), 281-292.

Bikerman, J.J., 2013. Foams (Vol. 10). Springer Science & Business Media.

Biterge, M. B., Hafez, H. H., Ouzzane, D., Khoury, J., & Safdar, M., 2014. Waterflood Surveillance in Lower Quality Carbonate Reservoir: History Matching of Fluid Front Beyond Wellbore Using Deeplook Electromagnetic Time-Lapse Surveys. In SPWLA 55th Annual Logging Symposium. OnePetro.

Bouchedda, A. and Giroux, B., 2015, December. Synthetic Study of CO2 monitoring using Time-lapse Down-hole Magnetometric Resistivity at Field Research Station, Alberta, Canada. In 2015 SEG Annual Meeting. Society of Exploration Geophysicists.

Bond, D.C. and Holbrook, O.C. Gas Drive Oil Recovery Process. 1958. United States Patent Office. 30 December. Patented number 2, 866, 507.

Boud, D.C. and O.C. Holbrook, Gas drive oil recovery process, 1958, Google Patents.

Bourdet, D., Ayoub, J. A., and Y. M. Plrard. 1989. Use of Pressure Derivative in Well-Test Interpretation. SPE Form Eval 4 (1989): 293–302. doi: https://doi.org/10.2118/12777-PA

Breen, S.J., et al., 2012. Bench-scale experiments to evaluate electrical resistivity tomography as a monitoring tool for geologic CO2 sequestration. International Journal of Greenhouse Gas Control, 2012. 9: p. 484-494.

Carrigan, C.R., et al., Electrical resistance tomographic monitoring of CO2 movement in deep geologic reservoirs., 2013. International Journal of Greenhouse Gas Control, 2013. 18: p. 401-408.

Chang, Kin-Shiung, and Robert Lemlich. 1980. A study of the electrical conductivity of foam." Journal of Colloid and Interface Science 73, no. 1 (1980): 224-232.

Chen, Q., Gerritsen, M.G., Kovscek, A.R. 2010. Modeling foam displacement with the local-equilibrium approximation: theory and experimental verification. SPE Journal 15 (1): 171–183

Cheng, L., A. B. Reme, D. Shan et al. 2000. Simulating Foam Processes at High and Low Foam Qualities. Proc., SPE/DOE Improved Oil Recovery Symposium, Tulsa, Oklahoma. SPE-59287-MS. https://doi.org/10.2118/59287-MS.

Chou, S.I., Vasicek, S.L., Pisio, D.L., Jasek, D.E., Goodgame, J.A. 1992. CO2 Foam Field Trial at North Ward Estes. Presented at the 67th SPE Annual Technical Conference and Exhibition, Washington, D.C., October 4-7, 1992.

Christensen, N. B., D. Sherlock, and K. Dodds. 2006. Monitoring CO2 injection with cross-hole electrical resistivity tomography." Exploration Geophysics 37.1 (2006): 44-49.

Cilliers, J.J., Wang, M. and Neethling, S.J., 1999. Measuring flowing foam density distributions using ERT. Ref, 5, pp.108-112.Clark, N. O. "The electrical conductivity of foam." Transactions of the Faraday Society 44 (1948): 13-15.

Cilliers, J.J., Xie, W., Neethling, S.J., Randall, E.W. and Wilkinson, A.J., 2001. Electrical resistance tomography using a bi-directional current pulse technique. Measurement Science and Technology, 12(8), p.997.

Daily, W., et al., 1992. Electrical resistivity tomography of vadose water movement. Water Resources Research, 1992. 28(5): p. 1429-1442.

Dholkawala, Z.F., Sarma, H.K. and Kam, S.I., 2007. Application of fractional flow theory to foams in porous media. Journal of Petroleum Science and Engineering, 57(1-2), pp.152-165.

Djuraev, U., S.R. Jufar, and P. Vasant, 2017. A review on conceptual and practical oil and gas reservoir monitoring methods. Journal of Petroleum Science and Engineering, 2017. 152: p. 586-601.

Du, D., P.L.J. Zitha, and M.G. Uijttenhout, 2007. Carbon dioxide foam rheology in porous media: a CT scan study. SPE Journal, 2007. 12(02): p. 245-252.

Enick, Robert Michael, David Kenneth Olsen, James Robert Ammer et al. 2012. Mobility and Conformance Control for CO2 EOR via Thickeners, Foams, and Gels -- A Literature Review of 40 Years of Research and Pilot Tests. Proc. SPE Improved Oil Recovery Symposium, 14-18 April, Tulsa, Oklahoma, USA. SPE-154122-MS. https://doi.org/10.2118/154122-MS.

Falls, A.H., Hirasaki G.J., Patzek, T.W., Gauglitz., P.A., Miller, D.D. and Ratulowski, T. 1988. Development of a Mechanistic Foam Simulator: The Population Balance and Generation by Snap-Off. SPE Reservoir Engineering 1988, 3 (03): 884-892. https://doi.org/10.2118/14961-PA

Farajzadeh, R., A. Andrianov, R. Krastev et al. 2012. Foam–oil interaction in porous media: Implications for foam assisted enhanced oil recovery. Advances in Colloid and Interface Science 183-184: 1-13. https://doi.org/10.1016/j.cis.2012.07.002.

Feitosa, K., Marze, S., Saint-Jalmes, A. and Durian, D.J., 2005. Electrical conductivity of dispersions: from dry foams to dilute suspensions. Journal of Physics: Condensed Matter, 17(41), p.6301.

Ferno, M. A., Gauteplass, J., Pancharoen, M., Haugen, A., Graue, A., Kovscek, A. R., & Hirasaki, G. J. 2014. Experimental Study of Foam Generation, Sweep Efficiency and Flow in a Fracture Network. Society of Petroleum Engineers. doi:10.2118/170840-MS

Gao, J., Zhao, Y., Li, X., & Wei, C., 2017. Foam displacement mechanisms and enhanced oil recovery in porous media: A review. Journal of Petroleum Science and Engineering, 155, 819-835.

Gargar, N.K., Mahani, H., Rehling, J.G., Vincent-Bonnieu, S., Kechut, N.I. and Farajzadeh, R., 2015, April. Fall-Off Test Analysis and Transient Pressure Behavior in Foam Flooding. In IOR 2015-18th European Symposium on Improved Oil Recovery.

Gauglitz, P. A., & Radke, C. J., 1990. Foam flow in porous media: Mechanisms and modeling. AIChE Journal, 36(11), 1639-1652.

Gauglitz, P. A., Friedmann, F., Kam, S. I., and Rossen, W. R., 2002. Foam Generation in Homogeneous Porous Media, Chem. Eng. Sci. 57 (2002), 4037-4052.

Ghosh, B. and D. Obasi., 2013. Eco-Friendly Surfactant for EOR in High Temperature, High Salinity Carbonate Reservoir. in SPE Enhanced Oil Recovery Conference. 2013. Society of Petroleum Engineers.

Haroun, M., Mohammed, A.M., Somra, B., Punjabi, S., Temitope, A., Yim, Y., Anastasiou, S., Baker, J.A., Haoge, L., Al Kobaisi, Aminzadeh, F., M., Karakas,

M., Corova, F., 2017. Real-Time Resistivity Monitoring Tool for In-Situ Foam Front Tracking. Society of Petroleum Engineers. doi:10.2118/188391-MS

Heller, J.P. 1966. Onset of Instability Patterns Between Miscible Fluids in Porous Media. Journal of Applied Physics 1966, 37, 1566-1579.

Heller, J.P., Boone, D.A., and Watts, R.J. 1985. Field Test of CO2-Foam Mobility Control at Rock Creek. Presented at the SPE 60th Annual Technical Conference and Exhibition, Las Vegas, Nevada USA. September 22-25, 1985. SPE-14395.

Hirasaki, G.J. and Lawson, J.B., 1985. Mechanisms of foam flow in porous media: apparent viscosity in smooth capillaries. Society of Petroleum Engineers Journal, 25(02), pp.176-190.

Hiraski, G.J., 1989. The steam-foam process. Journal of Petroleum Technology, 41(05): p. 449-456.

Hoefner, M.L. and Evans, E.M. 1995. CO2 Foam: Results from Four Developmental Fields Trials, SPE Reservoir Engineering, November 1995, p. 273-281.

Holm Le Roy, W., 1967. Method for recovering oil from subterranean formations, Google Patents.

Huh, D. and L. Handy, 1989. Comparison of steady and unsteady-state flow of gas and foaming solution in porous media. SPE reservoir engineering, 1989. 4(01): p. 77-84.

Iglauer, S., Paluszny, A., & Blunt, M. J. 2014. Experimental investigation of foam displacement mechanisms in porous media. Industrial & Engineering Chemistry Research, 53(42), 16324-16331.

Jian, G., Puerto, M. C., Wehowsky, A., Dong, P., Johnston, K. P., Hirasaki, G. J., & Biswal, S. L. 2016. Static adsorption of an ethoxylated nonionic surfactant on carbonate minerals. Langmuir, 32(40), 10244-10252.

Jian, Guoqing, Zhang, Leilei, Da, Chang, Puerto, Maura, Johnston, Keith P, Biswal, Sibani L, & Hirasaki, George J. 2019. Evaluating the Transport Behavior of CO2 Foam in the Presence of Crude Oil under High-Temperature and High-Salinity Conditions for Carbonate Reservoirs. Energy & Fuels, 33(7), 6038-6047.

Kam, S. I., Nguyen, Q. P., Li, Q., and W. R. Rossen. 2004. Dynamic Simulations With an Improved Model for Foam Generation. Paper presented at the SPE Annual Technical Conference and Exhibition, Houston, Texas, September 2004. doi: https://doi.org/10.2118/90938-MS

Kam, S.I., Nguyen, Q.P., Li, Q. and Rossen, W.R., 2007. Dynamic simulations with an improved model for foam generation. SPE Journal, 12(01), pp.35-48.

Karakas, M. and Kristensen, R. M., 2010 Cross-Well Pressure Measurements for CO2 and CO2-WAG Injection, Presented at the CO2 Monitoring Workshop at Schlumberger Dhahran Research Center, Dhahran, Saudi Arabia.

Karakas, M. and Aminzadeh, F., 2017, Optimization of CO2-Foam Injection through Resistivity and Pressure Measurements, Provisional US Patent Application, Serial No. 62/511,547.

Karakas, M., & Aminzadeh, F. 2018. Optimization of CO2-Foam Injection through Resistivity and Pressure Measurements. Society of Petroleum Engineers. doi:10.2118/190061-MS

Karakas, Metin, Alcorn, Zachary Paul, and Arne Graue. 2020. CO2 Foam Field Pilot Monitoring Using Transient Pressure Measurements. Paper presented at the SPE

Annual Technical Conference and Exhibition, Virtual, October 2020. doi: https://doi.org/10.2118/201406-MS

Karakas, M.; Alcorn, Z.P.; Aminzadeh, F.; Graue, A. 2022. Pressure Measurements for Monitoring CO2 Foam Pilots. Energies 2022, 15, 3035. https://doi.org/10.3390/en15093035

Karakas, M., Aminzadeh, F., & Graue, A. 2022. CO2-Foam Monitoring using Resistivity and Pressure Measurements. Global Journals of Research in Engineering, 22(J2), 33-46.

Khoshnevis Gargar, N., Mahani, H., Rehling, J. G., Vincent-Bonnieu, S., & Farajzadeh, R. 2015. Fall-off test analysis and transient pressure behavior in foam flooding.

Kiessling, D., Schmidt-Hattenberger, C., Schuett, H., Schilling, F., Krueger, K., Schoebel, B., Danckwardt, E., Kummerow, J. and CO2SINK Group, 2010. Geoelectrical methods for monitoring geological CO2 storage: first results from cross-hole and surface–downhole measurements from the CO2SINK test site at Ketzin (Germany). International Journal of Greenhouse Gas Control, 4(5), pp.816-826.

Kim, J. W., Xue, Z., & Matsuoka, T. 2010. Experimental Study on CO2 Monitoring and Saturation With Combined P-wave Velocity and Resistivity. Society of Petroleum Engineers. doi:10.2118/130284-MS

Kim, J., Dong, Y., & Rossen, W. R. 2005. Steady-State Flow Behavior of CO2 Foam. Society of Petroleum Engineers. doi:10.2118/89351-PA

Kim, J., Nam, M.J. and Matsuoka, T., 2016. Monitoring CO2 drainage and imbibition in a heterogeneous sandstone using both seismic velocity and electrical resistivity measurements. Exploration Geophysics, 47(1), pp.24-31.

Kim, Jisung, Yan Dong, and William R. Rossen. 2005. Steady-state flow behavior of CO2 foam. SPE journal 10.04 (2005): 405-415.

Kovscek, A. R., & Radke, C. J. 1994. Mechanisms of foam flow in porous media: Apparent viscosity in smooth capillaries. AIChE Journal, 40(9), 1487-1500.

Kovscek, A.R. and Radke, C.J., 1994. Fundamentals of foam transport in porous media.

Kovscek, A.R., Patzek, T.W. and Radke, C.J., 1995. A mechanistic population balance model for transient and steady-state foam flow in Boise sandstone. Chemical Engineering Science, 50(23), pp.3783-3799.

Kruglyakov, P., et al., Foam drainage. Current Opinion in Colloid & Interface Science, 2008. 13(3): p. 163-170.

Kuuskraa, V.A. and Koperna, G.J., 2006. Evaluating the potential for 'game changer'improvements in oil recovery efficiency from CO2 enhanced oil recovery. Prepared for US Department of Energy, Office of Fossil Energy—Office of Oil and Natural Gas.

Lai, S. H., & Radke, C. J. 1991. Foam flow in porous media: Experimental characterization of the steady state. AIChE Journal, 37(9), 1333-1349.

Law, D. H. S., Z. M. Yang, T. W. Stone. 1992. Effect of the Presence of Oil on Foam Performance: A Field Simulation Study. SPE Reservoir Engineering 7 (02). SPE-18421-PA. https://doi.org/10.2118/18421-PA.

Leeftink, T.N., Latooij, C.A. and Rossen, W.R. 2015. Injectivity errors in simulation of foam EOR. J Petrol Sci Eng 126, 26-34.

Lemlich, R., 1985. Semitheoretical equation to relate conductivity to volumetric foam density. Industrial & Engineering Chemistry Process Design and Development, 24(3), pp.686-687.

Lotfollahi, M., Farajzadeh, R., Delshad, M., Varavei, A., & Rossen, W. R. 2016. Comparison of Implicit-Texture and Population-Balance Foam Models. Society of Petroleum Engineers. doi:10.2118/179808-MS

Ma, K., Ren, G., Mateen, K., Morel, D., & Cordelier, P. 2015. Modeling Techniques for Foam Flow in Porous Media. Society of Petroleum Engineers. doi:10.2118/169104-PA

Ma, K.; Lopez-Salinas, J.L.; Puerto, M.C.; Miller, C.A.; Biswal, S.L.; Hirasaki, G.J. 2013. Estimation of Parameters for the Simulation of Foam Flow through Porous Media. Part 1: The Dry-Out Effect. Energy Fuels 2013, 27, 2363–2375.

Ma, Kun, Farajzadeh, Rouhi, Lopez-Salinas, Jose L, Miller, Clarence A, Biswal, Sibani Lisa, & Hirasaki, George J. 2014. Non-uniqueness, Numerical Artifacts, and Parameter Sensitivity in Simulating Steady-State and Transient Foam Flow Through Porous Media. Transport in Porous Media, 102(3), 325-348.

Ma, Kun, Jose L. Lopez-Salinas, Maura C. Puerto et al. 2013. Estimation of Parameters for the Simulation of Foam Flow through Porous Media. Part 1: The Dry-Out Effect. Energy & Fuels 27 (5): 2363-2375. https://doi.org/10.1021/ef302036s.

Mahani, H., Sorop, T., van den Hoek, P., Brooks, D., & Zwaan, M. 2011. Injection Fall-Off Analysis of Polymer flooding EOR. Society of Petroleum Engineers. doi:10.2118/145125-MS

Mannhardt, K., J.J. Novosad, and L.L. Schramm 1996. Core flood evaluation of hydrocarbon solvent foams. Journal of Petroleum Science and Engineering, 1996. 14(3-4): p. 183-195.

Martin, F.D., Heller., J.P., Weiss, W.W., and Tsau, J.S. 1992. CO2-Foam Field Verification Pilot Test at EVGSAU Injection Project Phase 1: Project Planning and Initial Results. Presented at the SPE Improved Oil Recovery Conference, Tulsa, Oklahoma, USA, 22-24 April, 1992. SPE/DOE-24176

Masoudi, R., Ann Giddins, M., Karkooti, H., Jalan, S., & Valero Gil, A. A. 2015. Foam simulation from coreflood to field scale. In SPE Asia Pacific Enhanced Oil Recovery Conference. OnePetro.

Matthews, C., Carbon dioxide flooding. Developments in Petroleum Science, 1989. 17: p. 129-156.

Mohanty, K. K., & Morrow, N. R. 1994. The effect of surfactant concentration on foam flow through porous media. SPE Reservoir Engineering, 9(2), 137-144.

Montaron, B. 2009. Connectivity Theory – A New Approach to Modeling Non-Archie Rocks. Society of Petrophysicists and Well-Log Analysts.

Moreno, J., & Flew, S. 2011. EOR: Challenges of translating fine scale displacement into full field Models. In SPE Enhanced Oil Recovery Conference. OnePetro.

Nakamura, Y., Mamoru T., and Abusaa E. 2015. Synthetic Analysis of Full-Waveform Crosshole Seismic Toward CO 2 EOR Monitoring in Abu Dhabi. Abu Dhabi International Petroleum Exhibition and Conference. Society of Petroleum Engineers, 2015.

Nakatsuka, Y., et al., 2010. Experimental study on CO2 monitoring and quantification of stored CO2 in saline formations using resistivity measurements. International Journal of Greenhouse Gas Control, 2010. 4(2): p. 209-216.

Namdar Zanganeh, M., & Rossen, W. 2013. Optimization of Foam Enhanced Oil Recovery: Balancing Sweep and Injectivity. Society of Petroleum Engineers. doi:10.2118/163109-PA

Nguyen, Q., Hirasaki, G., & Johnston, K. 2015. Novel CO2 Foam Concepts and Injection Schemes for Improving CO2 Sweep Efficiency in Sandstone and Carbonate Hydrocarbon Formations. Univ. of Texas, Austin, TX (United States).

Omar, S., et al. 2013. Monitoring Foam Stability in Foam Assisted Water Alternate Gas (FAWAG) Processes Using Electrokinetic Signals. in SPE Enhanced Oil Recovery Conference. 2013. Society of Petroleum Engineers.

Onishi, K., Ishikawa, Y., Yamada, Y. and Matsuoka, T., 2006, January. Measuring electric resistivity of rock specimens injected with gas, liquid and supercritical CO2. In 2006 SEG Annual Meeting. Society of Exploration Geophysicists.

Park, C. and S.W. Hermanowicz, 2014. A multi-point electrical resistance measurement system for characterization of foam drainage regime and stability. AIChE Journal, 2014. 60(9): p. 3143-3150.

Patzek, T., 1996. Field Application of Foam for Mobility Improvement and Profile Control. SPEREE 11 (2): 79–85, 1996, SPE-29612-PA. DOI: 10.2118/29612-PA.

Pereira, A. L. F., Rodrigues, R. B., & Schmitz, J. E. 2012. Foam flow in porous media: Effect of surfactant concentration on pressure drop. Chemical Engineering Science, 79, 235-244.

Prigiobbe, Valentina, et al. 2016. Transport of Nanoparticle-Stabilized CO2-Foam in Porous Media. Transport in Porous Media 111.1 (2016): 265-285.

Rognmo, A.; Heldal, S.; Fernø, M. 2018. Silica nanoparticles to stabilize CO2-foam for improved CO2 utilization: Enhanced CO2 storage and oil recovery from mature oil reservoirs. Fuel 2018, 216, 621–626.

Rognmo, A.U.; Fredriksen, S.B.; Alcorn, Z.P.; Sharma, M.; Føyen, T.; Eide, G.A.; Fernø, M. 2019. Pore-to-Core EOR Upscaling for CO2 Foam for CCUS. SPE J. 2019, 24, 2793–2803.

Rossen, W. and P. Gauglitz, 1990. Percolation theory of creation and mobilization of foams in porous media. AIChE Journal, 1990. 36(8): p. 1176-1188.

Rossen, W. R., & Gauglitz, P. A. 2000. Foam in porous media. CRC Press.

Rossen, W.R. 1996. Foams in Enhanced Oil Recovery. In Foams Theory, Measurements, and Applications. eds. Prud'homme, R.K. and Khan, S.A. volume 57, ch. 11, p 414-464, Marcel Dekker, Inc. New York

Rossen, W.R., Zeilinger, S.C., Shi, J.X. and Lim, M.T., 1999. Simplified Mechanistic Simulation of Foam Processes in Porous Media. SPE J. 4, 279-287.

Safouane, M., et al., 2006. Viscosity effects in foam drainage: Newtonian and non-newtonian foaming fluids. The European Physical Journal E: Soft Matter and Biological Physics, 2006. 19(2): p. 195-202.

Saint-Jalmes, A., Y. Zhang, and D. Langevin, 2004. Quantitative description of foam drainage: Transitions with surface mobility. The European Physical Journal E: Soft Matter and Biological Physics, 2004. 15(1): p. 53-60.

Sanchez, J. and R. Hazlett, 1992. Foam flow through an oil-wet porous medium: a laboratory study. SPE reservoir engineering, 1992. 7(01): p. 91-97.

Schmidt-Hattenberger, C., Bergmann, P., Labitzke, T. and Wagner, F., 2014. CO2 migration monitoring by means of electrical resistivity tomography (ERT)–Review on five years of operation of a permanent ERT system at the Ketzin pilot site. Energy Procedia, 63, pp.4366-4373.

Schramm, L. L. 1994. Foams: Fundamentals and Applications in the Petroleum Industry. Washington, DC: American Chemical Society.

Sharma, M.; Alcorn, Z.; Fredriksen, S.; Fernø, M.; Graue, A. 2017. Numerical Modeling Study for Designing CO2-foam Field Pilot. In Proceedings of the IOR 2017—19th European Symposium on Improved Oil Recovery, Stavanger, Norway, 24 April 2017.

Sharma, M., Alcorn, Z. P., Fredriksen, S. B., Rognmo, A. U., Fernø, M. A., Skjæveland, S. M., & Graue, A. 2020. Model calibration for forecasting CO2-foam enhanced oil recovery field pilot performance in a carbonate reservoir. Petroleum Geoscience, 26(1), 141-149.

Singh, R. and K.K. Mohanty, 2016. Foams with wettability-altering capabilities for oil-wet carbonates: a synergistic approach. SPE Journal, 2016. 21(04): p. 1,126-1,139.

Talebian, S. H., Masoudi, R., Tan, I. M., & Zitha, P. L. J. 2014. Foam assisted CO2-EOR: A review of concept, challenges, and future prospects. Journal of Petroleum Science and Engineering, 120, 202-215.

Tapp, H.S., Peyton, A.J., Kemsley, E.K. and Wilson, R.H., 2003. Chemical engineering applications of electrical process tomography. Sensors and Actuators B: Chemical, 92(1-2), pp.17-24.

Turta, A.T. and A.K. Singhal, 2002. Field foam applications in enhanced oil recovery projects: screening and design aspects. Journal of Canadian Petroleum Technology, 2002. 41(10).

Valincius, V., Weitz, D. A., & Lee, D. 2007. Foam in porous media: Dynamics and stability. Journal of Physics: Condensed Matter, 19(46), 463101.

Wang, M. and Cilliers, J.J., 1999. Detecting non-uniform foam density using electrical resistance tomography. Chemical Engineering Science, 54(5), pp.707-712.

Wassmuth, F., K. Green, and L. Randall, 2001. Details of in-situ foam propagation exposed with magnetic resonance imaging. SPE Reservoir Evaluation & Engineering, 2001. 4(02): p. 135-145.

Wiggers, F. 2001. An enhanced electrical resistance technique for foam drainage measurement. Colloids and Surfaces A: Physicochemical and Engineering Aspects, 2001. 189(1): p. 237-246.

Wu, Y., Hubbard, S. and Wellman, D., 2012. Geophysical monitoring of foam used to deliver remediation treatments within the vadose zone. Vadose Zone Journal, 11(4).

Xue, Z., Kim, J. W., Mito, S., Kitamura, K., & Matsuoka, T. 2009. Detecting and Monitoring CO2 With P-Wave Velocity and Resistivity From Both Laboratory and Field Scales. Society of Petroleum Engineers. doi:10.2118/126885-MS

Yang, X., et al., 2014. Uncertainty quantification of CO2 saturation estimated from electrical resistance tomography data at the Cranfield site. International Journal of Greenhouse Gas Control, 2014. 27: p. 59-68.

Yuan, H., & Chatzis, I. 2002. A network model for foam flow in porous media. Advances in Water Resources, 25(7), 823-839.

Zheng, Y., Muthuswamy, A., Ma, K., Wang, L., Farajzadeh, F., Puerto, M., Vincent-Bonnieu, S., Eftekhari, A.A., Wang, Y., Da, C., Joyce, J.C., Biswal, S.L. and Hirasaki, G.J. 2016. Insights on Foam Transport from a Texture- Implicit Local Equilibrium Model with an Improved Parameter Estimation Algorithm. Ind Eng Chem Res, 55 (28), 7819–7829.

Zhou B. and Greenhalgh S. A., 2000 Cross-hole resistivity tomography using different electrode configurations, Geophysical Prospecting, vol. 48, no. 5, pp. 887–912, 2000.

Scientific Papers

energies

MDPI

Article

Pressure Measurements for Monitoring CO_2 Foam Pilots

Metin Karakas [1,*], Zachary Paul Alcorn [1], Fred Aminzadeh [2] and Arne Graue [1]

[1] Department of Physics and Technology, University of Bergen, P.O. Box 7803, 5007 Bergen, Norway; zachary.alcorn@uib.no (Z.P.A.); arne.graue@uib.no (A.G.)
[2] FACT Inc., 3345 State St., Suite 3282, Santa Barbara, CA 93130-7001, USA; fred.aminzadeh@fact-corp.com
* Correspondence: metin.karakas@uib.no; Tel.: +1-310-795-5980

Abstract: This study focuses on the use of pressure measurements to monitor the effectiveness of foam as a CO_2 mobility control agent in oil-producing reservoirs. When it is applied optimally, foam has excellent potential to improve reservoir sweep efficiency, as well as CO_2 utilization and storage, during CO_2 Enhanced Oil Recovery (EOR) processes. In this study, we present part of an integrated and novel workflow involving laboratory measurements, reservoir modeling and monitoring. Using the recorded bottom-hole pressure data from a CO_2 foam pilot study, we demonstrate how transient pressures could be used to monitor CO_2 foam development inside the reservoir. Results from a recent CO_2 foam pilot study in a heterogeneous carbonate field in Permian Basin, USA, are presented. The injection pressure was used to evaluate the development of foam during various foam injection cycles. A high-resolution radial simulator was utilized to study the effect of foam on well injectivity, as well as on CO_2 mobility in the reservoir during the surfactant-alternating gas (SAG) process. Transient analysis indicated constant temperature behavior during all SAG cycles. On the other hand, differential pressures consistently increased during the surfactant injection and decreased during the subsequent CO_2 injection periods. Pressure buildup during the periods of surfactant injection indicated the development of a reduced mobility zone in the reservoir. The radial model proved to be useful to assess the reservoir foam strength during this pilot study. Transient analysis revealed that the differential pressures during the SAG cycles were higher than the pressures observed during the water-alternating gas (WAG) cycle which, in turn, showed foam generation and reduced CO_2 mobility in the reservoir. Although pressure data are a powerful indicator of foam strength, additional measurements may be required to describe the complex physics of in situ foam generation. In this pilot study, it appeared that the reservoir foam strength was weaker than that expected in the laboratory.

Keywords: CO_2 foam; pilot monitoring; pressure measurements; transient analysis; CO_2 EOR; CO_2 storage

Citation: Karakas, M.; Alcorn, Z.P.; Aminzadeh, F.; Graue, A. Pressure Measurements for Monitoring CO_2 Foam Pilots. *Energies* **2022**, *15*, 3035. https://doi.org/10.3390/en15093035

Academic Editors: Rouhi Farajzadeh and Dmitriy A. Martyushev

Received: 22 February 2022
Accepted: 18 April 2022
Published: 21 April 2022

1. Introduction

CO_2 foam injection is an effective method for controlling CO_2 mobility during enhanced oil recovery (EOR) processes in petroleum reservoirs [1]. When it is performed optimally, CO_2 foam has excellent potential to improve sweep efficiency [2–8] and CO_2 storage potential. Foam is a mixture consisting of a continuous liquid phase (surfactant solution) and a gas phase (CO_2). This mixture becomes discontinuous due to the generation of thin liquid films called lamellae [9]. The mobility of foam depends on its texture: the finer the foam's texture, the lower the CO_2 mobility. It has been shown that foam density is a direct function of the density of the lamellae [10]. Laboratory studies clearly show that foam strength is very important in achieving the desired reservoir displacement efficiency. Additionally, the solubility of the surfactant in CO_2 and water phases, as well as the adsorption of CO_2 on rocks, play a crucial role during foam displacement [11].

Surfactants are commonly used to generate and stabilize foams in porous media. They are screened to ensure the success of a CO_2 foam. Recent research has suggested various

surfactants (cationic, nonionic, and zwitterionic) as the main candidates for CO_2 foams in EOR [12]. Several studies have been conducted to examine the texture and stability of CO_2 foams as a function of the surfactant structure and formulation. These variables include the water/CO_2 ratio, surfactant concentration, water salinity, etc. Previous research shows that surfactant characteristics, along with foam strength, can be adjusted to ensure optimum foam displacement during CO_2 EOR processes. However, surfactant-based foams break down in the formation due to the presence of oil and the adsorption of the surfactant to rock, and at high temperatures and salinities. Therefore, it is also important to maintain foam strength (or stability) during the entire injection period in field applications. Recent work suggests that the addition of silica nanoparticles to surfactant-stabilized CO_2 foams may increase the strength and stability of foam systems [13].

There are several strategies to generate foam in porous media. These include the co-injection of gas (CO_2)/surfactant or surfactant-alternating gas (CO_2) injection (the SAG method). In the co-injection process, the gas (CO_2) and the surfactant solution are simultaneously injected, and foam is formed in situ. In the SAG method, the surfactant and CO_2 are injected in alternating slugs. In low-permeability reservoirs, SAG injection may be preferred due to increased gas injectivity. Additionally, with the use of the SAG method, the contact between CO_2 and water is minimized, which may reduce corrosion in surface facilities and piping [14].

Laboratory studies using reservoir cores are used to define the optimum recipe at a given reservoir pressure, temperature, and water salinity. For the application of foam in reservoirs where heterogeneity is involved, reservoir monitoring is carried out to assess foam development under reservoir conditions. While seismic, resistivity, electromagnetic and pressure measurements have been suggested in the oil industry, foam monitoring is typically carried out through flow and bottom hole pressure measurements, injection logging and the use of fluid tracers. These measurements are, in turn, used to assess the effectiveness of foam as a mobility control method and, hence, provide a way in which to remedy any underperforming CO_2 floods. In this way, the design of the foam can be adjusted to improve oil recovery, CO_2 utilization and storage.

In this study, we present the pressure monitoring part of an integrated and novel workflow involving laboratory measurements, reservoir modeling and monitoring. The laboratory studies were conducted on reservoir core samples to determine the optimal foam formulation. Reservoir modeling was carried out to decide on optimum injection strategy, and extensive reservoir monitoring was conducted to assess the effectiveness of the designed foam under reservoir conditions. The results of this integrated research work provide important knowledge for future CO_2 EOR field applications.

2. Pressure Testing for Foam Monitoring

In the petroleum industry, transient pressure testing is typically used to investigate reservoir characteristics such as permeability, reservoir boundaries, etc., as well as the well performance such as productivity or injectivity, skin effects, etc. Fall-off testing is an effective method for monitoring water or foam injection. Typically, fall-off tests are conducted by ceasing the injection and analyzing the transient pressure to assess any mobility changes near the injector [15]. In such tests, bottom-hole pressures are recorded at the injection well, and the data are used to examine the reservoir mobility changes caused by the injection. Foam injection affects the mobility distribution in the reservoir; therefore, the location of the foam front can be monitored, in principle, by fall-off tests. These tests rely on single-point pressure measurements and may lack the resolution required in layered formations.

Based on previous comparable studies with CO_2 injections [16], it has been suggested that crosswell pressure testing, in addition to seismic and electromagnetic data, could be deployed for CO_2 foam monitoring. In crosswell pressure testing, a series of pressure pulses is induced by shutting down the injector, and the pressure measurements are taken at the observation well. These measurements could be used to examine the inter-well

reservoir connectivity. The main advantage of these tests is the larger investigation volume away from the injector.

3. Field Pilot Description

A surfactant-stabilized foam was chosen to reduce the CO_2 mobility in this field. The surfactant system was selected based on laboratory measurements of surfactant adsorption. The foam stability was also verified during these laboratory studies. A surfactant-alternating gas (SAG) injection strategy was adapted, with 10 days of surfactant solution injection followed by 20 days of CO_2 injection. The pilot injection began in May 2019. Monitoring surveys during this pilot study included CO_2 injection profiles, CO_2 tracer tests, the collection of bottom-hole injection pressure/temperature and three-phase flow rates.

The pilot study was performed in the East Seminole Field, Permian Basin, West Texas, and the study area was an inverted 40 acre 5-spot pattern which included a central injection well and four surrounding producers (Figure 1). The oil was produced from the San Andres formation, which is classified as a heterogeneous cyclical carbonate. The reservoir interval had an average permeability of 13 mD, pay thickness of 110 ft, and consisted of six flow zones separated by impermeable flow barriers. The pilot area was selected based on rapid CO_2 breakthrough, high GORs in the producers as well as relatively short well distances [17,18]. Two production wells, P1 and P4, were the focus of the baseline data collection and pilot monitoring because they exhibited the most rapid CO_2 breakthrough time from tertiary CO_2 injection. Composite logs from the pilot injection well indicated a 10 ft thick high permeability streak of 200 mD. Historical injection profiles showed that this zone has been taking most of the injected CO_2. Therefore, this high permeability zone was targeted because foam can form in high permeability streaks and diverting flow to unswept regions of the reservoir with lower permeabilities. The reservoir and fluid properties are shown in Table 1.

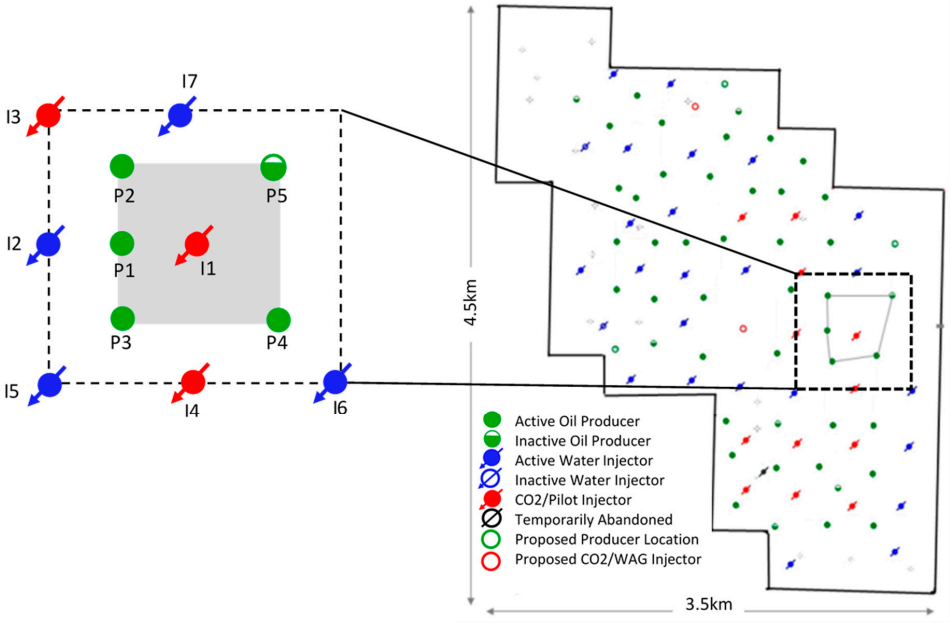

Figure 1. Pilot pattern (shaded area) and surrounding wells in East Seminole Field. The pilot injection well was I1, and the monitored producers were P1 through P4.

Table 1. Reservoir and fluid properties of the San Andres unit in the East Seminole Field.

Reservoir Characteristic	Value
Depth	5200 ft
Permeability	1 to 300 md (average: 13 md)
Porosity	3 to 28% (average: 12%)
Pay thickness	110 ft
Reservoir pressure (initial)	2500 psig
Reservoir pressure (current)	3400 psig
Fracture pressure	3900 psig
Reservoir temperature	104^0F
Oil gravity	31 °API
Formation brine salinity	70,000 ppm

4. Foam Formulation Design

The laboratory program aimed to determine the optimal foam formulation for the field test. This included surfactant-screening studies, evaluations of the optimal foam quality (gas fraction) and surfactant concentration and quantification of CO_2 EOR and CO_2 storage potential. Individual components of the laboratory program have been detailed elsewhere [12,13,17,18] and are briefly reviewed here.

Surfactant screening studies identified the nonionic water-soluble Huntsman L24-22, a linear ethoxylated alcohol (C12-14 EO22), for the field pilot study based upon minimal loss to the formation due to adsorption, adequate foam strength, and chemical stability [12]. Once the reservoir-specific surfactant was selected, the foam formulation was evaluated by determining the impact of surfactant concentration, gas fraction (foam quality) and flow velocity on foam strength at reservoir conditions [18]. The foam strength was quantitatively evaluated by the apparent foam viscosity, which was calculated from the steady-state pressure gradient at each gas fraction during foam quality scans and at each injection rate during foam rate scans [19]. As described in Section 6, foam model parameters for numeral modeling were derived from the foam quality and foam rate scans by curve-fitting regression [20–22].

5. Radial Model Set-Up and Initialization

In this pilot study, injection well pressures and temperatures were recorded using a down-hole memory pressure gauge during various surfactant, CO_2 and water injection periods. The transient analysis was conducted by examining the differential pressure (dP) and differential temperature (dT) over time for nine SAG cycles and one WAG cycle. A high-resolution two-dimensional radial foam simulator was used to history-match the measured transient pressure data. The simulation model included the porosity and permeability distribution from a validated sector-scale model of the pilot pattern and surrounding producers [21]. The simulation foam model was used to examine the impact of foam and/or relative permeability on injectivity and mobility reduction when switching between surfactant solution and CO_2 in an SAG process.

The objectives of this study were as follows:

- Evaluate whether foam has been generated based upon comparisons with measured BHP and injection rates;
- Tune foam model to observed pressures during pilot if foam has formed;
- Determine the foam propagation distance/rate if foam has formed.

The radial model used in this study was based upon a validated sector-level model of the pilot pattern and surrounding producers. The base sector model was calibrated to 40 years of waterflood and over 4 years of CO_2 injection data, before the pilot study. A workflow was developed to history-match the cumulative oil production and water-cut in the sector model [22].

The radial model included one injector (I1) which simulated the nine-cycle SAG pilot period. The grid contained 28 layers, which were refined from the validated sector model of

the pilot pattern and surrounding wells. The radial grid extended to 700 ft from the injector and the grid sizes increased logarithmically from the injector. Layers and perforations were from the history-matched (HM) sector model (reference to Mohan's PhD/papers with HM models). The model included historical water and CO_2 injections before the pilot study. The simulations during the pilot study were controlled by the actual injection rates, and the simulated rates were compared with historical rates to ensure that the model could adhere to these controls.

Figure 2 shows the permeability distribution in the radial model. Radial simulation model parameters are provided in Table 2.

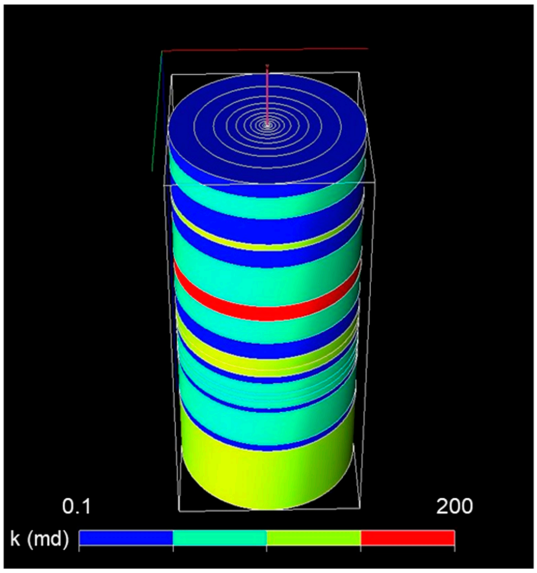

Figure 2. Permeability distribution in the radial model. The number of radial and vertical grid blocks are 20 and 28, respectively.

Table 2. Radial simulation model parameters.

Simulation Model Parameter	
Number of grid blocks	20 × 1 × 28 (r, theta, z)
Outer radius	700 ft
Total thickness	145 ft
Initial water saturation (Sw)	0.50
Starting reservoir pressure	3118 psia
Fracture pressure	3900 psig
Reservoir temperature	104^0F
Oil gravity	31 °API
Formation brine salinity	70,000 ppm
Permeability and porosity from the HM sector model	
Average permeability	13.5 md
Average porosity	0.08
Initial conditions on 1 April 2019.	

Base values for foam model parameters were obtained by performing regression analysis on the quality scan data to fit the empirical foam model [21,23]. Figure 3 shows the foam characteristics obtained based on the regression analysis.

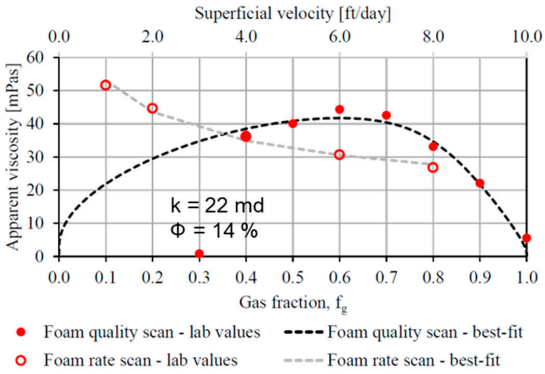

Figure 3. Laboratory foam quality (red filled circles) and rate (red open circles) scans used to derive foam model parameters for the local equilibrium foam model. The dashed lines show the model fit.

The simulation model was run using daily pilot study injection rates using the rate control option of the simulator.

6. Foam Modeling

There are two approaches to modeling foam transport in porous media: an explicit texture population balance model [10,24].and an implicit texture local equilibrium model [25,26]. Population balance models explicitly represent the dynamics of lamella creation and destruction along with the effect of the resulting foam on gas mobility. Gas mobility is reduced according to bubble size (determined by the rates of creation and destruction of lamellae). Local equilibrium models implicitly represent the effect of bubble size by introducing factors for reducing gas mobility by foam as a function of water saturation, oil saturation, surfactant concentration, and shear thinning due to the flow rate. Local equilibrium models assume that foam is present anywhere gas and water are present, along with an adequate surfactant concentration. The effect of foam was modeled in this study using the local equilibrium approach.

The decrease in gas mobility during foam floods is accounted for in local equilibrium models by scaling the gas relative permeability for no foam floods ($k_{rg}{}^{nf}$) by a mobility reduction factor (FM), whereas the water relative permeabilities remain unchanged.

$$k_{rg}^{f} = k_{rg}^{nf} \times FM \tag{1}$$

The effect of water saturation, shear rate, surfactant concentration and oil saturation [26] on the mobility reduction factor was studied, given by the expression:

$$FM = \frac{1}{1 + fmmmob \times F_{water} \times F_{shear} \times F_{oil} \times F_{surf}} \tag{2}$$

$fmmmob$ refers to the maximum gas mobility reduction that can be achieved. F_{water}, F_{shear}, F_{oil} and F_{surf} capture the water saturation, shear rate, oil saturation and surfactant concentration dependence, respectively, all lying in the range of 0 to 1 (Equations (3) through (6)). The capillary number, N_{ca}, represents the relative effect of viscous and capillary forces.

$$F_{water} = 0.5 + \frac{arctan[epdry(S_w - fmdry)]}{\pi} \tag{3}$$

$$F_{shear} = \begin{cases} \left(\frac{fmcap}{N_{ca}}\right)^{epcap} \; if \; N_{ca} > fmcap \\ 1 \; otherwise \end{cases} \tag{4}$$

$$F_{surf} = \left(\frac{Surfactant\ concentration}{fmsurf} \right)^{epsurf} \quad (5)$$

$$F_{oil} = \left(\frac{fmoil - So}{fmoil} \right)^{epoil} \quad (6)$$

Two water components were used to model foam behavior: one for surfactant solution and one for water. The base case foam parameters were derived from laboratory foam quality and rate scans and fitted to the empirical local equilibrium foam model by curve-fitting regression [19–21,25–27].

The surfactant selected for the pilot was found to have very low adsorption reservoir rock in the laboratory; thus, adsorption was excluded from the simulation study. Figure 3 shows the foam quality and rate scan used to derive the model parameters, and Table 3 shows the base case foam model parameters.

Table 3. Base case foam parameters.

Foam Parameter	Value
fmmob	192
fmdry	0.40
epdry	84
fmcap	9.0×10^{-7}
epcap	0.59

7. Measured Injection Rates and Pressures

The reservoir response to foam was evaluated by analyzing the bottom-hole pressure (BHP) response during surfactant and CO_2 injection. Figure 4 shows the injection rates of the CO_2 (red curve) and surfactant solution (green curve) and the measured BHP (black curve) at the injector well for nine complete pilot SAG cycles. The injection rates during the pilot study were 520 and 470 rb/day for the surfactant solution and CO_2, respectively. The volumetric ratio of injected CO_2 relative to the total volume of CO_2 and surfactant injected was used to evaluate injected foam quality per cycle. The aim was to inject foam at 70% quality (0.70 gas fraction) per cycle, as determined in the laboratory studies. The foam qualities ranged from 61% to 71%, which was within the designed target.

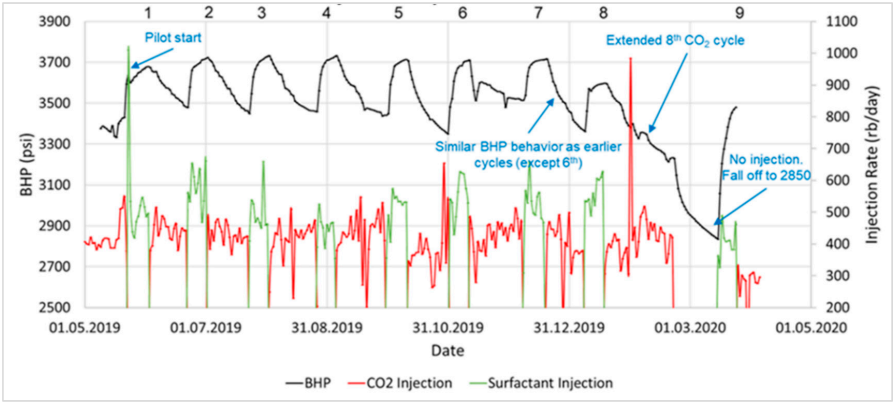

Figure 4. Plot showing the injection history along with measured bottom-hole pressures during the 9 SAG cycles.

8. Base Case Simulations

The simulated BHP was compared with actual surveys to evaluate foam generation and CO_2 mobility reduction. Figure 5 shows the surfactant-alternating gas (SAG) simulation

results, assuming the base case foam parameters (red curve). As can be seen in this plot, the simulated pressures were significantly higher than the measured BHP (black curve). In addition, the simulated pressures assuming a water-alternating gas (WAG) scenario are shown (blue curve), which were slightly lower but more consistent with the measured pressures, suggesting a weaker foam than that expected.

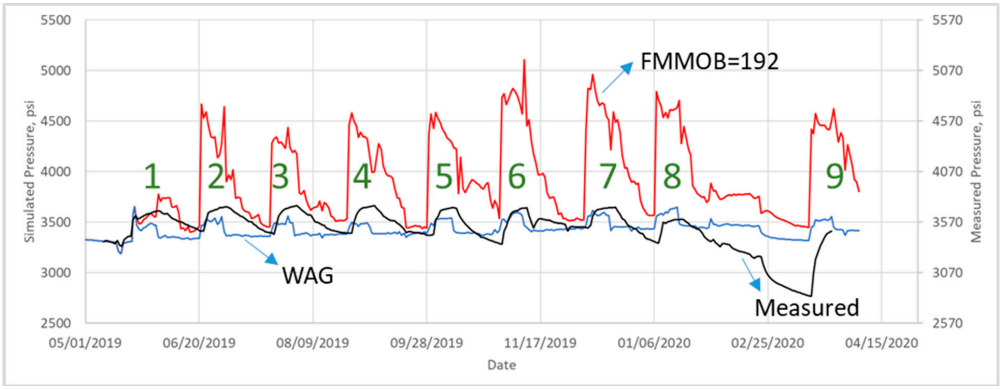

Figure 5. Simulated pressures using base case foam parameters.

The radial simulation model assumed a constant effect of nearby wells, and this may only be true for limited times. To check this assumption, the injection and production rates within the pilot pattern were also plotted. Figure 6 shows the total injection rates for the pilot pattern. As can be seen from this plot, the total CO_2 injection rate increased during Cycles 6 and 7 and decreased during Cycles 8 and 9. This is important since the radial well model only simulated the central injector and did not consider the effects of injection/production on the nearby wells. These non-steady conditions are addressed later in the transient analysis section.

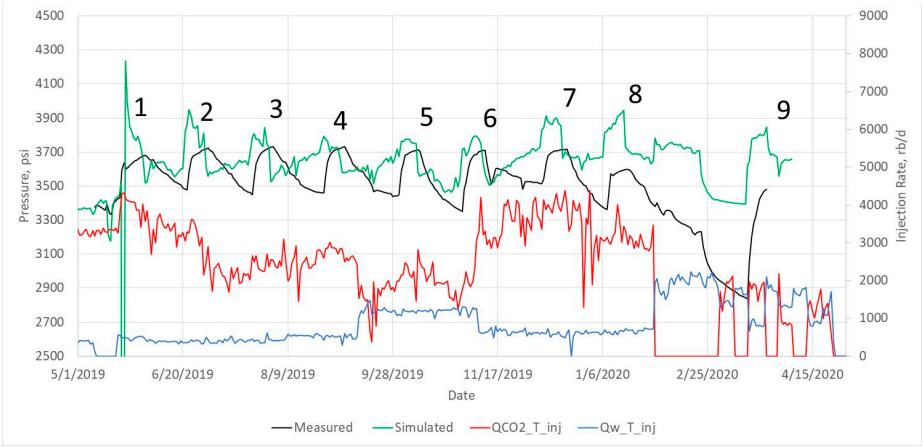

Figure 6. Total injection and BHP measured for the pilot study. The black curve shows the measured bottom-hole pressure data. The green curve shows simulated results from the base case model. Values for CO_2 and water injection rates (red and blue curves) are indicated on the secondary axis (rb/d).

9. Sensitivity Studies

Due to uncertainty in foam model parameters derived from laboratory data, sensitivity runs were set up to first test key foam model parameters. The following foam model parameters were adjusted for the sensitivity study:

- FMMOB: The reference mobility reduction factor;
- FMDRY: The limiting water saturation below which the foam is no longer effective;
- EPDRY: A weighting factor which controls the sharpness of the change in mobility;
- FOAMSO: The maximum oil saturation above which foam is no longer effective.

Table 4 shows the parameter ranges for the sensitivity study.

Table 4. Foam sensitivity parameters.

Simulation Run	FMMOB	FMDRY	EPDRY	FOAMFSO
Base Case	**192**	**0.4**	**84**	**0.28**
S1	92			
S2	19			
S3		0.45		
S4		0.35		
S5			42	
S6			168	
S7				0.18
S8				0.38

Figure 7 shows the sensitivity to foam strength parameters (FMMOB). As expected, the simulated pressures agreed better with the measured BHP, because the foam strength was controlled by the set FMMOB value. Sensitivity simulations for other foam parameters showed less of an impact; therefore, they are not shown here. These results clearly show that the foam was formed down-hole, and it was weaker than expected.

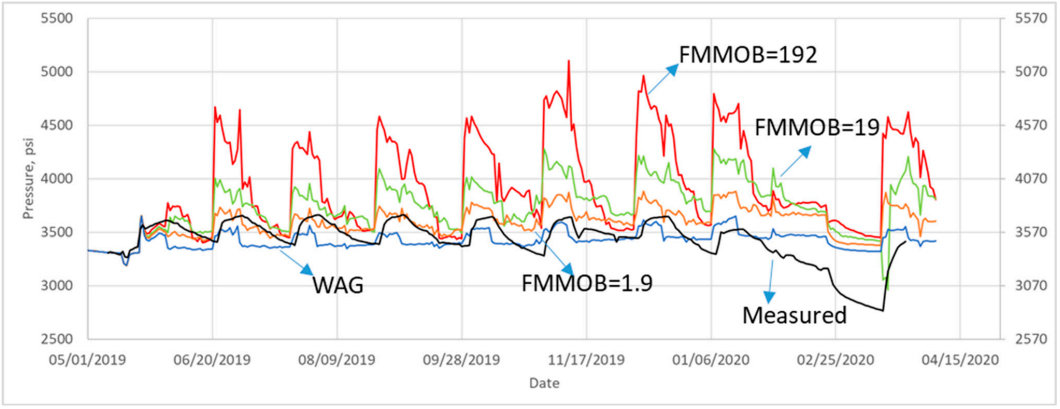

Figure 7. Simulated pressures using different foam strength parameters.

10. Transient Pressure Analysis

An alternative analysis was carried out using the pressure changes (instead of the absolute pressures) for each cycle. This analysis showed consistent results for both surfactant and CO_2 injection periods. Transient analysis represented a useful tool to analyze unsteady-state flow at the pilot injector. Figure 8 shows dP/dT over time for the first five SAG cycles. Delta pressure (dP) and delta temperature (dT) values were calculated by subtracting the absolute values from the last stabilized pressure and temperature before each injection cycle, a technique widely used in transient pressure analysis. Similarly, delta

t (dt) refers to the differential time from the start of a particular injection cycle. Differential pressure (dP) increased for each surfactant cycle, which may be related to a foam bank developing further into the reservoir. The dP values were in the order Cycle 1 < Cycle 2 < Cycle 3 < Cycle 4 < Cycle 5.

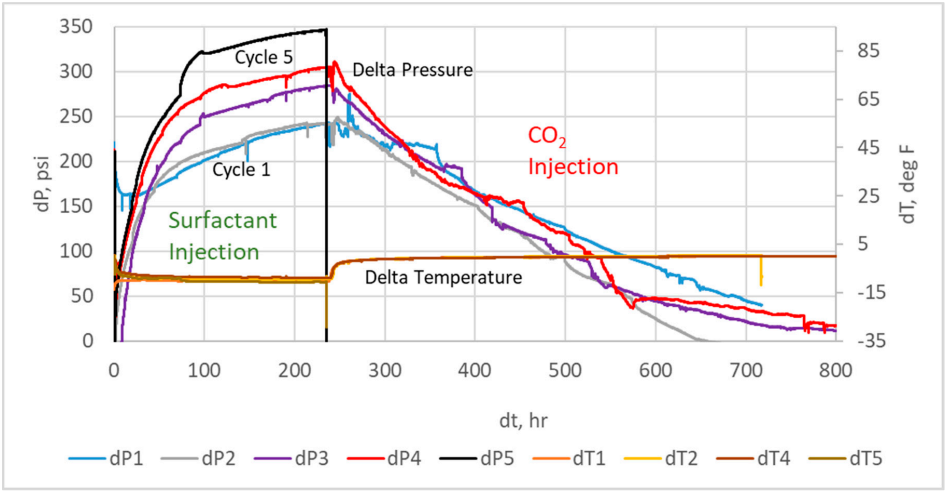

Figure 8. Transient pressures and temperatures for the first five SAG cycles. dP1 corresponds to slug 1, dP2 to slug 2, and so on.

The increased BHP during surfactant cycles could also be related to relative permeability and/or viscosity effects. A WAG was run at the end of the pilot to rule this out. As shown in Figure 9, the dP during the final SAG cycle (red curve) was higher than the dP observed during the final WAG (blue curve). The higher dP of the SAG cycles compared with the WAG indicated reduced the mobility during the SAG cycles and confirmed foam generation.

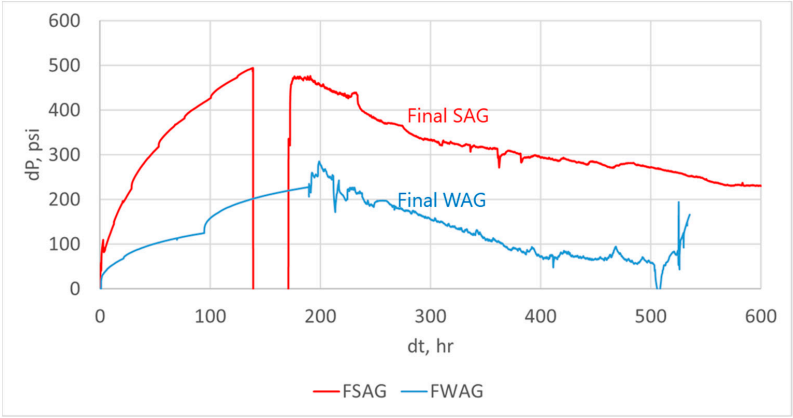

Figure 9. Transient bottom-hole pressure (dP) versus injection time (dt) for the final SAG cycle (red curve) and for the WAG cycle (blue curve).

The transient analysis was also applied to CO_2 injection periods independently. These results, along with the extended fall-off period, are shown in Figure 10.

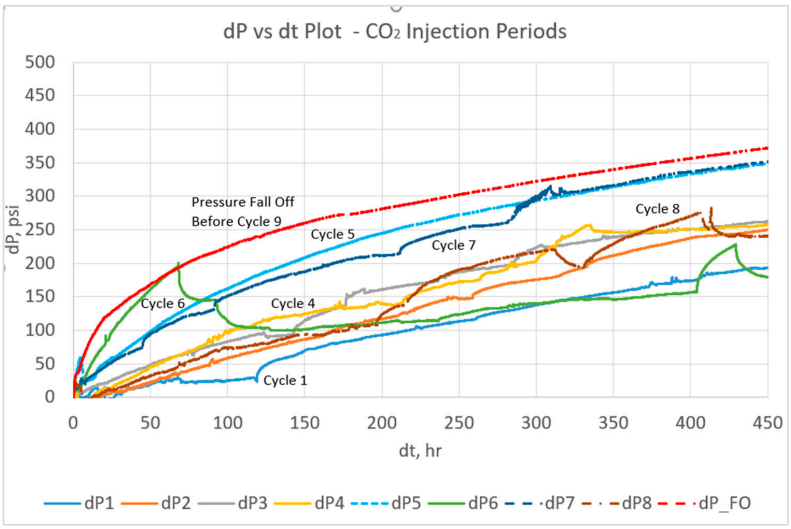

Figure 10. Transient analysis of CO_2 injection periods for the first 8 cycles. Additionally, the pressure fall-off results before Cycle 9 are shown.

11. Fall-Off Comparison

Due to operational reasons, the central injector was shut in for an extended period before Cycle 9. This created a fall-off test, which was also used to test different foam scenarios. Figure 11 shows the simulated results versus the measured dP/dT response during this fall-off period. As indicated, the simulated case with a lower FMMOB value (gray curve) followed the measured response more closely than the cases with higher mobility reduction (yellow and blue curves). In addition, the WAG case had a much lower pressure response, compared with the cases with foam and the observed data. This may indicate that a relatively weak foam was generated in the reservoir.

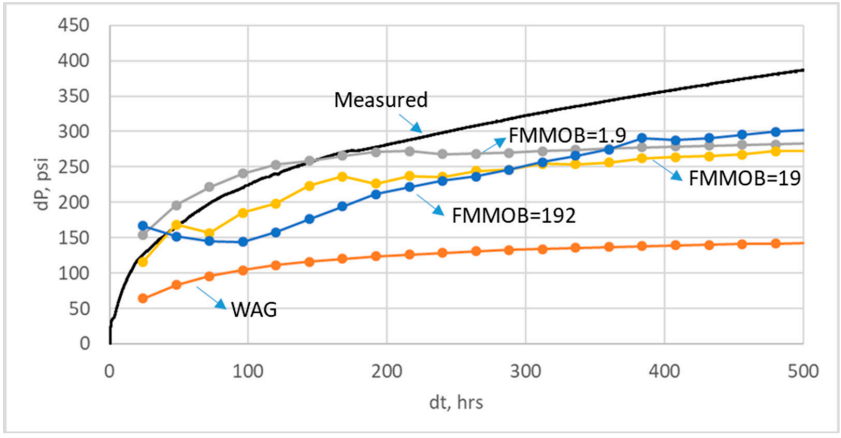

Figure 11. Simulated transient pressures during the fall-off period with different foam strength parameters.

12. Transient Surfactant and CO_2 Injection Comparisons

Transient data were also used to compare the model pressure response with the measured pressures during surfactant and CO_2 injection periods. These are shown in

Figures 12 and 13, respectively. These comparisons showed similar results to those observed during the fall-off period, suggesting weak foam strength.

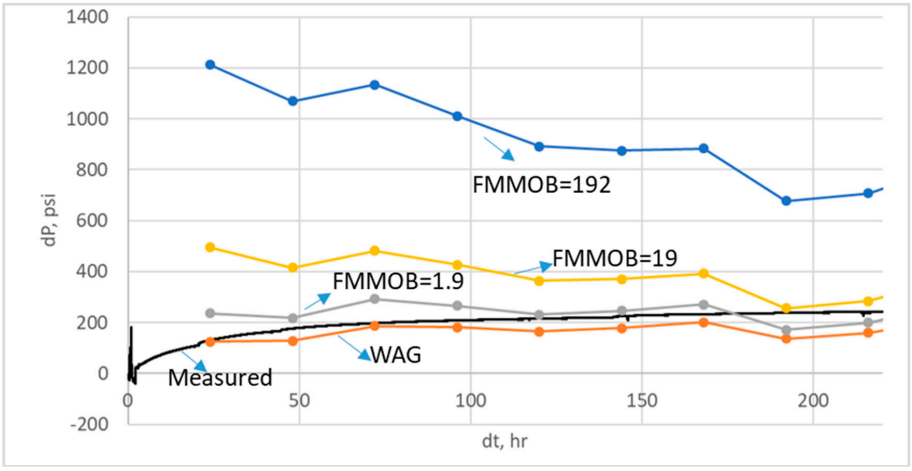

Figure 12. Simulated transient pressures of CO_2 injection during Cycle 2 with different foam strength parameters.

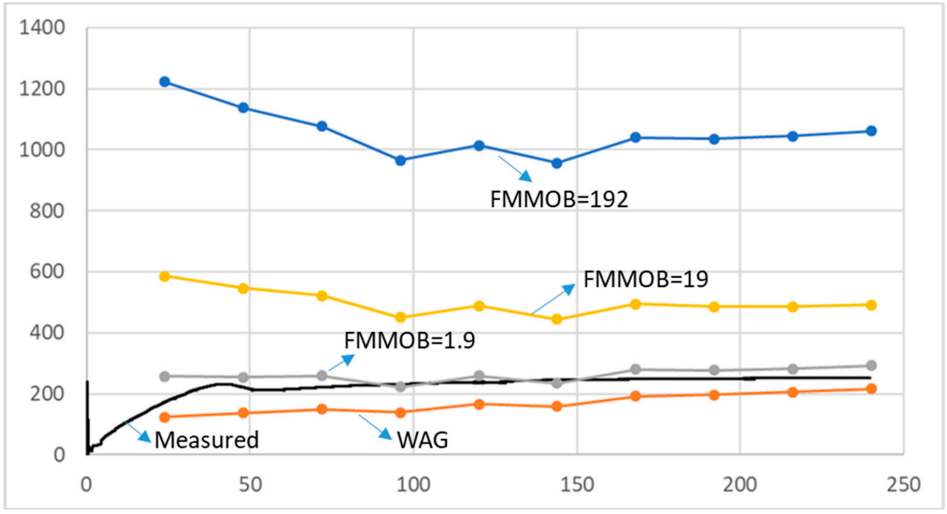

Figure 13. Simulated transient pressures of CO_2 injection during Cycle 8 with different foam strength parameters.

13. Foam Propagation

One of the important objectives of this study was to determine the foam propagation distance/rate if foam had formed. For this, a history-matched simulation model with tuned parameters was used. The simulator modeled foam as an effective concentration of surfactant transported in the gas (CO_2) phase. Figure 14 shows the simulated foam propagation for the weak foam case (FMMOB = 1.9) at the end of each surfactant/CO_2 cycle for Cycles 1, 5 and 8. These plots clearly indicate that foam had advanced deep in high-permeability layers during the pilot study.

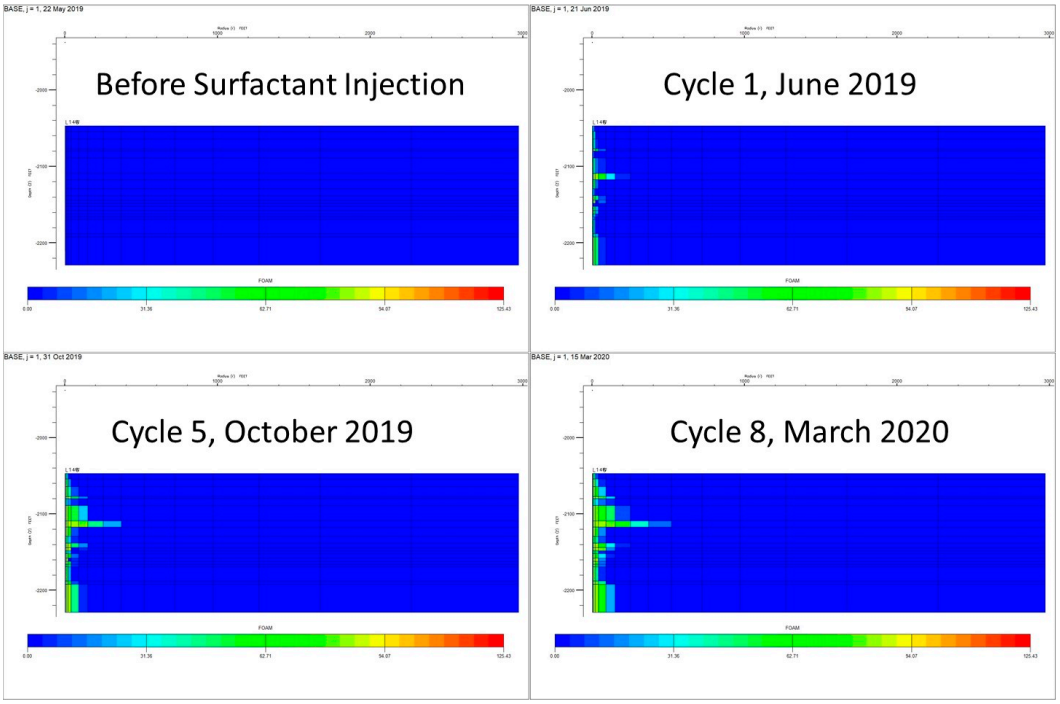

Figure 14. Cross-sectional (r-z) plot showing simulated foam concentrations for the weak foam case (FMMOB = 1.9) at the end of Cycles 1, 5 and 8.

14. Results and Discussion

The simulation model assuming the base case foam parameters for the SAG scenario gave significantly higher pressures than the measured pressures. This clearly shows that the simulated foam (or resistance) was stronger than that which occurred in reservoir conditions. The simulated WAG scenario (or no foam case) provided a lower bound for these pressures; therefore, based on the history-matched results, it could be concluded that the generated foam was weaker than expected.

Transient analysis showed that the temperature response was quite similar during all SAG cycles. On the other hand, differential pressures consistently increased during periods of surfactant injection and decreased during the subsequent CO_2 injection periods. The pressure increase (buildup) during surfactant injection clearly suggests the development of a mobility bank in the reservoir. Transient analysis also showed that the differential pressures during the SAG cycles were higher than the pressures observed during the WAG cycle. This revealed foam generation and reduced CO_2 mobility during this pilot development.

History matching using different foam parameters showed that a large reduction in the foam mobility reduction factor (FMMOB) was needed to match the measured bottomhole pressure data. Other foam parameters were also selectively adjusted, and results showed they had less of an impact on the overall pressure match. However, considering the non-unique nature of parameter estimation [28], the effects of these foam parameters should be addressed by more direct indicators of foam saturation, such as resistivity measurements [16].

The effectiveness of the foam could also be independently determined by improvements in the overall oil recovery against the base water/gas injection within the pilot area. A production analysis conducted after the pilot indicated a significant increase in both cumulative oil and water production compared to the baseline period before the pilot.

However, a large increase in water production was also observed, which may be related to a fracturing campaign conducted on pilot wells at the onset of the pilot. Therefore, no definite conclusions were drawn from this pilot with regard to the effectiveness of the foam based on the oil production increase.

15. Conclusions

In this study, we presented a novel technique to study the development of foam in reservoir conditions. The method was used to assess the effectiveness of CO_2 foam in a pilot study conducted in the East Seminole Field, Permian Basin, West Texas. In the selected pilot area, foam was utilized to reduce CO_2 mobility to improve sweep efficiency, oil recovery, and CO_2 storage potential. Injection pressure and temperature data were used to evaluate the reservoir response during various surfactant, CO_2 and water injection periods. Transient analyses were conducted for all SAG cycles, as well as one WAG cycle. A high-resolution two-dimensional radial flow model was used to history-match the measured differential pressures.

The radial model proved to be useful for assessing the reservoir foam strength during this pilot study. Although the pressure data alone may not be sufficient to describe the complex physics of in situ foam generation, this study shows that it is a strong indicator of foam strength. In this pilot, it appears that the reservoir foam strength was weaker than expected based on laboratory measurements.

The proposed method of transient analysis has been found to be quite useful in assessing the development and progression of foam in the reservoir. This analysis showed a consistent increase during all SAG cycles. In addition, differential pressures during the SAG periods were higher than those observed during a comparable WAG cycle. This revealed foam generation and reduced CO_2 mobility during the pilot. Based on the detailed comparisons and the transient analysis of measured bottom-hole pressure data, it could be concluded that foam was generated down-hole. However, the history-matched foam model was weaker than that expected based on laboratory studies.

Sensitivity studies show that the foam mobility reduction factor (FMMOB) is the most dominant parameter. Based on the history-matched model simulations, it could be concluded that the foam significantly advanced in high-permeability layers during this pilot study.

Author Contributions: Conceptualization, M.K., Z.P.A. and A.G.; methodology, M.K.; software, M.K. and Z.P.A.; validation, M.K. and Z.P.A.; formal analysis, M.K.; investigation, M.K. and Z.P.A.; resources, A.G.; data curation, M.K. and Z.P.A.; writing—original draft preparation, M.K. and Z.P.A.; writing—review and editing, M.K.; visualization, M.K. and Z.P.A.; supervision, A.G. and F.A.; project administration, A.G.; funding acquisition, A.G. All authors have read and agreed to the published version of the manuscript.

Funding: This research was funded by The Norwegian Research Council grant number 249742.

Institutional Review Board Statement: Not applicable.

Informed Consent Statement: Not applicable.

Data Availability Statement: Not applicable.

Acknowledgments: The authors acknowledge their industry partners: Shell Global Solutions, TOTAL E&P USA, Equinor ASA, and Occidental Petroleum. The authors also thank the field operator.

Conflicts of Interest: The authors declare no conflict of interest.

Nomenclature

f_g	Gas fraction or foam quality
cP	Centipoise
K	Permeability
mD	Millidarcy
MPa	Megapascal
Psig	Pound per square inch, gauge
Mscf	Thousand standard cubic feet
^0API	American Petroleum Institute gravity
rb/day	Reservoir barrels per day
Mscf/day	Thousand standard cubic feet per day
S_{or}	Residual oil saturation, fraction of pore volume
fmmob	Foam model, maximum gas mobility reduction factor
fmdry	Foam model parameter in Fwater
epdry	Foam model parameter in Fwater
fmsurf	Foam model parameter in Fsurf
epsurf	Foam model parameter in Fsurf
FM	Foam model, mobility reduction factor
$k_{rg}{}^{nf}$	Gas relative permeability with no foam

Abbreviations

CCUS	Carbon capture, utilization, and storage
CCS	Carbon capture and storage
EOR	Enhanced oil recovery
SAG	Surfactant-alternating gas
WAG	Water-alternating gas
DHPG	Down-hole pressure gauge
BHP	Bottom-hole pressure
MPZ	Main producing zone
ROZ	Residual oil zone
BT	Breakthrough
Wt %	Weight percentage
GOR	Gas/oil ratio
MRF	Mobility reduction factor
IWTT	Interwell CO_2 tracer test
PV	Pore volume

SI Metric Conversion Factors	
Acre × 4.046873	E + 03 = m^2
°API 141.5/(131.5 + °API)	= g/cm^3
bbl × 1.589873	E − 01 = m^3
cp × 1.0	E − 03 = Pa·s
°F (°F − 32)/1.8	= °C
ft × 3.048	E − 01 = m
psi × 6.894757	E + 00 = kPa

References

1. Enick, R.M.; Olsen, D.K.; Ammer, J.R.; Schuller, W. Mobility and Conformance Control for CO2 EOR via Thickeners, Foams, and Gels—A Literature Review of 40 Years of Research and Pilot Tests; SPE-154122-MS. In Proceedings of the SPE Improved Oil Recovery Symposium, Tulsa, OK, USA, 14–18 April 2012. [CrossRef]
2. Heller, J.P. Onset of Instability Patterns between Miscible Fluids in Porous Media. *J. Appl. Phys.* **1966**, *37*, 1566–1579. [CrossRef]
3. Heller, J.P.; Boone, D.A.; Watts, R.J. Field Test of CO2-Foam Mobility Control at Rock Creek; SPE-14395. In Proceedings of the SPE 60th Annual Technical Conference and Exhibition, Las Vegas, NV, USA, 22–25 September 1985.
4. Chou, S.I.; Vasicek, S.L.; Pisio, D.L.; Jasek, D.E.; Goodgame, J.A. CO_2 Foam Field Trial at North Ward Estes. In Proceedings of the 67th SPE Annual Technical Conference and Exhibition, Washington, DC, USA, 4–7 October 1992.

5. Martin, F.D.; Heller, J.P.; Weiss, W.W.; Tsau, J.S. CO2-Foam Field Verification Pilot Test at EVGSAU Injection Project Phase 1: Project Planning and Initial Results; SPE/DOE-24176. In Proceedings of the SPE Improved Oil Recovery Conference, Tulsa, OK, USA, 22–24 April 1992.
6. Hoefner, M.L.; Evans, E.M. CO_2 Foam: Results from Four Developmental Field Trials. *SPE Reserv. Eng.* **1995**, *10*, 273–281. [CrossRef]
7. Martin, F.D.; Stevens, J.E.; Harpole, K.J. CO_2-Foam Field Test at the East Vacuum Grayburg/San Andres Unit. *SPE Reserv. Eng.* **1995**, *10*, 266–272. [CrossRef]
8. Leeftink, T.N.; Latooij, C.A.; Rossen, W.R. Injectivity errors in simulation of foam EOR. *J. Pet. Sci. Eng.* **2015**, *126*, 26–34. [CrossRef]
9. Rossen, W.R. Foams in Enhanced Oil Recovery. In *Foams Theory, Measurements, and Applications*; Prud'homme, R.K., Khan, S.A., Eds.; Marcel Dekker, Inc.: New York, NY, USA, 1996; Volume 57, Chapter 11; pp. 414–464.
10. Falls, A.H.; Hirasaki, G.J.; Patzek, T.W.; Gauglitz, D.A.; Miller, D.D.; Ratulowski, T. Development of a Mechanistic Foam Simulator: The Population Balance and Generation by Snap-Off. *SPE Reserv. Eng.* **1988**, *3*, 884–892. [CrossRef]
11. Schramm, L.L. *Foams: Fundamentals and Applications in the Petroleum Industry*; American Chemical Society: Washington, DC, USA, 1994.
12. Jian, G.; Zhang, L.; Da, C.; Puerto, M.; Johnston, K.P.; Biswal, S.L.; Hirasaki, G.J. Evaluating the Transport Behavior of CO_2 Foam in the Presence of Crude Oil under High-Temperature and High-Salinity Conditions for Carbonate Reservoirs. *Energy Fuels* **2019**, *33*, 6038–6047. [CrossRef]
13. Rognmo, A.; Heldal, S.; Fernø, M. Silica nanoparticles to stabilize CO2-foam for improved CO_2 utilization: Enhanced CO2 storage and oil recovery from mature oil reservoirs. *Fuel* **2018**, *216*, 621–626. [CrossRef]
14. Haroun, M.; Mohammed, A.M.; Somra, B.; Punjabi, S.; Temitope, A.; Yim, Y.; Anastasiou, S.; Abu Baker, J.; Haoge, L.; Al Kobaisi, M.; et al. Real-Time Resistivity Monitoring Tool for In-Situ Foam Front Tracking. In Proceedings of the Abu Dhabi International Petroleum Exhibition & Conference, Abu Dhabi, United Arab Emirates, 13 November 2017. [CrossRef]
15. Gargar, N.K.; Mahani, H.; Rehling, J.G.; Vincent-Bonnieu, S.; Kechut, N.I.; Farajzadeh, R. Fall-Off Test Analysis and Transient Pressure Behavior in Foam Flooding. In Proceedings of the IOR 2015-18th European Symposium on Improved Oil Recovery. European Association of Geoscientists & Engineers, Dresden, Germany, 16 April 2015.
16. Karakas, M.; Aminzadeh, F. Optimization of CO_2-Foam Injection through Resistivity and Pressure Measurements. In Proceedings of the SPE Western Regional Meeting, Garden Grove, CA, USA, 22 April 2018. [CrossRef]
17. Alcorn, Z.P.; Fredriksen, S.B.; Sharma, M.; Rognmo, A.U.; Føyen, T.L.; Fernø, M.; Graue, A. An Integrated Carbon-Dioxide-Foam Enhanced-Oil-Recovery Pilot Program with Combined Carbon Capture, Utilization, and Storage in an Onshore Texas Heterogeneous Carbonate Field. *SPE Reserv. Eval. Eng.* **2019**, *22*, 1449–1466. [CrossRef]
18. Alcorn, Z.P.; Føyen, T.; Zhang, L.; Karakas, M.; Biswal, S.L.; Hirasaki, G.; Graue, A. CO_2 Foam Field Pilot Design and Initial Results; SPE-200450-MS. In Proceedings of the SPE Improved Oil Recovery Conference 2020, Virtual, 30 August 2020.
19. Rognmo, A.U.; Fredriksen, S.B.; Alcorn, Z.P.; Sharma, M.; Føyen, T.; Eide, G.A.; Fernø, M. Pore-to-Core EOR Upscaling for CO_2 Foam for CCUS. *SPE J.* **2019**, *24*, 2793–2803. [CrossRef]
20. Ma, K.; Lopez-Salinas, J.L.; Puerto, M.C.; Miller, C.A.; Biswal, S.L.; Hirasaki, G.J. Estimation of Parameters for the Simulation of Foam Flow through Porous Media. Part 1: The Dry-Out Effect. *Energy Fuels* **2013**, *27*, 2363–2375. [CrossRef]
21. Sharma, M.; Alcorn, Z.; Fredriksen, S.; Fernø, M.; Graue, A. Numerical Modeling Study for Designing CO_2-foam Field Pilot. In Proceedings of the IOR 2017—19th European Symposium on Improved Oil Recovery, Stavanger, Norway, 24 April 2017. [CrossRef]
22. Sharma, M.; Alcorn, Z.P.; Fredriksen, S.B.; Rognmo, A.U.; Ferno, M.A.; Skjaeveland, S.M.; Graue, A. Model calibration for forecasting CO_2-foam EOR field pilot performance in a carbonate reservoir. *Pet. Geosci.* **2019**, *26*, 141–149. [CrossRef]
23. Zeng, Y.; Muthuswamy, A.; Ma, K.; Wang, L.; Farajzadeh, R.; Puerto, M.; Vincent-Bonnieu, S.; Eftekhari, A.A.; Wang, Y.; Da, C.; et al. Insights on Foam Transport from a Texture-Implicit Local-Equilibrium Model with an Improved Parameter Estimation Algorithm. *Ind. Eng. Chem. Res.* **2016**, *55*, 7819–7829. [CrossRef]
24. Rossen, W.R.; Zeilinger, S.C.; Shi, J.-X.; Lim, M.T. Simplified Mechanistic Simulation of Foam Processes in Porous Media. *SPE J.* **1999**, *4*, 279–287. [CrossRef]
25. Cheng, L.; Reme, A.; Shan, D.; Coombe, D.; Rossen, W. Simulating Foam Processes at High and Low Foam Qualities; SPE-59287-MS. In Proceedings of the SPE/DOE Improved Oil Recovery Symposium, Tulsa, OK, USA, 3 April 2000. [CrossRef]
26. Farajzadeh, R.; Andrianov, A.; Krastev, R.; Hirasaki, G.; Rossen, W. Foam–oil interaction in porous media: Implications for foam assisted enhanced oil recovery. *Adv. Colloid Interface Sci.* **2012**, *183–184*, 1–13. [CrossRef] [PubMed]
27. Law, D.H.S.; Yang, Z.M.; Stone, T.W. Effect of the Presence of Oil on Foam Performance: A Field Simulation Study; SPE-18421-PA. *SPE Reserv. Eng.* **1992**, *7*, 228–236. [CrossRef]
28. Ma, K.; Farajzadeh, R.; Lopez-Salinas, J.L.; Miller, C.A.; Biswal, S.L.; Hirasaki, G.J. Non-uniqueness, Numerical Artifacts, and Parameter Sensitivity in Simulating Steady-State and Transient Foam Flow through Porous Media. *Transp. Porous Media* **2014**, *102*, 325–348. [CrossRef]

Global Journal of Researches in Engineering: J
General Engineering
Volume 22 Issue 2 Version 1.0 Year 2022
Type: Double Blind Peer Reviewed International Research Journal
Publisher: Global Journals
Online ISSN: 2249-4596 & Print ISSN: 0975-5861

CO_2-Foam Monitoring using Resistivity and Pressure Measurements

By Metin Karakas, Fred Aminzadeh & Arne Graue
University of Bergen

Abstract- This paper focuses on combining resistivity and pressure measurements to determine the effectiveness of foam as a mobility control method. It presents a theoretical framework to describe the expected resistivity changes during CO_2-foam displacements. With this objective, we first provide equations to estimate the resistivity for CO_2-foam systems and then utilize two distinct foam models to quantify these effects. Using analytical solutions based on the fractional flow theory, we present resistivity and mobility distributions for ideal and non-ideal reservoir displacement scenarios. Additionally, assuming pressure measurements only, we examine the inter-dependency between various foam parameters. Our results suggest that the combination of pressure and resistivity measurements in time-lapse mode could be deployed as an effective monitoring tool in field applications of the (CO_2) foam processes. The proposed method is novel as it could be employed to predict under-performing CO_2-foam floods and improve oil recovery and CO_2 storage.

GJRE-J Classification: DDC Code: 620 LCC Code: TP1183.F6

Strictly as per the compliance and regulations of:

CO_2-Foam Monitoring using Resistivity and Pressure Measurements

Metin Karakas [α], Fred Aminzadeh [σ] & Arne Graue [ρ]

Abstract- **This paper focuses on combining resistivity and pressure measurements to determine the effectiveness of foam as a mobility control method. It presents a theoretical framework to describe the expected resistivity changes during CO_2-foam displacements. With this objective, we first provide equations to estimate the resistivity for CO_2-foam systems and then utilize two distinct foam models to quantify these effects. Using analytical solutions based on the fractional flow theory, we present resistivity and mobility distributions for ideal and non-ideal reservoir displacement scenarios. Additionally, assuming pressure measurements only, we examine the inter-dependency between various foam parameters. Our results suggest that the combination of pressure and resistivity measurements in time-lapse mode could be deployed as an effective monitoring tool in field applications of the (CO_2) foam processes. The proposed method is novel as it could be employed to predict under-performing CO_2-foam floods and improve oil recovery and CO_2 storage.**

I. Introduction

Time-lapse seismic, resistivity, electromagnetic (EM), and pressure measurements have been used in the oil industry for water and CO_2 flooding and monitoring applications. For example, see: Passalacqua et al (2018), Davydycheva and Strack (2018) and Strack(2014). CO_2 foam injection is an effective method to control mobility during CO_2-Enhanced Oil Recovery processes in petroleum reservoirs. When it is done optimally, CO_2 foam can improve sweep efficiency, oil production, and CO_2 storage (Kuuskraaet al., 2006, Fernoet al., 2014). Laboratory studies show that foam strength is essential to achieve the desired reservoir efficiency. It has been demonstrated that the foam density is a direct function of the density of the lamellae (Kovscek and Radke, 1994). Additionally, the solubility of surfactant in CO_2 and water phases, as well as the adsorption of CO_2 on the rock, play a crucial role in these displacements. At a given reservoir temperature, the partitioning of the CO_2 soluble surfactants is dependent on pressure and strongly influenced by the attractiveness (CO_2-philicity) of the selected surfactant for foam application. Recent research indicates that various (cationic, nonionic, and zwitterionic) surfactants as the leading candidates for CO_2 foams. It is also critical to maintaining the foam strength for the entire injection period during reservoir applications. Additionally, the CO_2 mobility is higher than that of the foam, and under certain conditions, this can lead to less-than-optimal displacement in porous media.

Foam monitoring has been restricted to electrokinetic (streaming potential) measurements (Omar et al., 2013). Wo et al. (2012) ran foam experiments on unsaturated soil samples and investigated the possibility of using electrical measurements for foam monitoring. Of course, it should be realized that foam and CO_2 are charged. They connect and eventually build larger molecules. We need boundary to develop a bouble layer for charges to collect. Wo et al. (2012) reported significant changes in electrical properties with foam formation.

Karakas and Aminzadeh (2017) proposed time-lapse measurements with an array of permanently deployed sensors to detect the movement of the foam-CO_2-Oil interface in the reservoir due to CO_2-foam injection. With the proposed method, resistivity and pressure measurements are acquired simultaneously during the CO_2-foam Injection into reservoir, as shown in Fig. 1.

Author α ρ: University of Bergen, Norway.
Author σ: FACT Inc., United States. e-mail: metin.karakas@uib.no

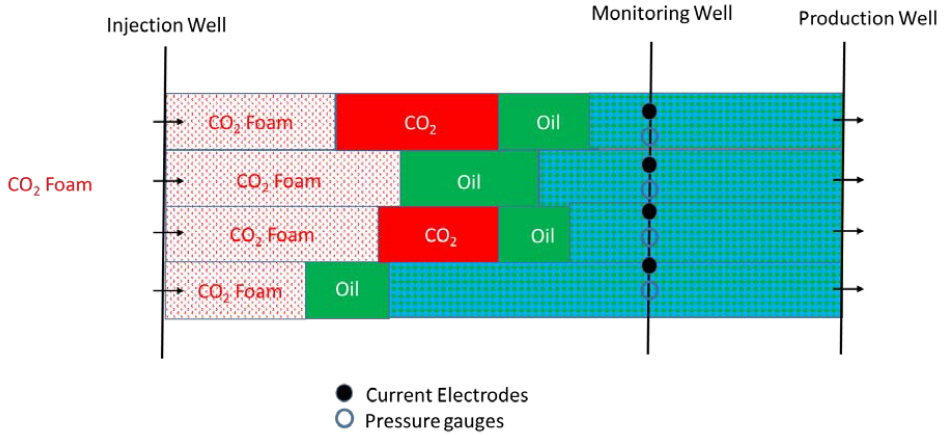

Fig. 1: Example of pressure and resistivity monitoring during a CO_2 Foam flood (Karakas and Aminzadeh, 2017).

In the proposed method by Karakas and Aminzadeh (2017), resistivity and pressure measurements are used to determine the effectiveness of foam as a mobility control method and hence, provide a way to remedy any under-performing foam (and CO_2-foam) floods to improve both oil recovery and CO_2 storage. This monitoring is crucial for applying foam (and CO_2 foam) in reservoirs where heterogeneity is involved. Figure 2 below illustrates this optimization process.

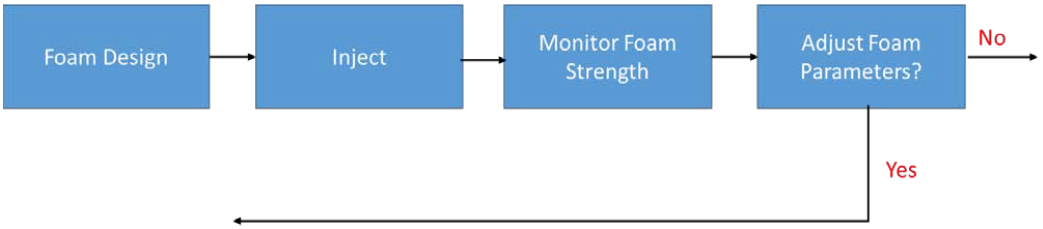

Fig. 2: Foam (and CO_2-Foam) optimization process (Karakas and Aminzadeh, 2017).

In terms of laboratory studies, Berge (2017) conducted resistivity measurements while injecting CO_2 and surfactant solution into saturated cores and Haroun et al. (2017) monitored resistivity and pressure changes during foam generation in the formation-brine saturated carbonate core plug samples. Haroun et al. (2017) reported significant increases in resistivity and pressure with foam development.

The main thrust of this paper is to the characterize the resistivity response and to present a theoretical foundation for resistivity monitoring during CO_2 foam displacements.

II. CO_2 Foam Transport Modeling

The transport of CO_2 foam can be described by several methods (Ma, K. et al., 2015). These include:

- Pore-network models
- Analytical methods
- Explicit population-based equation (PBE) methods
- Implicit foam methods

Pore-Network models provide a good insight into foam transport and are not yet practical for reservoir-scale applications. In this study, we focus on the Analytical and the explicit (or Population Based) methods. The analytical approach is based on the fractional-flow theory and steady-state foam development, as presented by Ashoori et al. (2010). The main assumptions are as follows:

- One-dimensional flow.
- Initially, the reservoir is at residual oil saturation (S_{or}) after waterflooding.
- CO_2 is injected at supercritical conditions.
- First-Contact Miscible (FCM) displacement of oil by the injected supercritical CO_2.
- The relative permeability depends on water saturation and the oil or CO_2 saturations.
- Foam effects are captured implicitly using steady-state assumption.

As demonstrated by Ashoori et al. (2010), there are two different solutions: the first one relates to an

ideal CO_2-foam displacement where the miscible (CO_2) and surfactant (foam) fronts travel at the same speed. In this case, three separate banks develop in the reservoir: Foam or surfactant (CO_2 plus water) bank, oil (with mobile water) bank, and water (with residual oil) bank. The second solution assumes a non-ideal CO_2-foam displacement. In this case, due to adsorption of the injected surfactant to the rock and its partitioning to the water phase, the foam front slows down, and the miscible (CO_2) front moves ahead of it. In this case, a separate CO_2 bank forms ahead of the foam (or surfactant) bank, which gives rise to an unfavorable mobility distribution in the reservoir. These reconstructed saturation profiles are provided in Appendix A. The fractional flow approach is based on the steady-state assumption and cannot capture the transient foam development during CO_2 foam injection (Kam S.I.,2008).

III. Population-Balance Method

In the Population Based (PBE) method, foam effects are captured explicitly by quantifying the bubble population (n_f) and correlating it to the foam mobility. In this work, we utilized the solution approach provided by Kam and Rossen (2003). The relevant foam equations are provided in Appendix B. Please note that this solution is based on the two-phase (CO_2 and water) flow, and the oil phase is ignored. This assumption is in line with most experimental work and gives good insight into foam development in porous media (Kam et al., 2004, Prigiobbe et al., 2016).

The solution of the PBE, due to nonlinear relations between injection rate and pressure gradient, is quite complex and may not be unique (Dholhawala, Z.F. et al., 2007). In this work, a numerical approach was taken for solving the transient foam equations. With this objective, a numerical foam simulator (FoamSim) was developed, in which upstream weighting was utilized to minimize the numerical dispersion effects. The numerical model was validated by comparing its results with that of Kam et al. (2004). These comparisons were made for both weak and strong foam states.

IV. Parameter Estimation using Pressure Measurements

One of the crucial considerations is the uniqueness of the model parameters obtained from pressure measurements. For this reason, we analyzed the inter dependency between various foam parameters. These included foam generation parameters (C_g & m), foam coalescence parameters (C_c& n), and the foam viscosity parameter (C_f). For this purpose, we utilized the published CO_2foam experiments by Prigiobbe et al. (2016). The foam parameters for these history matched experiments are as follows:

Table 1: Model Parameters used for Foam Simulations (From Prigiobbe et al., 2016).

	C_f	C_g	C_c	M	n	S_w*
Experiment 6	1.58E-15	3.02E+07	3.02E-01	0.588	0.73	0.121
Experiment 34	3.31E-17	3.72E+06	9.55E-03	1.140	0.29	0.01

We first ran forward simulations using FoamSim and compared our results with those of Prigiobbe et al. Two experiments (6 & 34) produced very similar (but not exact) results. The graph below shows the comparison for Experiment 6 using parameters from the table above.

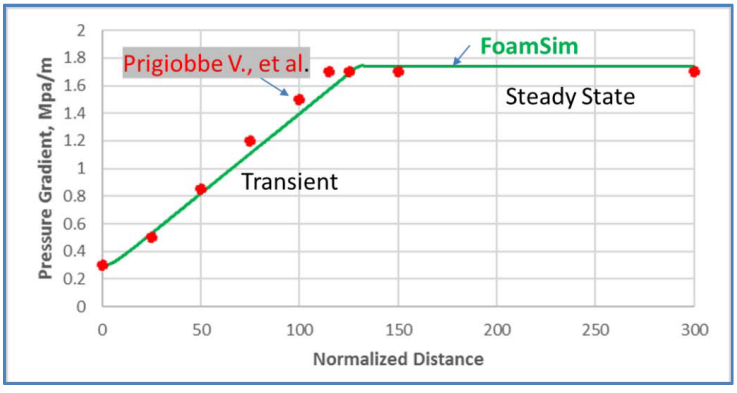

Fig. 3: Comparison of pressure gradients (experiment number 6).

The relevant sensitivity coefficients were generated using our numerical solver (FoamSim), and for experiments 6 and 34 and the duration of the lab experiments. In this analysis, the following parameters were considered:

$$X = \text{foam parameters } [C_g, C_c, C_f, m, n] \quad (1)$$

For most high-permeability systems, the critical water saturation (S_w^*) is relatively small. Therefore, due to potential numerical problems, it was not included in the analysis. In the calculations of sensitivity coefficients, we used the log transformation for all the foam parameters:

$$C_g' = \log_{10}(C_g) \quad (2)$$

The following plot shows the calculated sensitivity coefficients using data from experiment number 6:

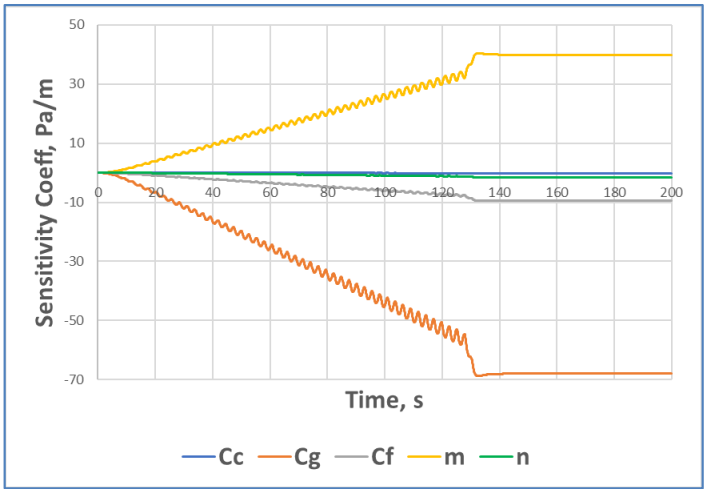

Fig. 4: Sensitivity coefficients for foam parameters (experiment number 6).

We also normalized sensitivity coefficients for an even comparison and calculated the determinant of the sensitivity matrix to examine the (ill) conditioning of the inverse problem. The determinant (d) is a function of time and is defined as follows:

$$d = [S^T S] \quad (3)$$

These calculations showed that the magnitude of the determinant increased with time (with more measurement samples):

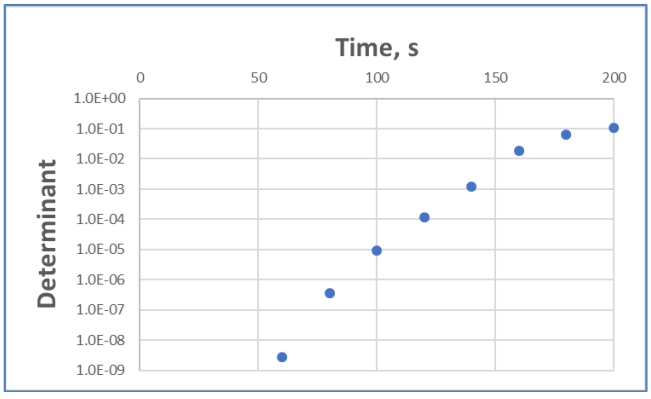

Fig. 5: Determinant of the sensitivity matrix.

We also calculated the determinant using the steady-state portion of the measurements only. For steady-state flow, the determinant became very small, which indicates a linear dependency between the selected foam parameters (Appendix B). This examination showed the following:

- Foam generation parameters, C_g & m, have by far the highest sensitivity.
- Foam viscosity coefficient, C_f, is of the middle rank.
- Foam coalescence parameters, C_c & n, have relatively less sensitivity.
- Linear independence is possible with transient data.
- Steady-State pressure measurements give rise to an ill-conditioned parameter estimation problem and the grouping of parameters is necessary.

V. CO_2 Foam Resistivity Characteristics and Modeling

Typically, nonionic surfactants are dissolved in the CO_2 phase, and the foam generation occurs in situ when injected the CO_2 plus surfactant meets the formation brine. CO_2 is highly resistive, whereas the thin water film is conductive (depending on the salinity of the in-situ reservoir fluid). During foam injection, these films enhance the electrical conductivity. With growing bubble size, these conduits become less effective, and overall, the resistivity of the foam system increases. However, with CO_2 injected brine already resistive this will only produce more resistive fluid. Reduction in resistivity will come from higher electron flow and resistivity reduction caused by pressure changes. See Boerner et al (2015) on electrical conductivity of CO_2-bearing pore waters at elevated pressure and temperature.

Assuming a uniform and hexagonal-prism shape foam, the foam conductivity σ_f is obtained using the Lemlich Relation (Lemlich, R., 1985):

$$K = \frac{D}{3} \tag{4}$$

Where K is the bulk foam conductivity. This relationship can also be written as follows:

$$K = \frac{\text{conductivity of dispersion}}{\text{conductivity of continous phase}} = \frac{\sigma_f}{\sigma_s} \tag{5}$$

Where D is the volumetric liquid fraction or = (1-X_f), and X_f is the foam quality. Using these relationships, we obtain:

$$\sigma_f = \frac{1}{3}\sigma_s\,(1 - X_f) \tag{6}$$

or another expression would be:

$$\sigma_f = c_1 * \sigma_s * (1\text{-}S_{co2}^f) \tag{7}$$

where:

c_1 = constant

S_{co2}^f = CO_2 saturation with foam

σ_s = conductivity of the thin film around bubbles

Assuming, σ_s = 1.0 S/m and X_f = 0.90 (foam quality), we obtain the following values for foam conductivity:

σ_f = 0.033 S/m (foam conductivity) or R_f = 30 ohm.m (foam resistivity)

These results suggest that foam conductivity will be order of (1 to 2) higher compared to that of the CO_2 phase only.

We propose to scale the foam conductivity with foam density as follows:

$$\sigma_f = c1\ \sigma_s\,(1\text{-}S_{co2}^f)\,(\frac{n_f}{n_{fmax}}) \tag{8}$$

where n_{fmax} is the maximum population density.

For a CO_2-Water system, lab results show that Archie's equation provides a reasonable approximation (Bergmannet al., 2013). Assuming a CO_2-Foam-Water system, the total system conductivity was calculated by utilizing the mixing law (Appendix D):

$$\sigma=\phi^2\,[S_{co2}^f\sigma_f{}^{½} + S_w\sigma_w{}^{1/2}]^{\,2} \tag{9}$$

Laboratory measurements using carbonate cores from Abu Dhabi (Harounet al., 2017) show a sharp increase in resistivity and a large pressure drop with the formation of foam during these high-temperature and high-pressure core floods. These experimental results are in line with the theoretical results provided here.

The difference between foam and CO_2 saturated reservoir depends on how much CO_2 is absorbed by the brine. However, strictly speaking, volumetrics are empirical correlations and do not often work for resistivity due to non-linearity of Archie. With fracture we increase complexity even further.

a) Resistivity Profiles

Using the simulated saturation and the foam densities, we can now estimate the resistivity (along with relative mobility) evolution during the CO_2-Foam displacements. For these simulations, we assumed the following bulk conductivities for water, CO_2, foam, and oil phases:

Table 2: Parameters Used For Resistivity Simulations

σ_w	5.00	S/m
σ_{CO2}	0.001	S/m
σ_f	0.100	S/m
σ_{oil}	0.001	S/m

The figure below shows the resistivity profile from one dimensional CO_2 foam flood assuming a moderately conductive water scenario. The resistivity profile has been calculated using the simulated foam densities from the FoamSim simulator, and the CO_2 foam resistivity model. To avoid using canonical resistivity values one would in practice scale the surface measurements to the borehole scale as shown by Strack et al (2022).

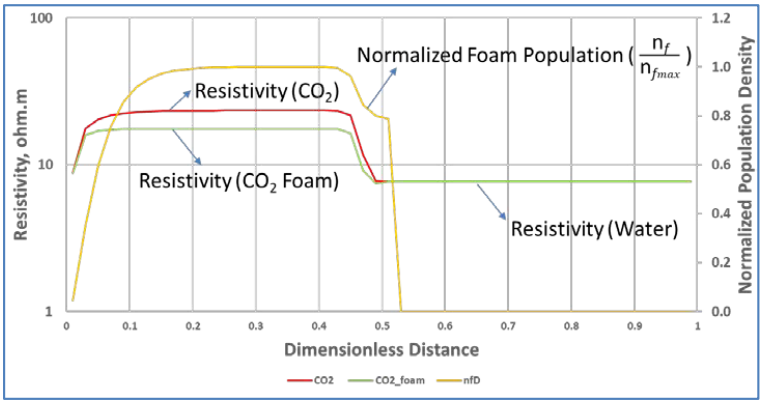

Fig. 6: Calculated resistivity profile during CO_2-Foam injection (PBE Solution).

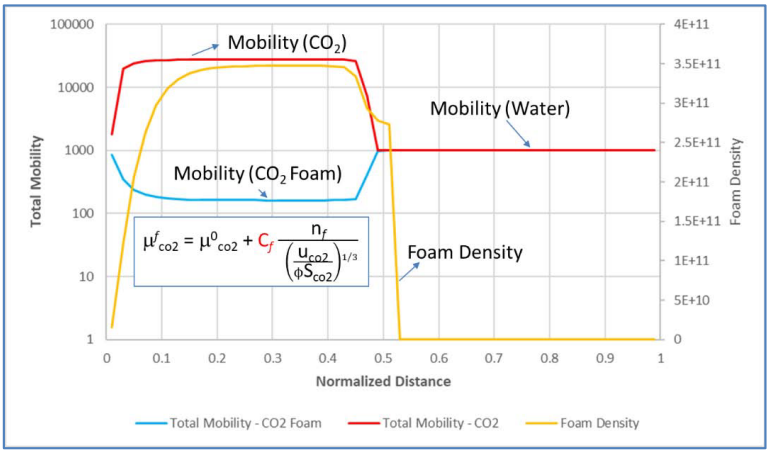

Fig. 7: Combined resistivity and mobility profile during CO_2-Foam injection (PBE Solution).

b) Resistivity Profiles – CO_2 Foam Displacement with Oil

The resistivity calculations for the CO_2 foam with oil were also made for CO_2-foam displacement with oil. For this model, the mobility effects were calculated using the steady-state assumption as outlined in Appendix A. The resistivity calculations were made assuming similar bulk conductivities as given in Table 2. The figures below show the calculated resistivity profiles for both ideal as well as non-ideal foam displacements:

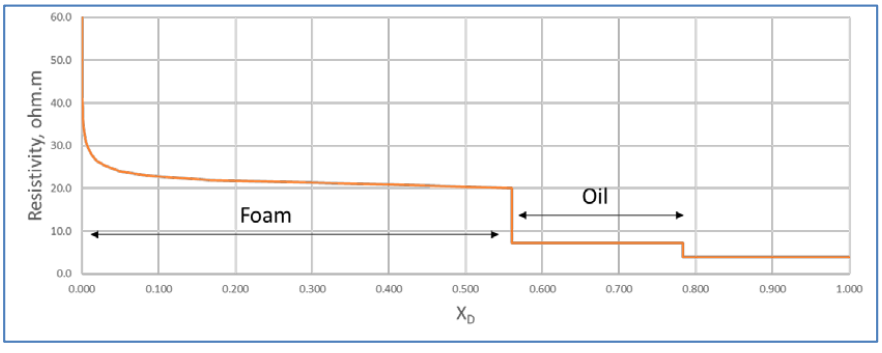

Fig. 8: Resistivity profile during ideal CO_2-Foam displacement.

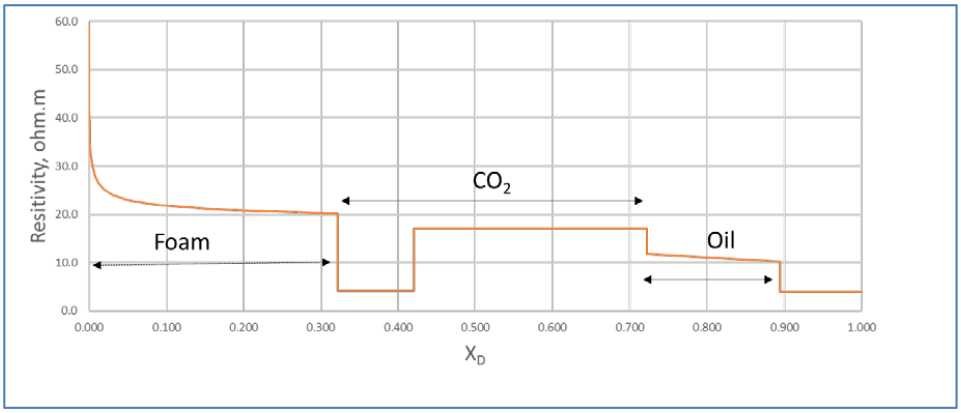

Fig. 9: Resistivity profile during non-deal CO_2-Foam displacement.

The figures below show the mobility distribution along with the resistivity profiles.

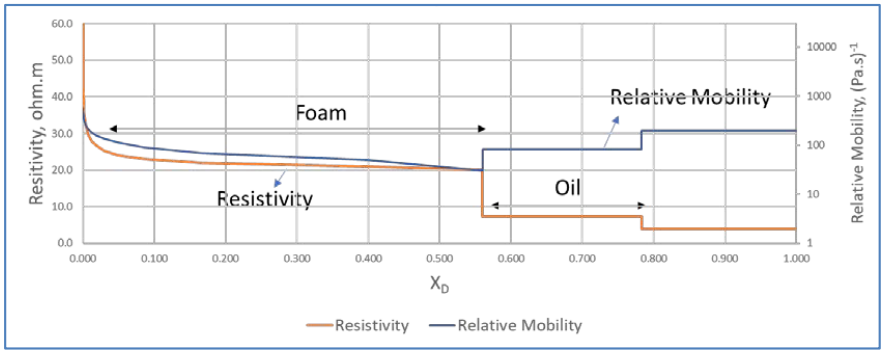

Fig. 10: Combined resistivity and mobility profile during CO_2-Foam injection (analytical Solution – ideal displacement).

As seen in Fig. 10, the resistivity profile during ideal displacement is like the PBE simulations shown earlier, and both models suggest a sharp resistivity contrast at the foam front. On the other hand, for non-ideal displacements, the resistivity profile is quite different. During these displacements, the resistivity profile, as shown in Fig. 11, indicate a staircase behavior, which extends into the miscible CO_2 bank.

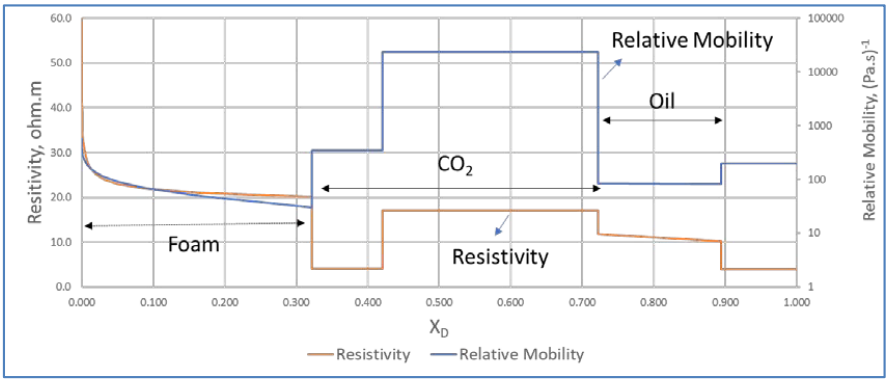

Fig. 11: Combined resistivity and mobility profile during CO_2-Foam injection (analytical solution – non-ideal displacement).

VI. Conclusions

In this paper, we presented a volumetric based foundation for resistivity and pressure monitoring during CO_2-foam displacements. Our results suggest that a combination of pressure and resistivity measurements in time-lapse mode could be deployed as an effective monitoring tool in field applications of the (CO_2) foam processes. The proposed method is novel as it could be employed to predict under-performing CO_2-foam floods and to improve oil recovery and CO_2 storage.

Other conclusions can be listed as follows:

- Pressure measurements during steady-state foam flow give rise to an ill-posed estimation problem and that grouping of foam parameters is necessary. For most reservoir applications, pressure measurements alone will not adequately describe the transient foam effects.
- Assuming brine in the reservoir, resistivity profiles during ideal CO_2 foam displacements should exhibit a distinctive signature at the foam front.
- During non-ideal CO_2 foam displacements, resistivity measurements by itself may not be enough to differentiate foam and miscible CO_2 banks. However, for these non-ideal cases, pressure measurements could be very utilized to locate these vastly contrasting mobility-fronts.

Acknowledgements

We would like to acknowledge financial support from Chevron for this research. We also acknowledge the input from Kurt Strack of KMS Technology.

Nomenclature

c_1 = a constant in the proposed foam conductivity model
C_c = a model parameter to represent foam coalescence
C_f = a model parameter to represent effective foam viscosity
C_g = a model parameter to represent foam generation
D = volumetric liquid fraction in the foam, fraction
d = value of determinant to capture the conditioning of the parameter estimation problem
epdry = a foam parameter used to capture the slope near critical water saturation
fmmob = a factor in steady-state foam model to represent the mobility factor
fmdry = a factor in steady-state foam model to represent the critical water saturation
epsurf = a steady-state foam parameter
f_{co2} = CO_2 phase fractional flow, fraction
f_w = water phase fractional flow, fraction
Fw = factor to capture the effect of water saturation on foam mobility reduction
K = bulk foam conductivity, (S/m)
k = permeability, m^2
k_{rCO2} = relative permeability to CO2 phase, fraction
k_{ro} = relative permeability to oil phase, fraction
k_{rw} = relative permeability to water phase, fraction
m = a model parameter for transient foam generation
M = measurement matrix
n = a model parameter for transient foam coalescence
R_{CO2} = resistivity of the CO_2 phase, ohm-m
R_f = resistivity of the foam, ohm-m
R_w = resistivity of water phase, ohm-m
n_f = foam texture or density, lamellae/unit volume
n_{fmax} = maximum foam density, lamellae/unit volume
r_c = foam (lamella) destruction rate
r_g = foam (lamella) generation rate
S = sensitivity matrix
S_{co2} = CO_2 saturation, fraction
S_o = oil saturation, fraction
S_w = water saturation, fraction
u_{co2} = CO_2 volumetric flux or superficial velocity, m/s
u_t = total velocity, m/s
u_w = water velocity, m/s
vf = volumetric fraction of rock and fluids, fraction
v_s = velocity of the foam front, m/s
v_w = velocity of the miscible (CO_2) front, m/s
X = vector defining the foam parameters
X_f = foam quality, fraction
μ_{co2}^0 = CO_2 viscosity (without foam), Pa.s
μ_{co2}^f = effective viscosity of the CO_2 foam phase, Pa.s
ϕ = porosity, fraction
σ_{co2} = CO_2 conductivity (without foam), S/m
σ_{co2}^f = CO_2 conductivity (with foam), S/m
σ_f = foam conductivity, S/m
σ_w = water conductivity, S/m
∇p = total pressure gradient, Pa/m
∇p_w = pressure gradient for the water phase, Pa/m

References Références Referencias

1. Agnihotri, A.K. and Lemlich, R., 1981. Electrical conductivity and the distribution of liquid in polyhedral foam. Journal of Colloid and Interface Science, 84(1), pp.42-46.
2. Ashoori, E., van der Heijden, T., & Rossen, W. (2010, June 1). Fractional-Flow Theory of Foam Displacements with Oil. Society of Petroleum Engineers. doi:10.2118/121579-PA.
3. Berge, C., 2017. An Experimental Study of Foam Flow in Water Saturated Porous Media, MS thesis, University of Bergen, Bergen, Norway.
4. Bergmann, P., Ivandic, M., Norden, B., Rücker, C., Kiessling, D., Lüth, S., Schmidt-Hattenberger, C. and Juhlin, C., 2013. Combination of seismic reflection and constrained resistivity inversion with an application to 4D imaging of the CO2 storage site, Ketzin, Germany. Geophysics, 79(2), pp. B37-B50.
5. Bikerman, J.J., 2013. Foams (Vol. 10). Springer Science & Business Media.

6. Boerner, J. B., Volker, H., Repke, J. U. and Spitzer, 2015. The electrical conductivity of CO2-bearing pore waters at elevated pressure and temperature: a laboratory study and its implications in CO2 storage monitoring and leakage detection, *Geophys. J. Int.* (2015) 203, 1072–1084 doi: 10.1093/gji/ggv331.
7. Bouchedda, A. and Giroux, B., 2015, December. Synthetic Study of CO2 monitoring using Time-lapse Down-hole Magnetometric Resistivity at Field Reseach Station, Alberta, Canada. In 2015 SEG Annual Meeting. Society of Exploration Geophysicists.
8. Chang, Kin-Shiung, and Robert Lemlich. "A study of the electrical conductivity of foam." Journal of Colloid and Interface Science 73, no. 1 (1980): 224-232.
9. Christensen, N. B., D. Sherlock, and K. Dodds. "Monitoring CO2 injection with cross-hole electrical resistivity tomography." Exploration Geophysics 37.1 (2006): 44-49.
10. Cilliers, J.J., Wang, M. and Neethling, S.J., 1999. Measuring flowing foam density distributions using ERT. Ref, 5, pp.108-112.Clark, N. O. "The electrical conductivity of foam." Transactions of the Faraday Society 44 (1948): 13-15.
11. Cilliers, J.J., Xie, W., Neethling, S.J., Randall, E.W. and Wilkinson, A.J., 2001. Electrical resistance tomography using a bi-directional current pulse technique. Measurement Science and Technology, 12(8), p.997.
12. Dholkawala, Z.F., Sarma, H.K. and Kam, S.I., 2007. Application of fractional flow theory to foams in porous media. Journal of Petroleum Science and Engineering, 57(1-2), pp.152-165.
13. Feitosa, K., Marze, S., Saint-Jalmes, A. and Durian, D.J., 2005. Electrical conductivity of dispersions: from dry foams to dilute suspensions. Journal of Physics: Condensed Matter, 17(41), p.6301.
14. Ferno, M. A., Gauteplass, J., Pancharoen, M., Haugen, A., Graue, A., Kovscek, A. R., & Hirasaki, G. J. (2014, October 27). Experimental Study of Foam Generation, Sweep Efficiency and Flow in a Fracture Network. Society of Petroleum Engineers. doi:10.2118/170840-MS.
15. Gargar, N.K., Mahani, H., Rehling, J.G., Vincent-Bonnieu, S., Kechut, N.I. and Farajzadeh, R., 2015, April. Fall-Off Test Analysis and Transient Pressure Behavior in Foam Flooding. In IOR 2015-18th European Symposium on Improved Oil Recovery.
16. Haroun, M., Mohammed, A.M., Somra, B., Punjabi, S., Temitope, A., Yim, Y., Anastasiou, S., Baker, J.A., Haoge, L., Al Kobaisi, Aminzadeh, F., M., Karakas, M., Corova, F. (2017, November 13). Real-Time Resistivity Monitoring Tool for In-Situ Foam Front Tracking. Society of Petroleum Engineers. doi:10.2118/188391-MS.
17. Hirasaki, G.J. and Lawson, J.B., 1985. Mechanisms of foam flow in porous media: apparent viscosity in smooth capillaries. Society of Petroleum Engineers Journal, 25(02), pp.176-190.
18. Kam, S.I., 2008. Improved mechanistic foam simulation with foam catastrophe theory. Colloids and Surfaces A: Physicochemical and Engineering Aspects, 318(1-3), pp.62-77.
19. Kam, S.I., Nguyen, Q.P., Li, Q. and Rossen, W.R., 2007. Dynamic simulations with an improved model for foam generation. SPE Journal, 12(01), pp.35-48.
20. Karakas, M. and Aminzadeh, F., 2017, Optimization of CO_2-Foam Injection through Resistivity and Pressure Measurements, Provisional US Patent Application, Serial No. 62/511,547.
21. Kiessling, D., Schmidt-Hattenberger, C., Schuett, H., Schilling, F., Krueger, K., Schoebel, B., Danckwardt, E., Kummerow, J. and CO2SINK Group, 2010. Geoelectrical methods for monitoring geological CO2 storage: first results from cross-hole and surface–downhole measurements from the CO2SINK test site at Ketzin (Germany). International Journal of Greenhouse Gas Control, 4(5), pp.816-826.
22. Kim, J., Dong, Y., & Rossen, W. R. (2005, December 1). Steady-State Flow Behavior of CO2 Foam. Society of Petroleum Engineers. doi:10.2118/89351-PA.
23. Kim, J., Nam, M.J. and Matsuoka, T., 2016. Monitoring CO2 drainage and imbibition in a heterogeneous sandstone using both seismic velocity and electrical resistivity measurements. Exploration Geophysics, 47(1), pp.24-31.
24. Kim, J. W., Xue, Z., & Matsuoka, T. (2010, January 1). Experimental Study On CO2 Monitroing and Saturation With Combined P-wave Velocity and Resistivity. Society of Petroleum Engineers. doi:10.2118/130284-MS.
25. Kovscek, A.R. and Radke, C.J., 1994. Fundamentals of foam transport in porous media.
26. Kovscek, A.R., Patzek, T.W. and Radke, C.J., 1995. A mechanistic population balance model for transient and steady-state foam flow in Boise sandstone. Chemical Engineering Science, 50(23), pp.3783-3799.
27. Kuuskraa, V.A. and Koperna, G.J., 2006. Evaluating the potential for 'game changer' improvements in oil recovery efficiency from CO2 enhanced oil recovery. Prepared for US Department of Energy, Office of Fossil Energy—Office of Oil and Natural Gas.
28. Lemlich, R., 1985. Semitheoretical equation to relate conductivity to volumetric foam density. Industrial & Engineering Chemistry Process Design and Development, 24(3), pp.686-687.
29. Lotfollahi, M., Farajzadeh, R., Delshad, M., Varavei, A., & Rossen, W. R. (2016, March 21). Comparison of Implicit-Texture and Population-Balance Foam

Models. Society of Petroleum Engineers. doi:10.2118/179808-MS.
30. Ma, K., Ren, G., Mateen, K., Morel, D., & Cordelier, P. (2015, June 1). Modeling Techniques for Foam Flow in Porous Media. Society of Petroleum Engineers. doi:10.2118/169104-PA.
31. Mahani, H., Sorop, T., van den Hoek, P., Brooks, D., & Zwaan, M. (2011, January 1). Injection Fall-Off Analysis of Polymer flooding EOR. Society of Petroleum Engineers. doi:10.2118/145125-MS.
32. Montaron, B. (2009, April 1). Connectivity Theory – A New Approach to Modeling Non-Archie Rocks. Society of Petrophysicists and Well-Log Analysts.
33. Nakatsuka, Y., Xue, Z., Garcia, H. and Matsuoka, T., 2010. Experimental study on CO2 monitoring and quantification of stored CO2 in saline formations using resistivity measurements. International Journal of Greenhouse Gas Control, 4(2), pp.209-216.
34. Namdar Zanganeh, M., & Rossen, W. (2013, January 30). Optimization of Foam Enhanced Oil Recovery: Balancing Sweep and Injectivity. Society of Petroleum Engineers. doi:10.2118/163109-PA.
35. Nguyen, Q., Hirasaki, G., & Johnston, K. (2015). Novel CO2 Foam Concepts and Injection Schemes for Improving CO2 Sweep Efficiency in Sandstone and Carbonate Hydrocarbon Formations. Univ. of Texas, Austin, TX (United States).
36. Omar, S., Jaafar, M. Z., Ismail, A. R., & Wan Sulaiman, W. R. (2013, July 2). Monitoring Foam Stability in Foam Assisted Water Alternate Gas (FAWAG) Processes Using Electrokinetic Signals. Society of Petroleum Engineers. doi:10.2118/165312-MS.
37. Onishi, K., Ishikawa, Y., Yamada, Y. and Matsuoka, T., 2006, January. Measuring electric resistivity of rock specimens injected with gas, liquid and supercritical CO2. In 2006 SEG Annual Meeting. Society of Exploration Geophysicists.
38. Passalacqua, H., S. Davydycheva, and K. Strack, 2018, Feasibility of multi-physics reservoir monitoring for Heavy Oil, Heavy Oil Conference Kuwait, SPE-193690-MS, doi: 10.2118/193690-MS.
39. Prigiobbe, Valentina, et al. "Transport of Nanoparticle-Stabilized CO_2-Foam in Porous Media." Transport in Porous Media 111.1 (2016): 265-285.
40. Schmidt-Hattenberger, C., Bergmann, P., Labitzke, T. and Wagner, F., 2014. CO2 migration monitoring by means of electrical resistivity tomography (ERT)–Review on five years of operation of a permanent ERT system at the Ketzin pilot site. Energy Procedia, 63, pp.4366-4373.
41. Strack, K. M., Hinojosa, H., Lüschen, E., and Martinez, Y., 2022, Using Electromagnetics for Geothermal and Carbon Capture, Utilization and Storage (CCUS) applications, European Geothermal Congress, Berlin, Germany | 17-21 October 2022, www.europeangeothermalcongress.eu
42. Strack, K.-M., 2014, Future directions of Electromagnetic Methods for Hydrocarbon Applications, Surveys in Geophysics, 35, 157-177, doi:10.1007/s10712-013-9237-z.)
43. Tapp, H.S., Peyton, A.J., Kemsley, E.K. and Wilson, R.H., 2003. Chemical engineering applications of electrical process tomography. Sensors and Actuators B: Chemical, 92(1-2) pp.17-24.
44. Wang, M. and Cilliers, J.J., 1999. Detecting non-uniform foam density using electrical resistance tomography. Chemical Engineering Science, 54(5), pp.707-712.
45. Wu, Y., Hubbard, S. and Wellman, D., 2012. Geophysical monitoring of foam used to deliver remediation treatments within the vadose zone. Vadose Zone Journal, 11(4).
46. Xue, Z., Kim, J. W., Mito, S., Kitamura, K., & Matsuoka, T., 2009, Detecting and Monitoring CO2 With P-Wave Velocity and Resistivity from both Laboratory and Field Scales. Society of Petroleum Engineers. doi:10.2118/126885-MS.

Appendix A – Analytical Solution

In the example provided by Ashoori et al. (2010), the following fluid and rock parameters are assumed:

Table A1: Model Parameters used for Analytical Simulations

μ_w	0.001	Pa.s
μo	0.005	Pa.s
μg	2E-05	Pa.s
ϕ	0.25	
S_{gr}	0.1	
S_{wc}	0.1	
S_{or}	0.1	

Water and Oil phase relative permeabilities are modeled as follows:

$$k_{rw}=0.20*((S_w-0.1)/0.8)^{4.2} \text{ (Water)} \quad \text{(A1)}$$

$$k_{ro}=0.94*((1-S_w-0.1)/0.8)^{1.3} \text{ (Oil)} \quad \text{(A2)}$$

Water and CO_2 phase relative permeabilities are represented by the following relationships:

$$k_{rw}=0.20*((S_w-0.1)/0.8)^{4.2} \text{ (Water)} \quad \text{(A3)}$$

$$k_{rg}^{0} = 0.94*((1-S_w-0.1)/0.8)^{1.3} \quad (CO_2 \text{ without foam}) \quad \text{(A4)}$$

In these models, foam reduces the CO_2 relative permeability, using the steady-state assumptions, as follows:

$$k_{rg}^{f} = k_{rCg}^{0} * \frac{1}{1+fmmob \ *\text{Fwater}} \quad \text{(A5)}$$

Where:

$$F_{water} = 0.5 + \pi^{-1} tan^{-1}[epdry(Sw - fmdry)] \quad \text{(A6)}$$

where fmdry and epdry are empirical parameters based on experimental data.

In the example by Ashoori et al., 2010, the following parameters were utilized:

Table A2: Foam Parameters used for Analytical Simulations

fmmob	55000
fmdry	0.316
epdry	1000
epsurf	100

Using these parameters, fractional flow curves for foam/water, CO_2/water and oil/water phases were reconstructed. Also, we used the two separate solutions; the first solution assumes an ideal displacement where the miscible fronts and the surfactant (foam) fronts travel at the same speed. For this to happen, there must be a minimal Surfactant adsorption as well as very favorable partitioning of the surfactant into the CO_2 phase. In the ideal displacement case, the solution paths are constructed by first drawing a tangent from the M=D=(1,1) point to the curve representing the fractional flow of foam, as shown in the figure below:

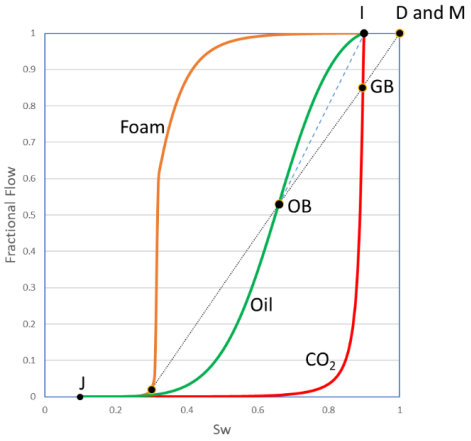

Fig. A1: Fractional flow – Ideal Displacement.

The saturation profile for the ideal displacement case is as follows:

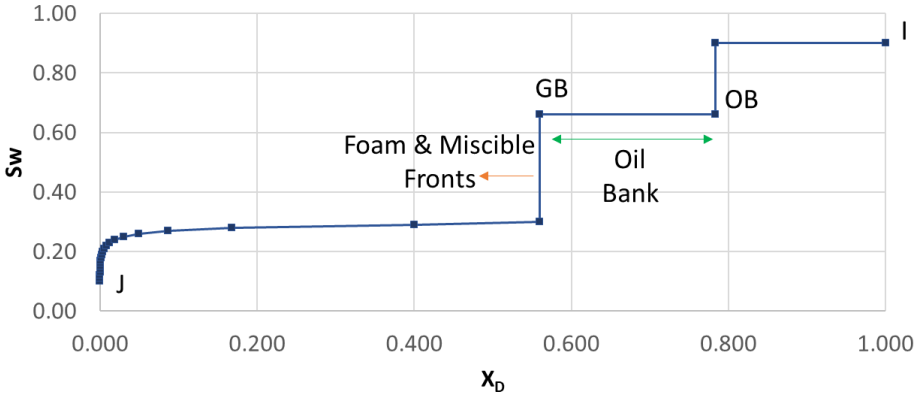

Fig. A2: Saturation profile – Ideal Displacement.

The second solution is non-ideal displacement where the miscible fronts and the surfactant (foam) fronts travel at different speeds. In this case, the surfactant adsorption as well as partitioning of the surfactant into the water phase slows down the speed of the foam (surfactant) front. On the other hand, the miscible (CO_2) front moves at the same speed as before. Therefore, miscible front shoots ahead of the foam (surfactant) front. Thus, a CO_2 bank forms. In this case, there are four different banks, and the construction of the solution paths starts first by drawing tangents from point D and the miscibility point, point M (1,1) to curves representing the fractional flow of oil and foam, respectively.

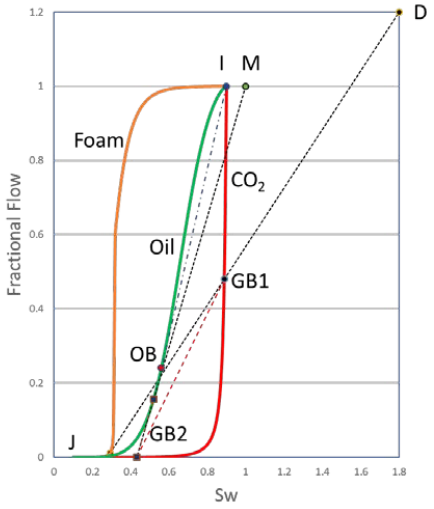

Fig. A3: Fractional flow, Non-Ideal displacement.

The saturation profile for the non-ideal displacement case is as follows:

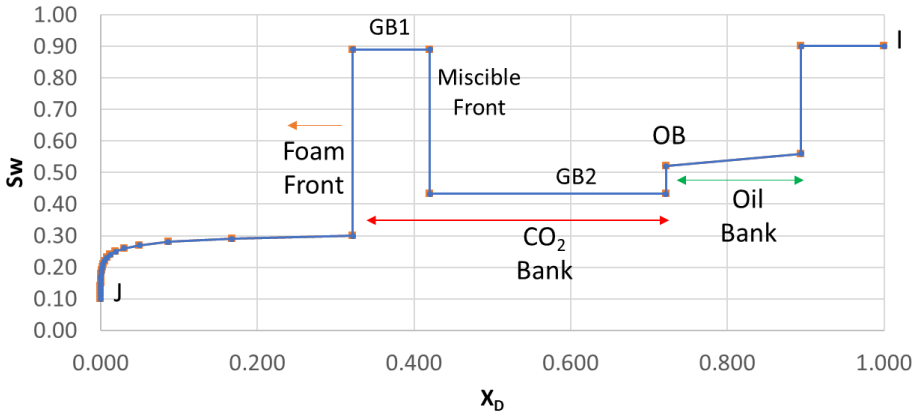

Fig. A4: Saturation profile, Non-Ideal displacement.

Appendix B – Population based Foam Model

Assuming one-dimensional flow of water and CO_2, the material balance of water is described by the following equation:

$$\phi \frac{\partial S_w}{\partial t} + u_t \frac{\partial f_w}{\partial x} = 0 \qquad \text{(B1)}$$

In this model, total flow rate (u_t) is assumed to be constant. As usual, water fractional flow is written as follows:

$$f_w = \frac{\frac{k_{rw}}{\mu_w}}{\frac{k_{rw}}{\mu_w} + \frac{k_{rco\,2}}{\mu^{f}_{co\,2}}} \qquad \text{(B2)}$$

where μ^{f}_{co2} is the CO_2– Foam viscosity and is given by (Hirasaki et al. 1985)

$$\mu^{f}_{co2} = \mu^{0}_{co2} + C_f \frac{n_f}{(\frac{u_{co\,2}}{\phi S_{co\,2}})^{1/3}} \qquad \text{(B3)}$$

In this equation, C_f is an empirical parameter based on experimental data.

Foam density ((n_f) equation is described by the following equation (Kovscek et al. 1995):

$$\phi \frac{\partial (S_{co2} n_f)}{\partial t} + u_t \frac{\partial (f_{co2} n_f)}{\partial x} = \varphi S_{co2} (r_g - r_c) \quad \text{(B4)}$$

The rate of foam generation is given by

$$r_g = C_g \nabla p^m \quad \text{(B5)}$$

and the rate of foam coalescence is given by

$$r_c = C_c n_f \left(\frac{S_w}{S_w - S_w^*}\right)^n \quad \text{(B6)}$$

Where C_g, C_c, m and n are model parameters. S_w^* is the water saturation linked with the critical capillary pressure for a foam–water system. In high permeability reservoirs, S_w^* is expected to be small. Also, the foam behavior around the critical water saturation could be quite abrupt.

The water rate is given by

$$u_w = - \frac{k\, k_{rw}}{\mu_w} \nabla p_w \quad \text{(B7)}$$

and the foam rate is given by:

$$u_{co2} = - \frac{k\, k_{rco2}}{\mu^o_{co2}} (\nabla p_w - \nabla p_c) \quad \text{(B8)}$$

At steady state conditions, the foam generation rate is equal to the foam destruction (or coalescence) rate.

$$r_g = r_c \quad \text{(B9)}$$

when this relationship is inserted into the foam-viscosity equation:

$$\mu^f_{co2} = \mu^0_{co2} + C_f \frac{n_f}{(\frac{u_{co2}}{\phi S_{co2}})^{\frac{1}{3}}} \quad \text{(B10)}$$

the following relationship is obtained, representing the foam viscosity:

$$\mu^f_{co2} = \mu^0_{co2} + \frac{C_g C_f}{C_c} \frac{\nabla p^m}{(\frac{S_w}{S_w - S_w^*})^n (\frac{u_{co2}}{\phi S_{co2}})^{\frac{1}{3}}} \quad \text{(B11)}$$

Appendix C - Sensitivity Coefficients

For a single-measurement (pressure) case, the Model response is defined as follows:

$$M(X) = \nabla p_{mod} (\bar{X}) \quad \text{(C1)}$$

Where M is a matrix representing the model response and X is a vector representing the system unknowns:

$$X = \text{foam parameters } [X_1, X_2, X_3, \ldots X_i \ldots, X_p] \quad \text{(C2)}$$

where p is the total number of unknows. In this case, the Sensitivity Coefficients are defined as follows:

$$S(X) = [\nabla_x M^T(X)] \quad \text{(C3)}$$

and the Sensitivity Matrix for the Single Response Case is defined as follows:

$$S = \begin{bmatrix} M_{11} \ldots\ldots\ldots\ldots M_{1p} \\ M_{k1} \ldots\ldots\ldots\ldots M_{kp} \end{bmatrix} \quad \text{(C4)}$$

or

$$S = \begin{bmatrix} \frac{\delta M_1}{\delta x_1} \ldots\ldots\ldots & \frac{\delta M_1}{\delta x_p} \\ \frac{\delta M_k}{\delta x_1} \ldots\ldots\ldots & \frac{\delta M_k}{\delta x_p} \end{bmatrix} \quad \text{(C5)}$$

where k is the number of measurements. Sensitivity of the Model response (M_i) to parameter vector X_j is defined as follows:

$$S^{(l)}_{ij} = \frac{\delta M_i}{\delta x_j} \Big|_{x^{(l)}} \quad \text{(C6)}$$

where $X^{(l)}$ represents the parameter vector which was used in generating the forward simulations.

Appendix D – Conductivity of Fluid Mixtures

Conductivity of fluid mixtures in porous media can be represented using the mixing law (Montaron, B., 2009). For a rock saturated with fluids, the total conductivity is expressed by the following equation:

$$\sigma^{1/2} = vf_1 \sigma_1^{1/2} + vf_2 \sigma_2^{1/2} + vf_3 \sigma_3^{1/2} \quad \text{(D1)}$$

where σ_i and vf_i represent the conductivity and the volumetric fraction of each component (rock and fluid), respectively. Additionally, the total volumetric fraction can be written as:

$$vf_1 + vf_2 + vf_3 = 1.0 \quad \text{(D2)}$$

for a water and oil/gas/CO_2 system these relationships become:

$$\sigma_1 = \sigma_R = 0, \qquad vf_1 = 1 - \phi \quad \text{(D3)}$$

$$\sigma_2 = \sigma_o = 0, \qquad vf_2 = S_o \phi \quad \text{(D4)}$$

$$\sigma_3 = \sigma_w, \qquad vf_3 = \sigma_w \phi \quad \text{(D5)}$$

and using the mixing law, we obtain:

$$\sigma = \sigma_w (S_w \phi)^2 \quad \text{(D6)}$$

This result is similar to Archie's law:

$$\sigma = \frac{\sigma_w S_w^n \phi^m}{a} \quad \text{(D7)}$$

where a, n and m are constants. For a CO_2-Foam and water system, the mixing law equations become:

$$\sigma_1 = \sigma_R = 0, \qquad vf_1 = 1 - \phi \quad \text{(D8)}$$

$$\sigma_2 = \sigma_f, \qquad vf_2 = S_{co2}^f \phi \quad \text{(D9)}$$

$$\sigma_3 = \sigma_w, \qquad vf_3 = \sigma_w \phi \quad \text{(D10)}$$

and finally:

$$\sigma = \phi^2 [S_{co2}^f \sigma_f^{1/2} + S_w \sigma_w^{1/2}]^2 \quad \text{(D11)}$$

energies

MDPI

Article

Unsteady-State CO_2 Foam Generation and Propagation: Laboratory and Field Insights

Zachary Paul Alcorn *, Aleksandra Sæle, Metin Karakas and Arne Graue

Department of Physics and Technology, University of Bergen, 5009 Bergen, Norway
* Correspondence: zachary.alcorn@uib.no

Abstract: This work presents a multiscale experimental and numerical investigation of CO_2 foam generation, strength, and propagation during alternating injection of surfactant solution and CO_2 at reservoir conditions. Evaluations were conducted at the core-scale and with a field-scale radial simulation model representing a CO_2 foam field pilot injection well. The objective of the experimental work was to evaluate foam generation, strength, and propagation during unsteady-state surfactant-alternating-gas (SAG) injection. The SAG injection rapidly generated foam based upon the increased apparent viscosity compared to an identical water-alternating-gas (WAG) injection, without surfactant. The apparent foam viscosity of the SAG continually increased with each subsequent cycle, indicating continued foam generation and propagation into the core. The maximum apparent viscosity of the SAG was 146 cP, whereas the maximum apparent viscosity of the WAG was 2.4 cP. The laboratory methodology captured transient CO_2 foam flow which sheds light on field-scale CO_2 foam flow. The single-injection well radial reservoir simulation model investigated foam generation, strength, and propagation during a recently completed field pilot. The objective was to tune the model to match the observed bottom hole pressure data from the foam pilot and evaluate foam propagation distance. A reasonable match was achieved by reducing the reference mobility reduction factor parameter of the foam model. This suggested that the foam generated during the pilot was not as strong as observed in the laboratory, but it has propagated approximately 400 ft from the injection well, more than halfway to the nearest producer, at the end of pilot injection.

Keywords: foam; CO_2; EOR; multiscale

Citation: Alcorn, Z.P.; Sæle, A.; Karakas, M.; Graue, A. Unsteady-State CO_2 Foam Generation and Propagation: Laboratory and Field Insights. *Energies* **2022**, *15*, 6551. https://doi.org/10.3390/en15186551

Academic Editors: Daoyong Yang, Shengnan Chen, Huazhou Li, Yin Zhang, Xiaoli Li and Zhaoqi Fan

Received: 18 August 2022
Accepted: 3 September 2022
Published: 7 September 2022

1. Introduction

Foam has emerged as a promising, cost effective technique to reduce CO_2 mobility for improved sweep efficiency during CO_2 enhanced oil recovery (EOR) and CO_2 storage processes [1–4]. Foam is a dispersion of gas in a continuous liquid phase where gas flow is impeded by thin liquid films called lamellae [5,6]. Lamellae are often stabilized by water-soluble surfactants which reduce surface tension and are screened to ensure minimal adsorption on reservoir rock. Foam is generated in-situ by simultaneous injection of CO_2 and surfactant solution (co-injection) or in alternating slugs of CO_2 and surfactant solution [7,8]. Once foam is generated, it is propagated through the porous medium at an initial unsteady-state and then later at steady-state. Unsteady-state foam is characterized by a rapidly increasing pressure drop, whereas the pressure drop is constant at steady-state and can be described with Darcy's Law [9,10]. In addition, significant differences in relative permeability have been observed between steady- and unsteady-state foam flow [11]. At the field scale, it is assumed that foam is at steady-state [12]. However, foam may encounter both unsteady-state and steady-state flow regimes, with unsteady-state flow dominating the near wellbore area.

Foam injection must balance injectivity, mobility reduction, and operational constraints. At laboratory scale, co-injection is the most common injection strategy because of the ability to achieve steady-state and for deriving foam model parameters [13]. In addition,

co-injection offers the most control of injected foam quality [14]. However, co-injection can be challenging at the field-scale because of operational limitations, extremely low injectivities, rapid pressure increases, and challenges associated with downhole corrosion [15]. This has led to most field tests using a surfactant-alternating-gas (SAG) injection strategy. Additionally, SAG processes have been shown to be the optimal injection strategy to overcome gravity override and to maintain injectivity [16].

Details on in-situ foam generation and propagation during unsteady-state flow are needed because they significantly impact injectivity, which is crucial to the success of foam applications for EOR and CO_2 storage. However, few attempts have been made to characterize transient CO_2 foam behavior during alternating injection of surfactant solution and CO_2 slugs at reservoir conditions. Moreover, the connection between laboratory and field-scale transient foam flow is unclear. To further complicate the matter, conventional reservoir simulations calculate injectivity assuming a uniform saturation and mobility in the injection-well grid block. Therefore, injectivity in a simulation of an SAG process is extremely poor [17]. In reality, foam in the near-well region rapidly dries out and injectivity is much greater than estimated in a finite-difference simulation. Foam dry-out occurs at high gas fractional flows due to foam coalescence and depletion of adequate surfactant solution. The large injectivity reduction can be compounded by limited variation in foam apparent viscosity at different gas fractions from experimental data used to derive foam model parameters. Therefore, an approach to capture foam dry-out in the near-well region is needed.

This work presents a multiscale investigation of unsteady-state CO_2 foam generation, strength, and propagation at reservoir conditions. The main objective of the experimental work was to evaluate foam generation and propagation during unsteady-state SAG injection at reservoir conditions to assist with field pilot interpretations. The aim was to develop a laboratory methodology for CO_2 foam quantification during SAG injection, representative of the near wellbore region. The objective of the field-scale modeling work was to calibrate a radial reservoir simulation model to the observed behavior from a recently completed CO_2 foam field pilot test. An approach to capture the foam dry-out effect near the well is proposed.

2. Pilot Overview

A surfactant-stabilized CO_2 foam pilot was conducted in a mature heterogeneous carbonate reservoir in East Seminole Field, Permian Basin USA [18]. The main objective was to achieve in-depth CO_2 mobility control to increase CO_2 sweep efficiency and improve the CO_2 utilization factor. The foam formulation was designed in the laboratory by measuring surfactant adsorption and verifying foam stability in the presence of residual oil [19–21].

The pilot area was an inverted 40 acre five-spot pattern with a central injection well and four surrounding producers. The pilot injection strategy was designed to mitigate injectivity losses due to strong foam generation and to volumetrically target the optimal 70% foam quality, as recommended from the laboratory studies. A rapid surfactant-alternating-gas (SAG) injection strategy began in May 2019. The injection strategy consisted of SAG cycles with 10 days of surfactant solution injection followed by 20 days of CO_2 injection. Eleven complete SAG cycles were injected for total of 10% hydrocarbon pore volume (HCPV) injected at the completion of the pilot in August 2020. Figure 1 shows the observed injection rates and bottom hole pressure (BHP) during the pilot.

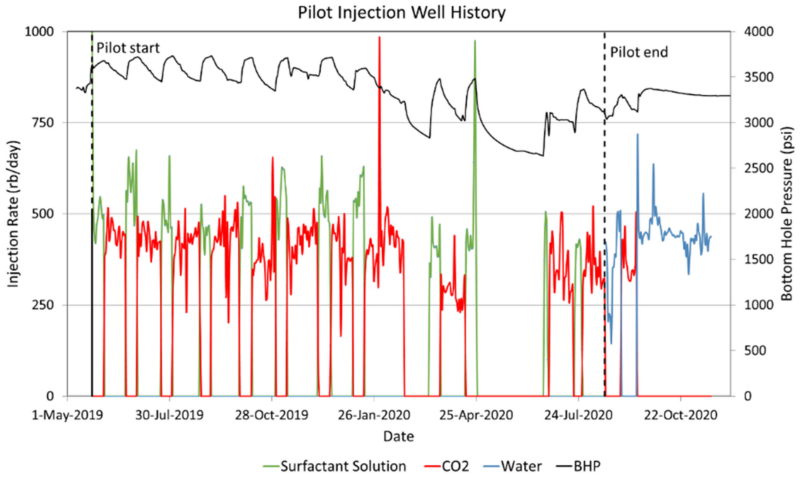

Figure 1. Observed injection rates and bottom hole pressure (BHP) during the foam pilot. The red curve corresponds to CO_2 injection, the green curve to surfactant solution injection, and the blue to water injection. The BHP is shown as the black curve.

Pilot Monitoring

The baseline data collection and pilot monitoring program aimed to obtain baseline from pre-pilot CO_2 and water injection periods and monitor pilot performance to evaluate reservoir response to foam injection. Foam was expected to reduce CO_2 mobility, thus the baseline period focused on characterizing interwell connectivity and injectivity of CO_2 and water. The baseline data collection program consisted of CO_2 injection profile logs, an interwell CO_2 tracer test (IWTT) and collection of injection and production flow rates for comparison to repeat surveys during the pilot. The pilot monitoring program included repeat CO_2 injection profiles, an IWTT, three-phase production monitoring and collection of downhole pressure data for evaluation of reservoir response to foam injection. The injection bottom hole pressure and temperature were monitored by mounting a downhole pressure gauge (DHPG) in the pilot injection well. Produced fluids were also collected, before the pilot and once a week during the pilot, for chemical analysis to determine surfactant breakthrough time.

Foam generation was confirmed during the pilot based upon a delay in CO_2 breakthrough compared to the baseline CO_2 breakthrough time, higher BHP values during the pilot compared to pre-pilot values, and more evenly distributed injection profiles during the pilot compared to the pre-pilot period. In addition, an increase in oil production was observed with less volumes of CO_2 injected during the pilot, compared to conventional CO_2 injection, thereby improving the CO_2 utilization factor and the economics of the project. Pilot results are discussed in detail in [22]. Observed BHP values and injection rates were used in this work to calibrate the radial reservoir model as discussed below.

3. Experimental Materials

The objective of the unsteady-state CO_2 foam experiments was to evaluate foam generation, strength, and collapse during alternating injection of CO_2 and surfactant solution to assist in the interpretation of the recently completed field pilot. The aim was to develop a laboratory methodology for CO_2 foam quantification during unsteady-state SAG injection, representative of the near wellbore region.

3.1. Rock and Fluid Properties

An outcrop Bentheimer sandstone was used for all experiments to maintain constant core properties. Bentheimer is a homogeneous, water-wet sandstone with a composition consisting of quartz (92%), clay minerals (3%) and feldspar (5%). The permeability was measured at an average of 2.14 ± 0.03 Darcy. Rock properties are shown in Table 1.

Table 1. Rock properties of the sandstone core material used in the experimental work.

Property	Value
Length (cm)	24.40 ± 0.01
Diameter (cm)	3.80 ± 0.01
Permeability (D)	2.14 ± 0.03
Pore Volume (mL)	62.16 ± 0.01
Porosity (%)	21.54 ± 0.10

Brine was prepared by dissolving 3.5 wt.% NaCl and distilled water. The foaming agent was a nonionic surfactant from Huntsman, SURFONIC L24-L22, that was dissolved in brine. The surfactant concentration was 0.50 wt% as also used in the pilot test. The SURFONIC L24-L22 surfactant demonstrated low adsorption in carbonate rock material, both in the absence and presence of CO_2 [19]. In addition, it is expected to have low adsorption on the surface of the Bentheimer sandstone. CO_2 of 99.999% purity was used during the foam injections. Isopropyl alcohol solution consisting of 87.5 wt.% isopropyl and 3.5 wt.% distilled water was injected to clean the core between each experiment. See Table 2 for an overview of fluid compositions used in the experimental work.

Table 2. Properties of the fluids used in the experimental work.

Fluid	Composition
Brine	Distilled water + 3.5 wt% NaCl
Surfactant solution	Brine + 0.5 wt% SURFONIC L24-L22
CO_2	>99.999% CO_2
Isopropyl alcohol	Distilled water + 87.5 wt% Di-propanol

3.2. Experimental Setup

Figure 2 shows a schematic of the experimental setup used for the unsteady-state CO_2 foam experiments. The temperature and pressure were set to reservoir conditions of 40 °C and 198 bar. The core was wrapped in a layer of nickel foil and placed inside of a Teflon rubber sleeve to prevent CO_2 diffusion into the sleeve [23]. The core was then inserted into a vertically-oriented hassler core holder. The system was pressurized by an N_2 tank connected with two Equilibar back pressure regulators (BPR) connected in series to reduce fluctuations and keep a constant pressure in the system. An ISCO pump kept the confinement pressure 70 bar over the system pressure. The confinement pressure, pressure at the inlet and outlet of the core and the pressure over the BPRs were measured and monitored by ESI-pressure transducers (Figure 2). The differential pressure over the core was used to calculate foam apparent viscosity and was measured by Aplisens Smart Differential Pressure Transmitter.

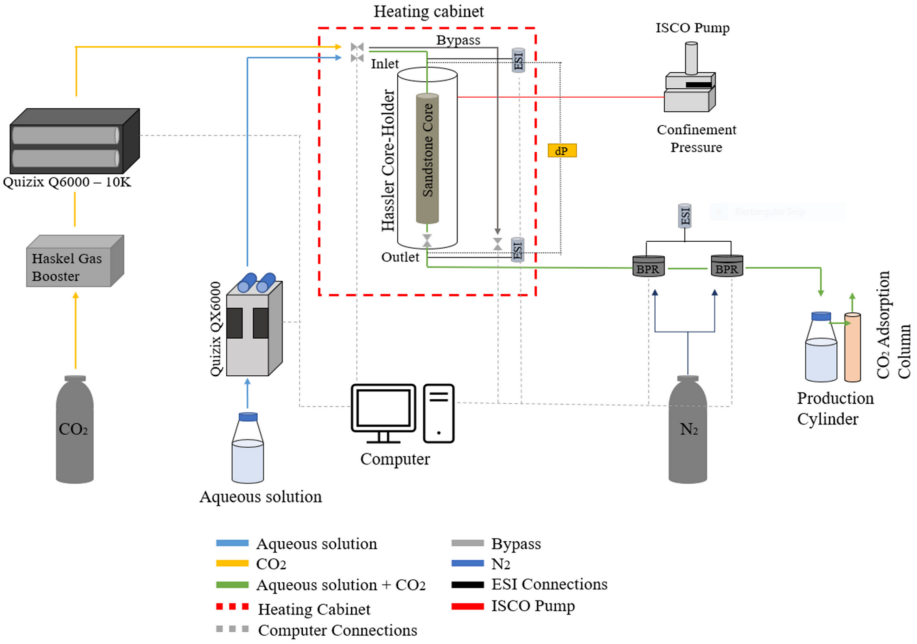

Figure 2. Illustration of experimental setup used for unsteady-state foam injections.

The aqueous solutions were injected through a Quizix QX6000-pump and CO_2 was injected through a Quizix Q6000-10K pump. CO_2 was pressurized by a Haskel gas booster to achieve a supercritical phase before it was injected through the pump and into the core. The production cylinder accumulated the production fluids from the outlet. The fluids were depressurized to atmospheric conditions and CO_2 was separated from the liquid solution by an adsorption column.

4. Experimental Methods

Foam generation, strength and stability were investigated during unsteady-state alternating slug injection of surfactant solution and CO_2. An identical WAG injection (without surfactant) was also conducted to establish a baseline for comparison. Foam generation and strength was quantified by calculating apparent viscosity (μ_{app}), which is based on the pressure measured across the core and is defined as:

$$\mu_{app} = \frac{k}{\mu_{gas} + \mu_{liquid}} \nabla \mathrm{p}\,, \tag{1}$$

where k is the absolute permeability of the core, μ_{gas} and μ_{liquid} are the superficial velocities of gas and liquid, respectively, and ∇p is the pressure gradient across the core [24]. A higher apparent viscosity value corresponds to a stronger foam and increased resistance to flow.

The experimental procedure and injection strategy were designed to represent unsteady-state flow in the near wellbore region. The experimental procedure for the baseline water-alternating-gas (WAG) and surfactant-alternating-gas (SAG) are shown in Figure 3 and are discussed below.

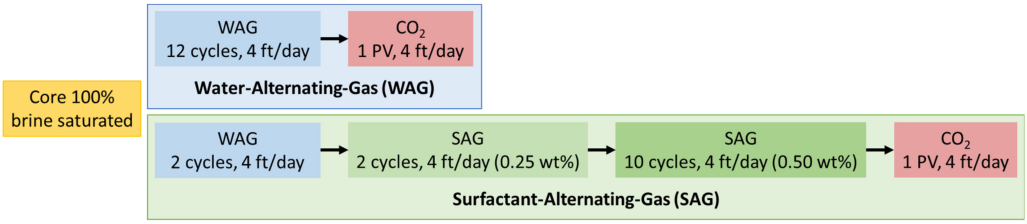

Figure 3. Experimental injection sequence for the baseline water-alternating-gas (WAG) and the surfactant-alternating-gas (SAG). The core was initially 100% saturated with brine and all injection rates were 4 ft/day. Individual WAG or SAG cycles injected 0.25 pore volumes (PV).

4.1. Baseline Water Alternating Gas (WAG)

The core was initially 100% saturated with brine by injecting brine at a low rate for five pore volumes (PV). The WAG injection was then conducted by injecting alternating slugs of brine and CO_2 at an injection rate of 4 ft/day. One brine slug and one CO_2 slug comprised one complete WAG cycle. The WAG injection procedure first injected brine for 0.10 PV. Next, the first CO_2 slug was injected for 0.15 PV to achieve the targeted 0.60 gas fraction. The WAG injection procedure was repeated until 12 complete WAG cycles were injected. Continuous CO_2 was then injected for 1 PV to study foam dry-out.

4.2. Surfactant Alternating Gas (SAG)

The core was initially 100% saturated with brine by injecting brine at a low rate for 5 PV. An initial 2-cycle WAG was conducted, followed by a diluted 2-cycle SAG and finally a 10-cycle SAG with 0.50 wt% surfactant solution. Pure CO_2 was injected at the end of the experiment for 1 PV. All injection rates were 4 ft/day at a gas fraction of 0.60, identical to the baseline WAG injection.

5. Modeling Methods

A single injection well radial reservoir simulation model was set up to investigate foam generation, strength, and propagation during the field pilot. The objective was to tune the foam model to match the simulated BHP to the observed BHP from the foam pilot. In addition, the sensitivity of foam model parameters on foam generation and propagation were studied. Previous simulation studies with the radial model have also been reported elsewhere [25]. The radial model was based upon a sector scale model that was history matched to the historical water and CO_2 injection periods in East Seminole Field [26].

The radial grid was composed of 560 active grid cells with 28 layers in the *z*-direction (Figure 4). Cell thicknesses, permeabilities, porosities and saturations were derived from the last step of the history matched sector model. The radial grid was centered around the pilot injection well and grid cell sizes increased logarithmically from the injector to a total of 700 ft. The radial model parameters are shown in Table 3. A commercially available conventional finite-difference compositional reservoir simulator was used for all simulations (ECLIPSE 300). The compositional model utilized the Peng–Robinson (PR) equation of state (EoS) model with six components that were tuned to PVT data. The model included two C7+ components where the lighter components were lumped as CO_2, N_2 + C1, H_2S + C2 + C3, C4 + C5 + C6. Two aqueous phases were included in the model, one for water and one for surfactant. See [26] for a complete description of the fluid model.

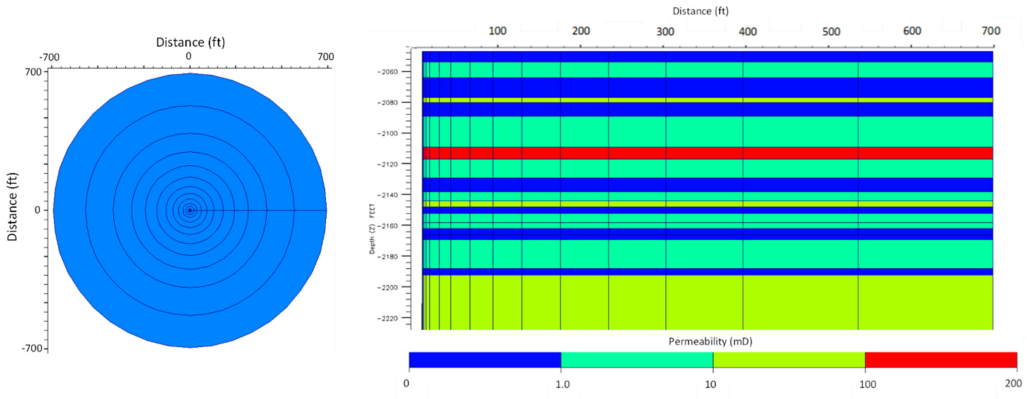

(**a**) (**b**)

Figure 4. (**a**) Top view of the radial model. The injection well was placed in the center of the grid. (**b**) Permeability distribution of a 2D slice ($r-z$) of the radial simulation model. Properties were derived from the last step of the history matched sector model.

Table 3. Radial model properties.

Parameter	Value
Grid Dimensions (r, θ, z)	$20 \times 1 \times 28$
Outer Radius	700 ft
Total Thickness	145 ft
Initial Water saturation	0.50
Initial Reservoir Pressure	3118 psig
Reservoir Temperature	104 °F
Average Permeability	13.5 mD
Average Porosity	0.08

5.1. Foam Modeling

Foam was modeled with an implicit texture local-equilibrium (LE) model. LE foam models represent the effect of bubble size implicitly by introducing factors for reducing gas mobility by foam as a function of water saturation, oil saturation, surfactant concentration and shear-thinning due to flow rate [27,28]. LE models assume foam is present anywhere gas and water are present along with adequate surfactant concentration.

The decrease in gas mobility during foam floods is accounted for in LE models by scaling the gas relative permeability in the absence of foam (k_{rg}^{nf}) by a mobility reduction factor (FM), whereas the water relative permeabilities remain unchanged.

$$k_{rg}^{f} = k_{rg}^{nf} \times FM. \tag{2}$$

The effect of water saturation, shear rate, surfactant concentration and oil saturation on mobility reduction factor was modeled, given by the expression:

$$FM = \frac{1}{1 + fmmmob \times F_{water} \times F_{shear} \times F_{oil} \times F_{surf}}, \tag{3}$$

where $fmmmob$ refers to the maximum gas mobility reduction that can be achieved. Below are the equations for F_{water}, F_{shear}, F_{oil} and F_{surf} which capture the water saturation, shear rate, oil saturation and surfactant concentration dependence, all lying in the range of 0 to 1.

The reduction of gas mobility due to the presence of water is defined as:

$$F_{water} = 0.5 + \frac{\alpha \tan[epdry(S_w - fmdry)]}{\pi}. \quad (4)$$

The capillary number, N_c, describes the relative effect of capillary and viscous forces.

$$F_{shear} = \begin{cases} \left(\frac{fmcap}{N_c}\right)^{epcap} & if\ N_c > fmcap \\ 1 & otherwise \end{cases}. \quad (5)$$

The individual reduction by surfactant concentration indicates that low surfactant concentrations and weak foam results in a low F_{surf}, while higher surfactant concentrations result in a higher individual mobility reduction.

$$F_{surf} = \left(\frac{C_s}{C_s^r}\right)^{epsurf}, \quad (6)$$

where C_s is defined as the surfactant concentration, C_s^r is the surfactant concentration reference and $epsurf$ indicated the rate change when $C_s = C_s^r$.

$$F_{oil} = \left(1 - \frac{S_o}{fmoil}\right)^{epoil}. \quad (7)$$

Foam model parameters (*fmmob*, *fmdry* and *epdry*) were obtained by fitting the empirical foam model to foam quality scan data through curve fitting regression [13,29]. The base values for *fmcap* and *epcap* were obtained by fitting the empirical foam model to rate scan data, assuming *fmmob*, *fmdry* and *epdry* to be invariable for regression. Figure 5 shows the model fit to a foam quality and rate scan conducted on a reservoir core at 2500 psi and 104F. The complete experimental procedure for foam quality and rate scans is given in [30].

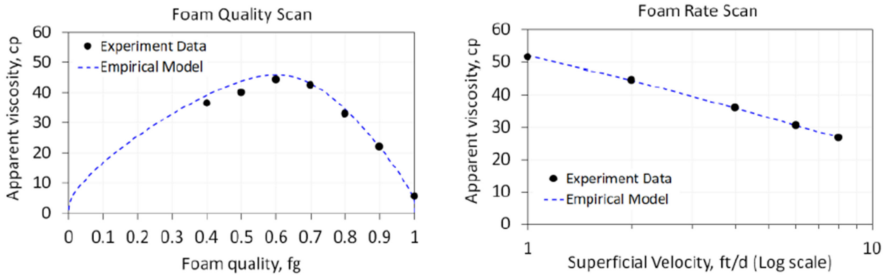

Figure 5. Foam quality scan (**left**) and foam rate scan (**right**) for the base case foam model. The empirical foam model (dashed lines) was fit to experimental data (black dots). Modified from [30].

The surfactant selected for the pilot had very low adsorption on the reservoir rock. Therefore, surfactant adsorption was not included in the model. The critical micellar concentration (CMC) was 0.01 wt% (0.035 lb/bbl) for the selected surfactant. The minimum concentration for foam generation was set at CMC, and the reference concentration for transition from weak to strong foam was assumed five times the CMC. The base value of *fmsurf* was therefore set as 0.05 wt% (0.175 lb/bbl). Due to unavailability of data to characterize the steepness in the change of mobility reduction due to surfactant concentration, the base value of *epsurf* was assumed 1. Based upon earlier CO_2 foam EOR experiments, the maximum oil saturation above which foam ceased to exit (*fmoil*) was 0.28 [18]. Due to unavailability of data to characterize the steepness in the change of mobility reduction due to oil saturation, the base value of *epoil* was assumed 1. To model foam dry-out during an SAG process near the injection well, the grid cells connected to the injector were assigned an *fmmob* of 0. This allowed modeling of a no foam region within a radius of 20 ft around injector to mimic foam dry out near the well.

5.2. Model Initialization

The model was initialized from the last step of the history matched sector model. The simulated injection schedule was identical to the observed injection from the pilot. Figure 6 shows an illustration of the injection schedule. Blue bars correspond to water injection, red to CO_2, and green to surfactant solution injection. The black bars indicate periods of observed field shutdowns that were also included in the simulation schedule. The pre-pilot period (1 April 2019–23 May 2019) included both the historical water injection and CO_2 injection periods. The pilot period (24 May 2019–23 August 2020) was the rapid SAG injection. The post-pilot injection period consisted of a one cycle WAG and then continuous water injection. The model did not capture the effect of nearby production wells on injection BHP because the model contained only the injection well.

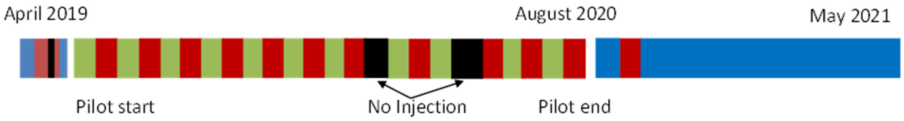

Figure 6. Injection overview of the radial model for East Seminole Field. Water injections (blue), CO_2 injections (red), surfactant injections (green), no injection periods (black).

5.3. Baseline Water Alternating Gas (WAG and Base Case Surfactant Alternating Gas (SAG)

A water-alternating-gas (WAG) case was set up to establish a baseline and to determine the CO_2 relative permeability reduction in a WAG process. The baseline WAG case injected only brine (no surfactant) and CO_2 at the targeted gas fraction of 0.70. The injection strategy consisted of 11 complete WAG cycles with alternating slugs of CO_2 for 20 days and water for 10 days. The simulation was run in history match mode where injection rates were set to the observed values from the pilot. The simulated BHP response was compared to the base rapid SAG and to the observed pilot values. The base case SAG was identical to the baseline WAG but included a surfactant component to model foam transport. Base foam model parameters were derived foam quality and rate scans conducted on reservoir core at reservoir temperature and pressure [30].

5.4. Foam Model Sensitivity Study

The objective of the foam model sensitivity was to investigate the impact of different experimentally derived foam models on foam generation and CO_2 mobility reduction. Injection BHP results were compared to the observed BHP data to determine which foam model best represented foam behavior at the field-scale. All foam model parameters were derived from laboratory foam quality and rate scans as described previously. Three cases were set up with different foam models for the sensitivity study. The foam model parameters are shown in Table 4.

Table 4. Foam model parameters used in the sensitivity study. Foam model 2 was used in the base case.

Model Parameter	1	2 (Base)	3
fmmob	41.5	192	248
fmdry	0.595	0.40	0.313
epdry	35	84	46.8
fmcap	2.14×10^{-6}	9.00×10^{-7}	8.50×10^{-7}
epcap	0.87	0.59	0.71

The base foam model was used in a sensitivity study of the foam model parameter, *fmmob*. As discussed previously, *fmmob* is the maximum gas mobility reduction that can be achieved with foam. Previous modeling results have shown that this parameter has the most impact on the simulated BHP [25].

6. Results and Discussion

6.1. Experimental: Unsteady-State CO_2 Foam Corefloods

Figure 7 shows apparent viscosity versus pore volume (PV) injected for the first seven cycles (2 PVs injected) of the baseline WAG (blue curve) and the base SAG (green curve). As mentioned previously, the first two cycles for both experiments were WAG cycles which generated no foam. The fluctuation in apparent viscosity between 0 cP and 2 cP during the first two cycles of each experiment was related to reduced CO_2 relative permeability in the presence of high water saturations in a WAG process [31]. The apparent viscosity of the baseline WAG stabilized at an average of 1.66 cP with a maximum value of 2.4 ± 0.2 cP. Therefore, an apparent viscosity of 2.4 cP was used as the foam generation limit for comparison to the SAG experiment (i.e., an apparent viscosity value higher than 2.4 cP indicated foam generation). Once surfactant was injected during the third cycle of the SAG experiment, the apparent viscosity increased above the WAG baseline, indicating foam generation. The apparent viscosity of the SAG continued to increase with each subsequent cycle indicating continued foam generation and propagation into the core.

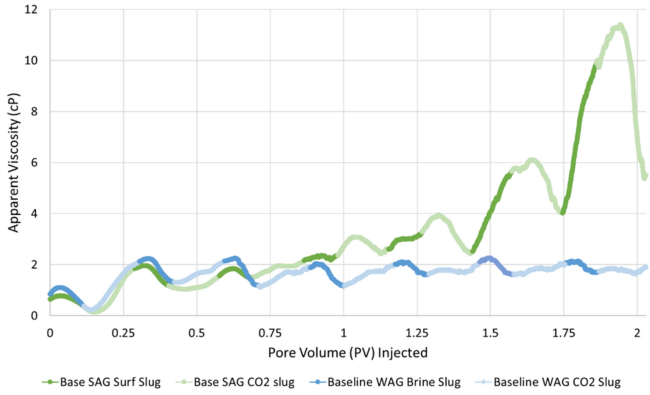

Figure 7. The first seven cycles for the Baseline WAG (blue curve) and Base SAG (green curve) experiments. Surfactant, or water, slugs are indicated with darker colors whereas the CO2 slugs are lighter colored. The maximum apparent viscosity value of WAG is indicated with the dotted red line.

Figure 8 shows apparent viscosity versus pore volume (PV) injected for the baseline WAG (blue curve) and the base SAG (green curve) for the entire experiment. The apparent viscosity of the base SAG increased continuously from SAG cycle 4 until cycle 12, reaching a peak value of 146 ± 0.4 cP, whereas the baseline WAG had a peak apparent viscosity value of 2.4 ± 0.1 cP.

Foam is usually generated in a drainage-like process where higher capillary pressure results in a snap-off mechanism [32,33]. However, apparent viscosity also increased during surfactant injection (imbibition-like injection). This may be related to foam generation or the viscosity contrast between CO_2 and surfactant solution. The increasing apparent viscosity from cycles 3 until 12 indicated continued foam generation and propagation through the core. The final CO_2 slug was injected for 1 PV to investigate foam stability and foam dry out during a prolonged period of pure CO_2 injection. The highest apparent viscosity value was reached in this slug (146 cP) before foam collapsed due to an effective drainage process, resulting in foam dry-out.

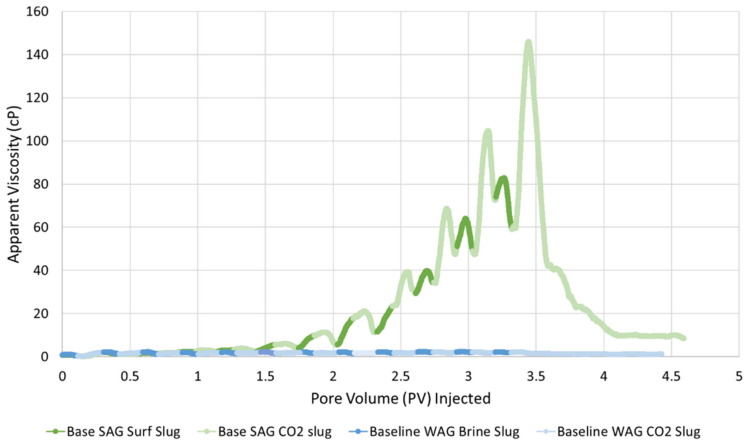

Figure 8. Apparent viscosity versus pore volume (PV) injected for 12 complete cycles for the Baseline WAG (blue curve) and the Base SAG (green curve). Surfactant solution, or water, slugs are indicated with darker colors whereas the CO_2 slugs are lighter colored.

6.2. Radial Model: Baseline WAG and Base Case SAG

The injection BHP of the baseline WAG and base case SAG simulation cases were used to evaluate foam generation and strength with surfactant present. The results were also compared to the observed BHP response from the foam pilot to determine the degree of CO_2 mobility reduction during the pilot. Figure 9 shows the simulated injection BHP through time for the baseline WAG (blue curve) and the base case SAG (green curve). The observed BHP is shown as the black circles. As discussed earlier, the injection well was run in history match mode at a set injection rate that was consistent with the observed injection rate.

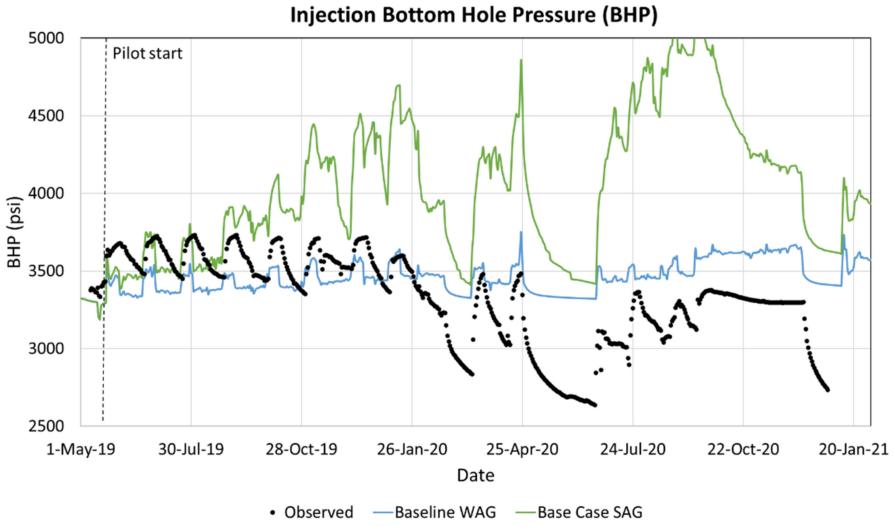

Figure 9. Injection bottom hole pressure (BHP) through time for the baseline WAG (blue curve) and the base case SAG (green curve). The observed BHP is shown as the black circles.

The simulated BHP values for the base case SAG (Figure 9, green curve) were higher than the baseline WAG (Figure 9, blue curve), indicating that foam was generated with surfactant present. Foam generation was also confirmed during the pilot based upon the higher observed BHP values compared to the baseline WAG [21]. However, the base case SAG's BHP values were significantly higher than the observed BHP, especially after the fourth SAG cycle. This suggests that the foam generated during the pilot was not as strong as in laboratory studies as also observed in [25]. In addition, the simulated BHP did not match the observed pressure fall-off after the seventh cycle because the model did not capture the effect of nearby production wells on injection BHP. As mentioned previously, the model contained only the injection well and did not include production that was observed in the field. The increase in BHP during surfactant solution slugs and subsequent decrease during CO_2 slug injection may be related to the viscosity difference between CO_2 and surfactant solution at these conditions. However, it may also be related to increased CO_2 injectivity due to water displacement in the near well area during CO_2 injection [34]. Indeed, the decreased BHP during CO_2 slugs, compared to surfactant solution slugs, at the same injection rates, increased CO_2 injectivity.

6.3. Foam Model Sensitivity Study

The foam model sensitivity study investigated the impact of different experimentally derived foam models on foam generation and CO_2 mobility reduction. Figure 10 shows the injection BHP for the simulation cases with three different experimentally derived foam models. See Table 4 for an overview of the foam model parameters.

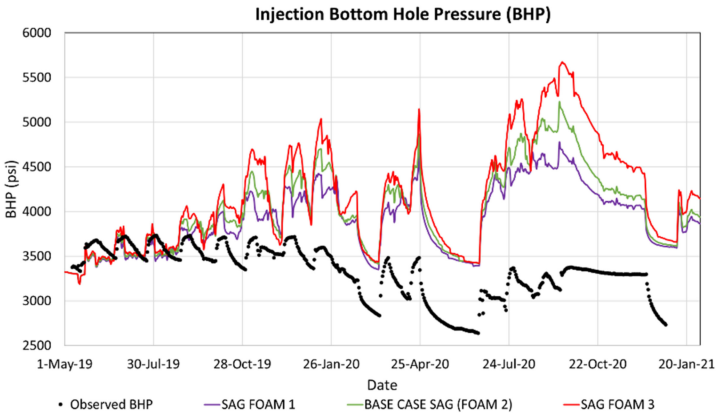

Figure 10. Injection bottom hole pressure (BHP) through time for the foam model sensitivity study. The red curve used foam model 1, the green curve is the base case SAG with foam model 2, and the purple curve used foam model 3. The observed BHP is shown as the black circles.

All three experimentally derived foam models generated foam which reduced CO_2 mobility and propagated foam into the reservoir based upon the increasing pressure build-up for each SAG cycle. Foam model 3 (Figure 10, red curve), with the highest value of *fmmob* generated the strongest foam whereas foam model 1 (Figure 10, purple curve), with the lowest *fmmob* value, generated the weakest foam relative to other cases. Thus, the most significant foam model parameter impacting injection BHP in the studied cases was *fmmob*. It was determined that the base case foam model *fmmob* parameter would be tuned to the observed BHP data to shed light on field-scale foam generation and propagation observed during the pilot. Figure 11 shows the injection BHP for the base foam model with the tuned *fmmob* value. The tuned foam model is shown at right.

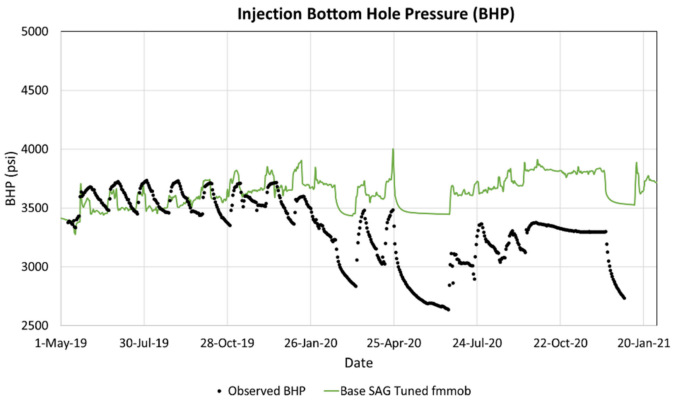

Model Parameter	Base Tuned
fmmob	1.9
fmdry	0.4
epdry	84
fmcap	9×10^{-7}
epcap	0.59

Figure 11. Injection bottom hole pressure (BHP) through time for the tuned base foam model (green curve). The observed BHP is shown as the black circles.

Reducing the *fmmob* value of the base case foam model brought the simulated BHP in closer agreement with the observed BHP response (Figure 11, black circles). Therefore, this case was used to evaluate field-scale foam propagation during the pilot. Figure 12 shows the simulated foam concentration in a 2D slice (r-z) of the radial model from before the pilot (Figure 12a), after the 1st SAG cycle (Figure 12b), after the 5th SAG cycle (Figure 12c), and after the 11th (final) SAG cycle (Figure 12d). Injection was from left to right in each figure. The permeability distribution is shown Figure 4b.

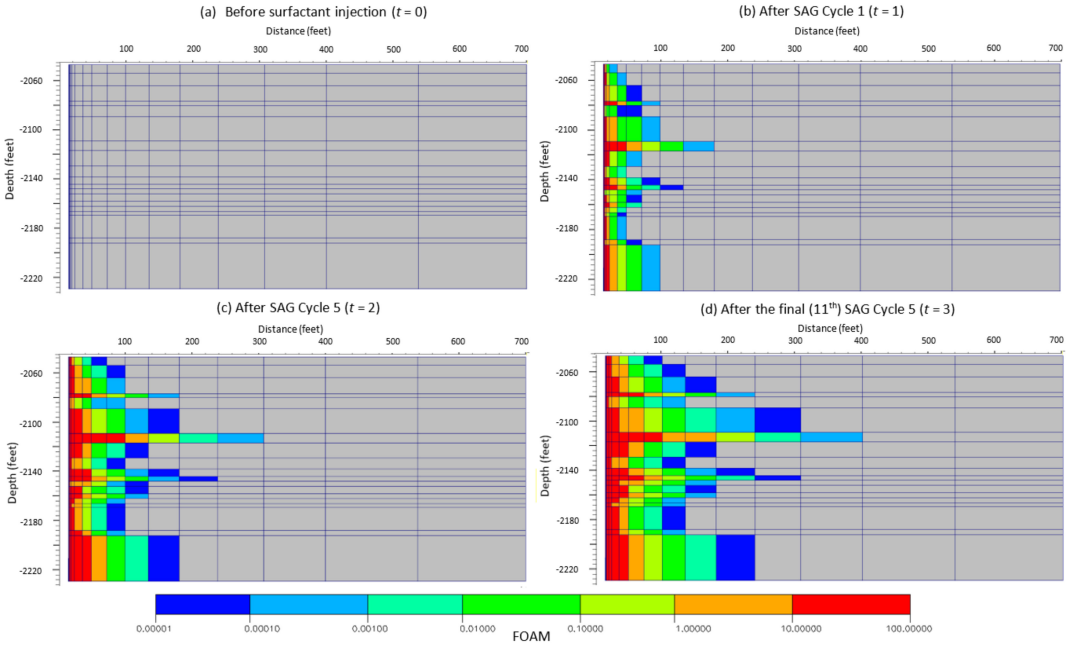

Figure 12. Foam concentration in a 2D slice ($r-z$) of the radial simulation model from (**a**) before surfactant injection, (**b**) after the 1st surfactant-alternating-gas (SAG) cycle, (**c**) after the 5th SAG cycle, and (**d**) after the 11th (final) SAG cycle. Injection was from left to right in each figure.

Figure 12b shows that foam propagated nearly 200 ft through the highest permeability layer after injection of the first SAG cycle. Foam continued to propagate as SAG injection continued, reaching a peak distance of 400 ft from the injection well (Figure 12d). Foam propagation distance was directly linked to permeability, with the highest permeability layers propagating foam the furthest. Foam more readily generates and propagates in higher permeability layers due to decreased capillary pressure.

7. Conclusions

This work presented a multiscale experimental and numerical investigation of CO_2 foam mobility control. CO_2 foam generation, strength, and propagation were evaluated at the core-scale at reservoir conditions and in a field-scale radial simulation model representing a recently completed CO_2 foam field pilot. The main objective of the experimental work was to evaluate foam generation, strength, and propagation during unsteady-state surfactant-alternating-gas (SAG) injection at reservoir conditions. The SAG injection rapidly generated foam upon the introduction of surfactant into the system. The apparent viscosity of the SAG continually increased with each subsequent SAG cycle indicating continued foam generation and propagation into the core. During a period of prolonged CO_2 injection, after SAG injection, the highest apparent viscosity value was reached before foam was destroyed in an effective drainage process, resulting in foam dry-out. Overall, the maximum apparent viscosity of the SAG was 146 cP, whereas the maximum apparent viscosity of an identical water-alternating-gas (without surfactant) injection was 2.4 cP. The laboratory methodology captured unsteady-state CO_2 foam flow and sheds light on field-scale CO_2 foam flow.

The radial reservoir simulation model investigated foam generation, strength, and propagation during a recently completed field pilot. The objective was to tune the model to match the observed bottom hole pressure (BHP) data from the foam pilot. The simulated BHP values for the base case SAG were higher than the baseline WAG, indicating that foam was generated with surfactant present. However, the base case SAG's simulated BHP values were significantly higher than the observed BHP from the pilot. This suggests that the foam generated during the pilot was not as strong as observed in laboratory studies. The foam model sensitivity study investigated the impact of different experimentally derived foam models on foam generation and strength. The most significant foam model parameter impacting injection BHP in the studied cases was the reference mobility reduction factor (*fmmob*). A reasonable match was achieved by tuning the reference mobility reduction factor. The model included a method to capture foam dry-out in the near wellbore region and indicated that foam had propagated approximately 400 ft from the injection well, more than halfway to the nearest producer, at the end of pilot injection.

Author Contributions: Conceptualization, Z.P.A.; methodology, Z.P.A., A.S. and M.K.; investigation, Z.P.A., A.S. and M.K.; writing—original draft preparation, Z.P.A.; writing—review and editing, A.S., M.K. and A.G.; supervision, Z.P.A. and A.G.; funding acquisition, Z.P.A. and A.G. All authors have read and agreed to the published version of the manuscript.

Funding: This research was funded by The Norwegian Research Council project number 249742.

Institutional Review Board Statement: Not applicable.

Acknowledgments: The authors acknowledge industry partners: Shell Global Solutions, TOTAL E&P USA, Equinor ASA and Occidental Petroleum. The authors also thank the field operator.

Conflicts of Interest: The authors declare no conflict of interest.

Nomenclature

f_g	Gas fraction or foam quality
ft	Feet
cP	Centipoise
K	Permeability
mD	Millidarcy
D	Darcy
MPa	Megapascal
Psig	Pound per square inch, gauge
rb/day	Reservoir barrels per day
ft/day	Foot per day
t	Time
S_{or}	Residual oil saturation, fraction of pore volume
fmmob	Foam model, maximum gas mobility reduction factor
fmdry	Foam model parameter in Fwater
epdry	Foam model parameter in Fwater
fmsurf	Foam model parameter in Fsurf
epsurf	Foam model parameter in Fsurf
fmcap	Foam model parameter in Fshear
epcap	Foam model parameter in Fshear
FM	Foam model, mobility reduction factor
$k_{rg}{}^{nf}$	Gas relative permeability with no foam

Abbreviations

CCUS	Carbon capture, utilization, and storage
CCS	Carbon capture and storage
EOR	Enhanced oil recovery
SAG	Surfactant-alternating gas
WAG	Water-alternating gas
DHPG	Down-hole pressure gauge
BHP	Bottom hole pressure
wt%	Weight percentage
IWTT	Interwell CO_2 tracer test
HCPV	Hydrocarbon pore volume

References

1. Bernard, G.G.; Holm, L.W.; Harvey, C.P. Use of Surfactant to Reduce CO_2 Mobility in Oil Displacement. *SPE J.* **1980**, *20*, 281–292. [CrossRef]
2. Blaker, T.; Aarra, M.G.; Skauge, A.; Rasmussen, L.; Celius, H.K.; Martinsen, H.A.; Vassenden, F. Foam for gas mobility control in the Snorre field: The FAWAG project. *SPE Reserv. Eval. Eng.* **2002**, *5*, 317–323. [CrossRef]
3. Enick, R.M.; Olsen, D.K.; Ammer, J.R.; Schuller, W. Mobility and Conformance Control for CO_2 EOR via Thickeners, Foams, and Gels—A Literature Review of 40 Years of Research and Pilot Tests; SPE-154122-MS. In Proceedings of the SPE Improved Oil Recovery Symposium, Tulsa, OK, USA, 14–18 April 2012. [CrossRef]
4. Føyen, T.; Brattekås, B.; Fernø, M.A.; Barrabino, A.; Holt, T. Increased CO_2 storage capacity using CO_2-foam. *J. Greenh. Gas Control* **2020**, *96*, 103016. [CrossRef]
5. Falls, A.H.; Hirasaki, G.J.; Patzek, T.W.; Gauglitz, D.A.; Miller, D.D.; Ratulowski, T. Development of a Mechanistic Foam Simulator: The Population Balance and Generation by Snap-Off. *SPE Res. Eng.* **1988**, *3*, 884–892. [CrossRef]
6. Rossen, W.R. Foams in Enhanced Oil Recovery. In *Foams Theory, Measurements, and Applications*; Prud'homme, R.K., Khan, S.A., Eds.; Marcel Dekker, Inc.: New York, NY, USA, 1996; Volume 57, Chapter 11; pp. 414–464.
7. Friedmann, F.; Jensen, J.A. Some Parameters Influencing Formation and Propagation of Foam in Porous Media. In Proceedings of the SPE California Regional Meeting, Oakland, CA, USA, 2–4 April 1986. [CrossRef]
8. Rossen, W.R.; Gauglitz, P.A. Percolation Theory of Creation and Mobilization of Foam in Porous Media. *AIChE J.* **1990**, *36*, 1176. [CrossRef]
9. Ashoori, E.; Marchesin, D.; Rossen, W.R. Roles of transient and local equilibrium foam behavior in porous media: Traveling wave. *Colloids Surf. A Physicochem. Eng. Asp.* **2011**, *377*, 228–242. [CrossRef]
10. Holm, L.W.; Garrison, W.H. CO_2 Diversion with Foam in an Immiscible CO_2 Field Project. *SPE Res. Eng.* **1988**, *3*, 112–118. [CrossRef]
11. Huh, D.G.; Handy, L.L. Comparison of Steady and Unsteady-State Flow of Gas and Foaming Solution in Porous Media. *SPE Res. Eng.* **1989**, *4*, 77–84. [CrossRef]

12. Castillo, R.O.S. Scale up of Surfactant Alternating Gas Foam Processes. Ph.D. Thesis, Delft University of Technology, Delft, The Netherlands, 2019. [CrossRef]
13. Ma, K.; Lopez-Salinas, J.L.; Puerto, M.C.; Miller, C.A.; Biswal, S.L.; Hirasaki, G.J. Estimation of Parameters for the Simulation of Foam Flow through Porous Media. Part 1: The Dry-Out Effect. *Energy Fuels* **2013**, *27*, 2363–2375. [CrossRef]
14. Hoefner, M.L.; Evans, E.M. CO_2 Foam: Results from Four Developmental Field Trials. *SPE Res. Eng.* **1995**, *10*, 273–281. [CrossRef]
15. Chou, S.I.; Vasicek, S.L.; Pisio, D.L. CO_2 Foam Field Trial at North Ward-Estes. In Proceedings of the SPE Annual Technical Conference and Exhibition, Washington, DC, USA, 4–7 October 1992. [CrossRef]
16. Shan, D.; Rossen, W.R. Optimal Injection Strategies for Foam IOR. *SPE J.* **2004**, *9*, 132–150. [CrossRef]
17. Leeftink, T.N.; Latooij, C.A.; Rossen, W.R. Injectivity errors in simulation of foam EOR. *J. Petrol. Sci. Eng.* **2015**, *126*, 26–34. [CrossRef]
18. Alcorn, Z.P.; Fredriksen, S.B.; Sharma, M.; Rognmo, A.U.; Føyen, T.L.; Fernø, M.A.; Graue, A. An Integrated CO_2 Foam EOR Pilot Program with Combined CCUS in an Onshore Texas Heterogeneous Carbonate Field. *SPE Resv. Eval. Eng.* **2019**, *22*, 1449–1466. [CrossRef]
19. Jian, G.; Puerto, M.C.; Wehowsky, A.; Dong, P.; Johnston, K.P.; Hirasaki, G.J. Static Adsorption of an Ethoxylated Nonionic Surfactant on Carbonate Minerals. *Langmuir* **2016**, *32*, 10244–10252. [CrossRef] [PubMed]
20. Jian, G.; Alcorn, Z.P.; Zhang, L.M.; Biswal, L.S.; Hirasaki, G.; Graue, A. Evaluation of a Nonionic Surfactant Foam for CO_2 Mobility Control in a Heterogeneous Carbonate Reservoir. *SPE J.* **2020**, *25*, 3481–3493. [CrossRef]
21. Alcorn, Z.P.; Sharma, M.; Fredriksen, S.B.; Rognmo, A.U.; Fernø, M.A.; Graue, A. CO_2 Foam Field Pilot Test for EOR and CO_2 Storage in a Heterogeneous Carbonate Reservoir: Operational Design, Data Collection and Pilot Monitoring Program. In Proceedings of the 80th EAGE Annual Conference and Exhibition, Copenhagen, Denmark, 11–14 June 2018. [CrossRef]
22. Alcorn, Z.P.; Karakas, M.; Graue, A. CO_2 Foam Pilot in a Heterogenous Carbonate Reservoir: Analysis and Results. In Proceedings of the SPE Improved Oil Recovery Conference, Virtual, 25–28 April 2022. [CrossRef]
23. Al-Menhali, A.; Krevor, S. The Impact of Crude Oil Induced Wettability Alteration on Remaining Saturations of CO_2 in Carbonates Reservoirs: A Core Flood Method. In Proceedings of the 2016 SPE Europec featured at 78th EAGE Conference and Exhibition, Vienna, Austria, 30 May–2 June 2016.
24. Jones, S.A.; Laskaris, G.; Vincent-Bonnieu, G.; Farajzadeh, R.; Rossen, W.R. Surfactant Effect on Foam: From Core Flood Experiments to Implicit-Texture Foam-Model Parameters. In Proceedings of the SPE Improved Oil Recovery Conference, Tulsa, OK, USA, 11–13 April 2016.
25. Karakas, M.; Alcorn, Z.P.; Graue, A. Pressure Measurements for Monitoring CO_2 Foam Pilots. *Energies* **2022**, *15*, 3035. [CrossRef]
26. Sharma, M.; Alcorn, Z.; Fredriksen, S.; Fernø, M.; Graue, A. Numerical Modeling Study for Designing CO_2-foam Field Pilot. In Proceedings of the IOR 2017—19th European Symposium on Improved Oil Recovery, Stavanger, Norway, 24 April 2017.
27. Cheng, L.; Reme, A.; Shan, D.; Coombe, D.; Rossen, W. Simulating Foam Processes at High and Low Foam Qualities. In Proceedings of the SPE/DOE Improved Oil Recovery Symposium, Tulsa, OK, USA, 3 April 2000.
28. Farajzadeh, R.; Andrianov, A.; Krastev, R.; Hirasaki, G.; Rossen, W. Foam–oil interaction in porous media: Implications for foam assisted enhanced oil recovery. *Adv. Colloid Interface Sci.* **2012**, *183–184*, 1–13. [CrossRef] [PubMed]
29. Sharma, M.; Alcorn, Z.P.; Fredriksen, S.B.; Fernø, M.A.; Skjæveland, S.; Graue, A. Model Calibration for Forecasting CO_2-Foam EOR Field Pilot Performance in a Carbonate Reservoir. *Pet. Geosci.* **2020**, *26*, 141–149. [CrossRef]
30. Rognmo, A.U.; Fredriksen, S.B.; Alcorn, Z.P.; Sharma, M.; Føyen, T.; Eide, G.A.; Fernø, M. Pore-to-Core EOR Upscaling for CO_2 Foam for CCUS. *SPE J.* **2019**, *24*, 2793–2803. [CrossRef]
31. Lake, L.W. *Enhanced Oil Recovery*; Society of Petroleum Engineers: Richardson, TX, USA, 2010.
32. Chou, S.I. Conditions for Generating Foam in Porous Media. In Proceedings of the SPE Annual Technical Conference and Exhibition, Dallas, TX, USA, 6–9 October 1991.
33. Ransohoff, T.C.; Radke, C.J. Mechanisms of Foam Generation in Glass-Bead Packs. *SPE Res. Eng.* **1988**, *3*, 573–585. [CrossRef]
34. Patzek, T.W. Field Applications of Steam Foam for Mobility Improvement and Profile Control. *SPE Res. Eng.* **1996**, *11*, 79–86. [CrossRef]

Graphic design: Communication Division, UiB / Print: Skipnes Kommunikasjon AS

uib.no

ISBN: 9788230861516 (print)
9788230863329 (PDF)